TITLE:
Martensitic Transformation from Ultrafine Grained Meta-stable Austenite in Fe-Ni-C Alloy(Dissertation_全文)

AUTHOR(S):
Hamidreza Jafarian

CITATION:
Hamidreza Jafarian. Martensitic Transformation from Ultrafine Grained Meta-stable Austenite in Fe-Ni-C Alloy. 京都大学, 2012, 博士(工学)

ISSUE DATE:
2012-01-23

URL:
https://doi.org/10.14989/doctor.k16502

RIGHT:

京都大学学術情報リポジトリ
KURENAI 紅
Kyoto University Research Information Repository

Martensitic Transformation from Ultrafine Grained Meta-stable Austenite in Fe-Ni-C Alloy

2011

Hamidreza Jafarian

Martensitic Transformation from Ultrafine Grained Meta-stable Austenite in Fe-Ni-C Alloy

By

Hamidreza Jafarian

A Dissertation submitted to Kyoto University for

Doctor of Engineering

Department of Materials Science and Engineering

Graduate School of Engineering

Kyoto University

2011

Chapter 1. Background and purpose

1.1. Ultrafine-grained (UFG) or nano-structured materials

In recent decades, a new class of material having mean grain size between 100 nm-1 μm has been developed by severe plastic deformation (SPD) [1-14]. This kind of material is so-called ultrafine-grained (UFG) or nano-structured materials. It is expected that in the UFG materials having mean grain size below 1 μm, volume fraction of grain boundary significantly increases compared with coarse-grained materials. It is well known that mechanical properties of materials can be improved by grain refinement, so that grain refinement has been an important issue in research field of metallic materials. So far, however, the minimum grain size of bulky metallic materials that could be achieved is about 10 μm. It is expected that the UFG materials or nano-structured materials exhibit superior high strength, though the UFG or nano-structured materials often have limited uniform elongation. The UFG or nano-structured materials also exhibit peculiar properties that have never seen in conventional metallic materials having coarse-grained structures. Tsuji et al. [8] reported that yielding behavior with Lüders bands appears during tensile test in pure Al when the grain size becomes ultrafine. Huang et al. [13] reported the peculiar phenomenon of bulk nano-structured Al, that is, "hardening by annealing and softening by deformation". In general, metallic materials are softened by annealing and hardened by deformation. Nano-structured Al fabricated by SPD process, however, exhibits completely opposite behaviors [13].

The unique properties of UFG materials have prompted material scientists to study them in more detail, in both fundamental and application issues, under the demands for lightweight or high strength materials.

1.2. Accumulative roll bonding (ARB) process

Several techniques of SPD process have been developed to fabricate UFG materials, such as cyclic extrusion compression (CEC) [1], equal channel angular pressing (ECAP) [2,5], high pressure torsion (HPT) [3], accumulative roll-bonding (ARB) [4,6], repetitive corrugation and straightening (RCS) [7], severe torsion straining (STS) [10] and torsion extrusion (TE) [12]. Among these techniques, in the present study, the ARB process was used to fabricate UFG material. The ARB process has some unique features. Firstly, unlike the ECAP, CEC and HPT processes which require special forming machines with large capacity and expensive dies, the ARB process can be performed by a conventional rolling mill without any special dies. Secondly, in comparison to the other methods, the productivity of the ARB process is relatively high.

The ARB process was invented by Saito et al. [4] in 1998. The ARB process is an only SPD process using rolling deformation itself. The principle of the ARB is schematically shown in **Fig. 1.1**. Rolling is the most advantageous metalworking process for continuous production of plates, sheets and bars. However, the total reduction applied to the materials is substantially limited in conventional rolling because of the decrease in the thickness of the materials with increasing the reduction. In the ARB process, 50% rolled sheet is cut into two, stacked to be the initial dimension after degreasing and wire brushing the contact surfaces, and then rolled again. In order to obtain one-body solid materials, the rolling in the ARB process is not only a deformation process but also a bonding process (roll-bonding). To achieve good bonding, the roll-bonding process is sometimes carried out at elevated temperatures below recrystallization temperature of the material. The ARB process can apply significant amount of plastic strain into the materials, because the above mentioned

procedures can be repeated limitlessly. **Table 1.1** summarizes the geometrical changes of the specimen during the ARB, when two pieces of the sheets 1 mm thickness are stacked and roll-bonded by 50% reduction per cycle. The number of the initial sheets included in the 6-cycle ARB processed sheet is 64, so that the mean thickness of the initial sheet after 6-cycle ARB process is about 15 μm. The 6-cycle ARB process corresponds to a total reduction in thickness of 98.4%, i.e., an equivalent strain of 4.8. The major difficulty in the ARB process is the occurrence of edge-cracks in the sheets, because rolling is not a hydrostatic process.

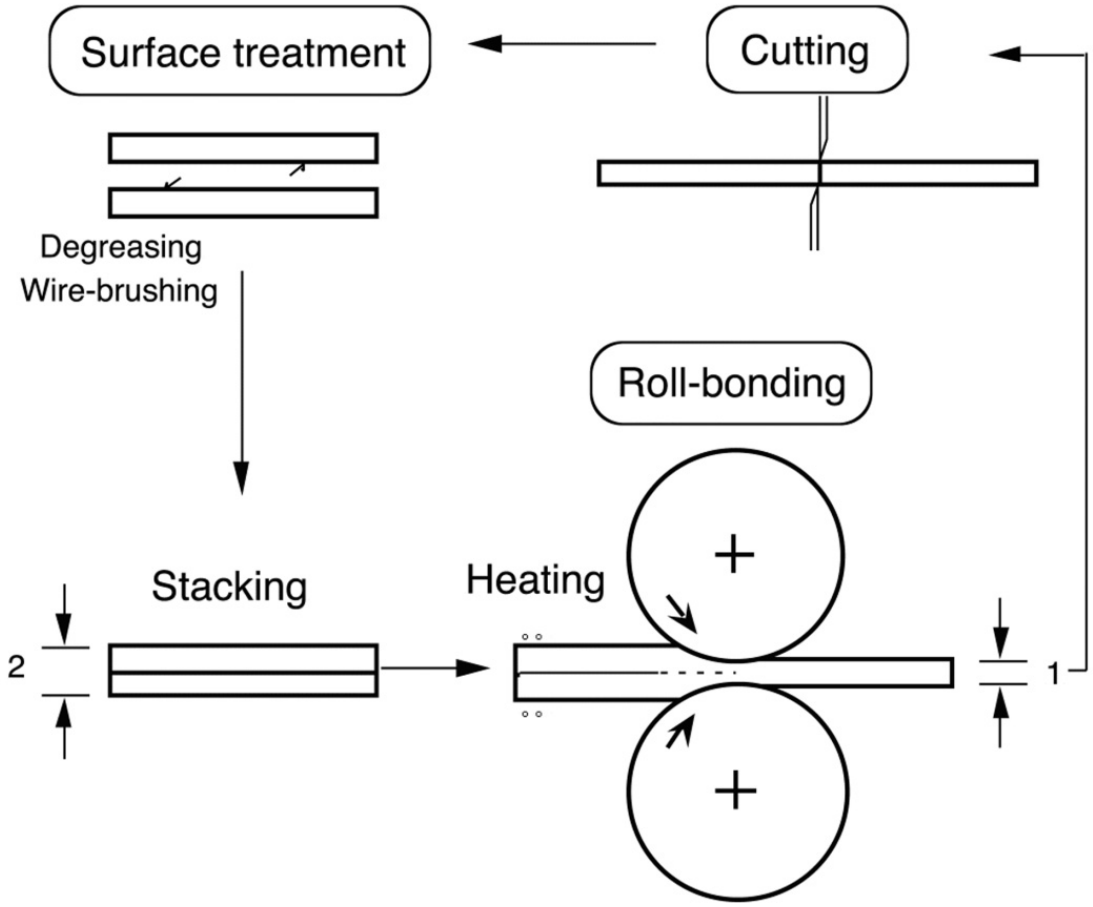

Fig. 1.1. Schematic illustration showing the principle of the ARB process [6].

Table 1.1. Geometrical changes of the materials during the ARB where two pieces of the sheets 1 mm thick are roll-bonded by 50% reduction per cycle [9].

No. of cycles	1	2	3	4	5	6	n
No. of layers	2	4	8	16	32	64	2^n
No. of bonded boundaries	1	3	7	15	31	63	$2^n - 1$
Layer intervals (μm)	500	250	125	62.5	31.2	15.6	$1000/2^n$
Total reduction (%)	50	75	87.5	93.8	96.9	98.4	$(1 - 1/2^n) \times 100$
Equivalent strain	0.8	1.6	2.4	3.2	4.0	4.8	$(\frac{2}{\sqrt{3}} ln2)\, n = 0.8n$

1.3. Objective and strategy of the present research

Although the UFG or nano-structured materials can exhibit outstanding strength, the largest issue of the UFG or nano-structured materials is poor tensile ductility. Besides SPD process, another possible way to achieve finer microstructure and good mechanical properties is using phase transformation, especially martensitic transformation in steels. In addition, one of the promising ways to overcome the poor ductility in the UFG or nano-structured materials is using transformation induced plasticity (TRIP) phenomenon that is caused by deformation-induced martensitic transformation. The details of TRIP phenomenon will be explained later in this chapter. On this basis, the combination of UFG structure and martensitic transformation is desired to fabricate finer UFG materials having both superior strength and enough ductility. **Figure 1.2** illustrates the motivation of this doctoral study. The aim of this thesis is to clarify the characteristics of martensitic transformation from UFG austenite fabricated by ARB process and subsequent annealing.

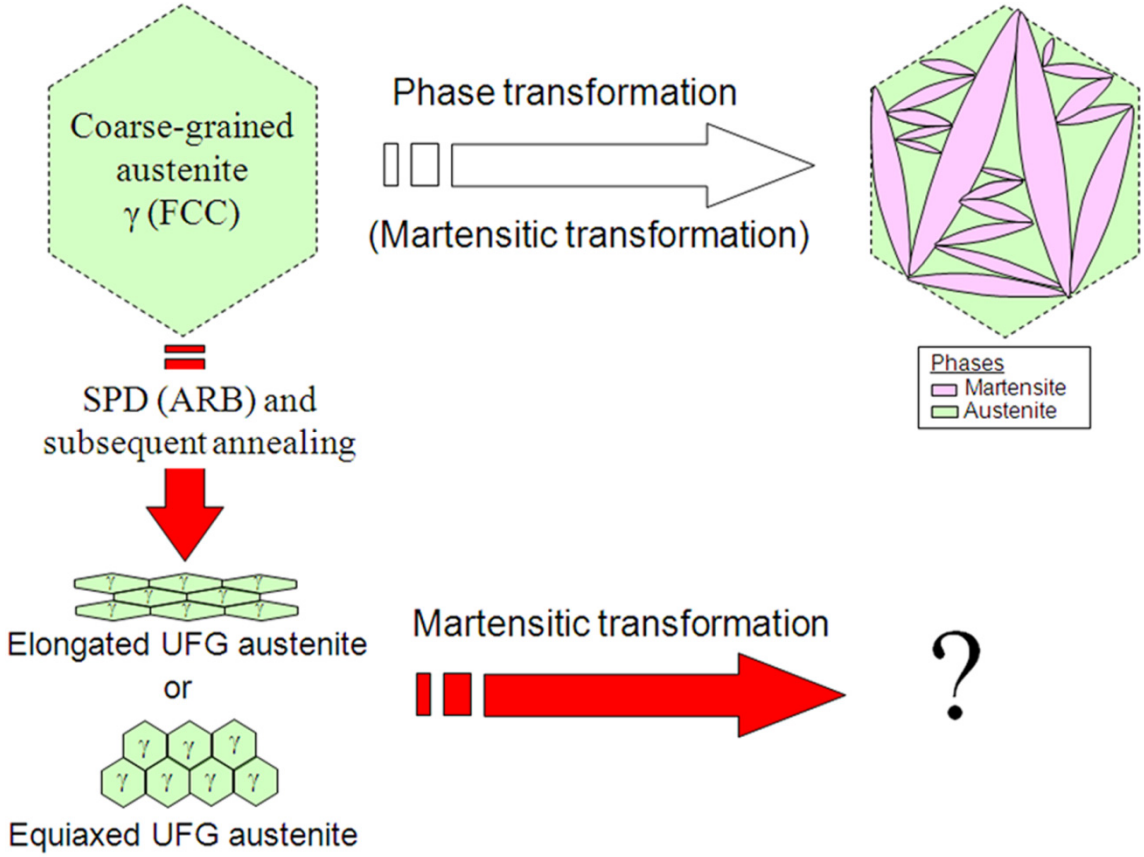

Fig. 1.2. Schematic illustration showing the major objective of this study on martensitic transformation from coarse-grained austenite, elongated UFG austenite or equiaxed UFG austenite.

1.3.1. Martensitic transformation from coarse-grained austenite

Martensitic transformation is a diffusionless and displacive solid state phase transformation that takes place by cooperative atomic movement. Characteristics of martensite transformed from conventional austenite with coarse-grained structure, such as morphology, martensite starting (M_s) temperature, crystallographic features (orientation relationship, variant selection), etc., have been well studied [16-29]. There are four kinds of morphology in α′-martensite (with b.c.c or b.c.t structure), i.e., lath, butterfly, lenticular and thin plate types, depending on the alloy composition or the M_s temperature. Typical optical micrographs of the four kinds of martensite are shown in **Fig. 1.3**. Among these martensite morphologies, lath martensite forms at the highest M_s

temperature. Lath martensite is an important structure from a practical point of view, because it exhibits high strength. On the other hand, thin plate martensite forms at the lowest M_s temperature and exhibits shape memory effect or super-elasticity. It has been reported that the M_s temperature is determined by not only chemical composition but also austenite grain size. Previous studies [20-21] reported that M_s temperature decreases significantly and monotonously with decreasing the austenite grain size, resulting in the change of the morphology of martensite even in the same alloy. However, the previous works studied martensitic transformation from the austenite having grain sizes larger than 5 μm. Hence, studying martensitic transformation from UFG austenite is desirable, and the present study focuses on it.

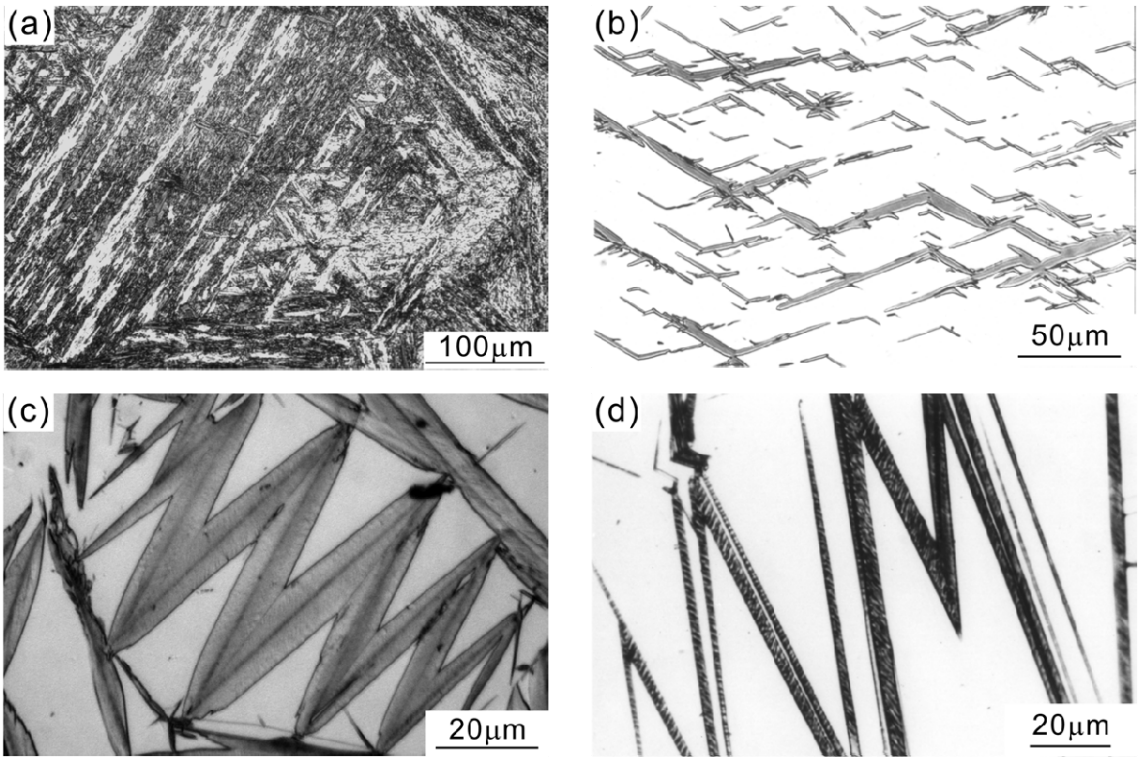

Fig. 1.3. Optical microscope images of the four kinds of typical martensite, (a) lath martensite, (b) butterfly martensite, (c) lenticular martensite, and (d) thin plate martensite [22].

It is well known that martensite holds an orientation relationship with respect to austenite mother phase. Concerning martensitic transformation in iron-based alloys, three kinds of orientation relationships were reported [16-19]; Kurdjumov-Sachs (K-S) relationship ($\{111\}_A$ // $\{011\}_M$, $<\bar{1}01>_A$ // $<\bar{1}\bar{1}1>_M$), Nishiyama-Wasserman (N-W) relationship ($\{111\}_A$ // $\{011\}_M$, $<\bar{1}\bar{1}2>_A$ // $<0\bar{1}1>_M$) and Greninger-Troiano (G-T) relationship ($\{111\}_A$ 1° from $\{011\}_M$, $<\bar{1}\bar{1}2>_A$ 2.5° from $<0\bar{1}1>_M$), where subscripts of A and M represent austenite and martensite, respectively. Previous studies [25, 28] demonstrated that orientation relationship between martensite and austenite can be greatly influenced by morphology of martensite. Thus, study on orientation relationship of martensite transformed from the UFG austenite is curious.

Due to the crystal symmetry of austenite and martensite, there are many equivalent crystallographic variants of martensite that are transformed from a single grain of austenite. There are 24 variants of martensite under the K-S orientation relationship while 12 variants of martensite under the N-W orientation relationship. When plastic deformation is applied to austenite before martensitic transformation, these variants of martensite do not form equally but some specific variants are preferentially formed, resulting in the development of transformation texture [29]. This is so-called variant selection. Because martensite plate cannot grow across the austenite grain boundary, austenite grain size and grain shape would significantly affect the variant selection of martensite.

Another important phenomenon of martensitic transformation in metastable austenitic steels is the TRIP phenomenon. The driving force for martensitic transformation can be provided not only by cooling (thermal driving force) but also by applying mechanical work (mechanical driving force). Therefore, martensitic

transformation can also happen in metastable austenitic steel during deformation (deformation-induced martensitic transformation) [30]. The formation of martensite during deformation can inhibit the propagation of necking area in the tensile specimens, resulting in large plasticity (TRIP phenomenon). Since the stability of austenite affects the TRIP phenomenon, it is expected that grain size and microstructure of austenite would also influence the TRIP phenomenon.

1.3.2. Martensitic transformation from ultrafine-grained austenite

As mentioned in the sections of 1.3.1 and 1.3.2 of this chapter, previous studies have indicated that grain size and microstructure of austenite influence the characteristics of martensite. On this basis, it is expected that martensitic transformation behaviors from the UFG austenite can be significantly different compared with those from coarse-grained austenite. Several researchers have studied martensitic transformation behavior from UFG austenite in steels. Tadaki et al. [31] studied martensite transformation in nano-powder particles of Fe-Ni alloys. They found that austenite is stabilized significantly in the nano-powders. However, the martensitic transformation of powder particles with free surface must be essentially different from that of bulky polycrystalline austenite having fine-grained structures. Takaki et al. [32] reported that UFG structure of austenite reduces the number of martensite variants within an austenite grain. Kitahara et al. [33] also studied the effect of austenite grain size on morphology and M_s temperature of martensite transformed from UFG austenite fabricated by ARB process. Han and Xu [34] reported that martensite plate transformed from UFG austenite fabricated by severe plastic deformation in a Fe–32%Ni alloy exhibited fragmented shape, which was different from that transformed from coarse-grained

austenite. Although several interesting phenomena have been reported, there is no systematic study on martensitic transformation from UFG austenite.

1.4. Outline of the thesis

In this thesis, a metastable austenitic steel with mean grain size of 35 μm is used as the starting material. The chemical composition of the studied alloy (the starting material) is shown in **Table 1.2**. The sheets of the starting material were subjected to the ARB process (with pre-heating at 873 K for 0.6 ks) up to 6 cycles and then subsequently annealed between 773-873 K to obtain UFG austenite. This thesis studies the characteristics of martensite transformed from austenite having various UFG structures, in order to clarify the mechanism of martensitic transformation from UFG austenite. The thesis consists of 6 chapters.

Table 1.2. Chemical composition of the alloy studied (wt.%)

Fe	C	Ni	Si	Mn	P	S	O	N
bal.	0.29	24.09	0.01	0.07	<0.005	<0.0005	0.0008	0.0006

In **chapter 1** (this chapter), background and purpose of this thesis are explained.

In **chapter 2**, change in microstructure and texture of austenite ARB processed and subsequently annealed is studied. Mechanical properties of the austenite are also investigated.

In **chapter 3**, characteristics of martensite, i.e., morphology and M_s temperature, transformed from austenite ARB processed and subsequently annealed are studied from a view point of the change in austenite structure.

In **chapter 4**, orientation relationship between martensite and austenite is studied from view points of austenite grain size and austenite microstructure.

In **chapter 5**, effects of austenite grain size and austenite microstructure on the variant selection in martensitic transformation are studied.

In **chapter 6**, conclusions and achievements in this thesis are summarized.

References

[1] J. Richert, M. Richert, Aluminium 62 (1986), pp. 604-607.

[2] R.Z. Valiev, N.A. Krasilnikov, N.K. Tsenev, Mater. Sci. and Eng. A 137 (1991), pp. 35-40.

[3] Z. Horita, D.J. Smith, M. Furukawa, N. Nemoto, R.Z. Valiev, T.G. Langdon, Mater. Res. 11 (1996), pp. 1880-1890.

[4] Y. Saito, N. Tsuji, H. Utsunomiya, T. Sakai, R.G. Hong, Scripta Mater. 39 (1998), pp. 1221-1227.

[5] N. Nemoto, Z. Horita, M. Furukawa, T.G. Langdon, Met. Mater. 4 (1998), pp. 1181-1186.

[6] Y. Saito, N. Tsuji, H. Utsunomiya, T. Sakai, Acta Mater. 47 (1999), pp. 579-583.

[7] J.Y. Huang, Y.T. Zhu, H. Jiang, T.C. Lowe, Acta Mater. 49 (2001), pp. 1497–1505.

[8] N. Tsuji, Y. Ito, Y. Saito, Y. Minamino, Scripta Mater. 47 (2002), pp. 893-899.

[9] N. Tsuji, Y. Saito, S.H. Lee, Y. Minamino, Adv. Eng. Mater. 5 (2003), pp. 338-344.

[10] K. Nakamura, K. Neishi, K. Kaneko, M. Nakagaki, Z. Horita, Mater. Trans. 45 (2004), pp. 3338–3342.

[11] R.Z. Valiev, Nature Mater. 3 (2004), pp. 511-516.

[12] S. Mizunuma, Mater. Sci. Forum 503–504 (2005), pp. 185–190.

[13] X. Huang, N. Hansen, N. Tsuji, Science 312 (2006), pp. 249-253.

[14] A. Azushima, R. Kopp, A. Korhonen, D.Y. Yang, F. Micari, G.D. Lahoti, P. Groche, J. Yanagimoto, N. Tsuji, A. Rosochowski, A. Yanagida, CIRP Annals-Manufacturing Technology 57 (2008), pp. 716-735.

[15] http://www.bnm.mtl.kyoto-u.ac.jp

[16] G. Kurdjumov, G. Sachs, Z. Phys, 64 (1930), pp. 325-343.

[17] A.B. Greninger, A.R. Troiano, Trans. ASM 140 (1940), pp. 307-336.

[18] A.B. Greninger, A.R. Troiano, Trans. AIME 145 (1941), pp. 289-291.

[19] Z. Nishiyama, K. Shimizu, Acta Metall. 9 (1961), pp. 980-981.

[20] T. Maki, S. Shimooka, I. Tamura, Metall. Trans. 2 (1971), pp. 2944-2955.

[21] M. Umemoto, W.S. Owen, Metall. Trans. 5 (1974), pp. 2041-2046.

[22] A. Shibata, PhD thesis, Kyoto University, (2005).

[23] A. Shibata, S. Morito, T. Furuhara, T. Maki, Scripta Mater. 53 (2005), pp. 597-602.

[24] H. Kitahara, R. Ueji, M. Ueda, N. Tsuji, Y. Minamino, Mater. Character. 54 (2005), pp. 378-386.

[25] A. Shibata, S. Morito, T. Furuhara, T. Maki, Scripta Mater. 53 (2005), pp. 597-602.

[26] H. Kitahara, R. Ueji, N. Tsuji, Y. Minamino, Acta Mater. 54 (2006), pp. 1279-1288.

[27] A. Shibata, S. Morito, T. Furuhara, T. Maki, Acta Mater. 57 (2009), pp. 483-492.

[28] H. Sato, S. Zaefferer, Acta Mater. 57 (2009), pp. 1931–1937.

[29] S. Kundu, H.K.D.H. Bhadeshia, Scripta Mater. 55 (2006), pp. 779-781.

[30] P.C. Maxwell, A. Goldberg, J.C. Shyne, Metall. Trans. 5 (1974), pp. 1305-1318.

[31] T. Tadaki, Y. Murai, A. Koreeda, Y. Nakata, Y. Hirotsu, Mater. Sci. and Eng. A 217–218 (1996), pp. 235-238.

[32] S. Takaki, K. Fukunaga, J. Syarif, T. Tsuchiyama, Mater. Trans. 45 (2004), pp. 2245-2251.

[33] H. Kitahara, N. Tsuji, Y. Minamino, Mater. Sci. and Eng. A 438–440 (2006), pp. 233-236.

[34] B. Han, Z. Xu, Mater. Sci. and Eng. A 487 (2008), pp. 64-67.

Chapter 2. Characteristics of austenite processed by accumulative roll bonding (ARB) and subsequent annealing

2.1. Introduction

Ultrafine-grained (UFG) materials having grain size smaller than 1 μm exhibit outstanding mechanical properties [1-2]. Such properties of UFG materials have prompted many materials scientists to study UFG materials. One of the promising ways to produce UFG materials with bulky shapes is the severe plastic deformation (SPD) [1-2], such as accumulative roll bonding (ARB) [3], equal channel angular pressing (ECAP) [4], high pressure torsion (HPT) [5] and cyclic extrusion compression (CEC) [6]. In the present study, the ARB process is used to fabricate UFG materials among aforementioned techniques, because the ARB process can produce UFG sheet with larger dimensions [7-8].

As described in chapter 1, the goal of this study is to clarify the characteristics of martensite transformed from UFG austenite. The detailed characterization of microstructural evolution in austenite during the ARB process is necessary to understand the martensitic transformation behavior from the UFG austenite, because martensitic transformation is greatly affected by microstructure of mother phase, i.e., austenite. So far, however, UFG structures of metastable austenitic steels, such as Fe-Ni-C have been rarely studied systematically. The aim of this chapter is to characterize the microstructure and texture of metastable austenitic steel with the chemical composition of Fe-24Ni-0.3C (wt.%) processed by the ARB. The author also evaluates the change in mechanical properties of the material during the ARB and subsequent annealing processes.

2.2. Experimental procedure

An Fe-24Ni-0.3C (wt.%) alloy was used in the present study, of which chemical composition is shown in **Table 1.2** (chapter 1). A cast ingot of the alloy was hot-rolled and then cold-rolled to make a sheet with thickness of 1 mm and austenitized at 1173 K for 3.6 ks. The produced sheets were used as the starting material. To obtain UFG austenite structures, the sheets were subjected to the ARB process under lubrication condition. Figure 1.2 (chapter 1) is a schematic illustration showing the principle of the ARB process. In the ARB process, two pieces of the sheets are stacked after degreasing and wire brushing the contact surfaces. The stacked sheets are rolled by 50% reduction in one pass. Then, the rolled sheet is cut into two, stacked to have the initial dimensions before rolling, and rolled again. The rolling in the ARB process is not only a deformation process but also a bonding process (roll-bonding). The ARB process can apply significant amount of plastic strain into the materials, because the procedures can be repeated limitlessly. In order to prevent deformation-induced martensitic transformation during the ARB process resulting in fully austenitic structures, stacked sheets were held at 873 K, at which austenite phase was stable, for 0.6 ks and subsequently roll-bonded by 50% reduction in thickness in one pass. The roll-bonded sheets were immediately cooled in water. A two-high mill with 310 mm diameter rolls was used for rolling process. The ARB was repeated up to 6-cycle, so that the total equivalent strain accumulated was 4.8. The 6-cycle ARB processed specimens were annealed at 773, 823 and 873 K for 1.8 ks to obtain UFG austenite with partly recrystallized or fully recrystallized microstructures.

The microstructures of the ARB processed specimens were characterized by scanning electron microscopy (SEM) using a field-emission type SEM machine (Philips XL30S-FEG) equipped with electron backscatter diffraction (EBSD) system operated at

15 kV, and transmission electron microscopy (TEM) using Philips CM200-FEG operated at 200 kV. The section of the specimen for EBSD observation was polished mechanically and then electrolytically in a 900 ml CH_3COOH + 100 ml $HClO_4$ solution at approximately 284 K with a voltage of 20 V. The obtained EBSD data were analyzed by TSL-OIM Analysis software. Thin foils for TEM observation were prepared by twin-jet electropolishing in the same solution as that for the SEM/EBSD observation. All the microstructures were observed from the transverse direction (TD) of the sheets. Dislocation density in the austenite ARB processed to various strains was measured by X-ray diffraction (XRD) with Cr-K_α radiation. The XRD data were analyzed based on the Williamson-Hall method [9]. In order to evaluate mechanical properties of the material, tensile specimens with gage length of 10 mm, gage width of 5 mm and thickness of 1 mm were prepared form the sheets after different ARB cycles.

2.3. Results and discussion

2.3.1. Change in microstructure of austenite during ARB process and subsequent annealing treatment

A SEM image of the starting material is shown in **Fig. 2.1**. The starting microstructure is an equiaxed and fully recrystallized austenite with mean grain size of 35 μm. In **Fig. 2.2**, change in microstructure during the ARB process is illustrated by grain boundary and phase maps, normal direction (ND) orientation color maps and rolling direction (RD) orientation color maps obtained by EBSD measurements and analysis. The phase maps of Fig. 2.2(a)-(e) demonstrate 100% austenite structures, indicating that deformation-induced martensitic transformations did not occur during the ARB process at 873 K.

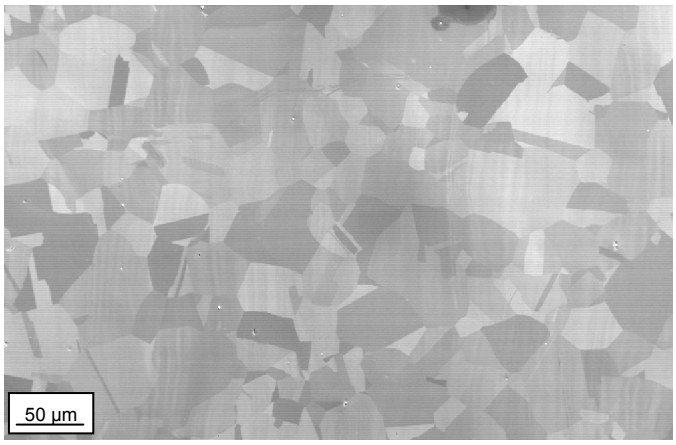

Fig. 2.1. SEM image of the starting material before the ARB process.

The grain boundary maps are superimposed on phase maps in Fig. 2.2(a)-(e). In the grain boundary maps, high angle boundaries with misorientation larger than 15° are drawn in black lines and low angle boundaries with misorientation between 2° and 15° are drawn in red lines. The grain boundary map of Fig. 2.2(a) indicates that the starting material consists of fully recrystallized and coarse grained austenite that has been shown in Fig. 2.1. The 1-cycle ARB process, corresponding to 50% rolling and an equivalent strain of 0.8, introduced a large amount of low angle boundaries into the austenite. Till 2-cycle of ARB process (75% rolling), the microstructures exhibit typical deformation microstructures which mainly involve pancake shape austenite grains having low angle boundaries (dislocation structures) inside. Increasing the number of ARB process up to 6-cycle causes significant grain refinement as shown in Fig. 2.2(a)-(e). Change in austenite grain size with increasing the number of ARB cycle is summarized in **Fig. 2.3**. Interception method was used to measure the grain size (or interval of boundaries) along ND. Here, both high angle boundaries and low angle boundaries were took into account for the grain size (d^{all}) measurement. In addition, the size of the grains surrounded by high angle boundaries (d^{HAGB}) is also indicated in Fig. 2.3. The figure indicates that the grain sizes (d^{all} and d^{HAGB}) monotonously decreases with increasing strain (ARB cycle), and UFG austenite with mean grain size of 300 nm was obtained by 6-cycle ARB process.

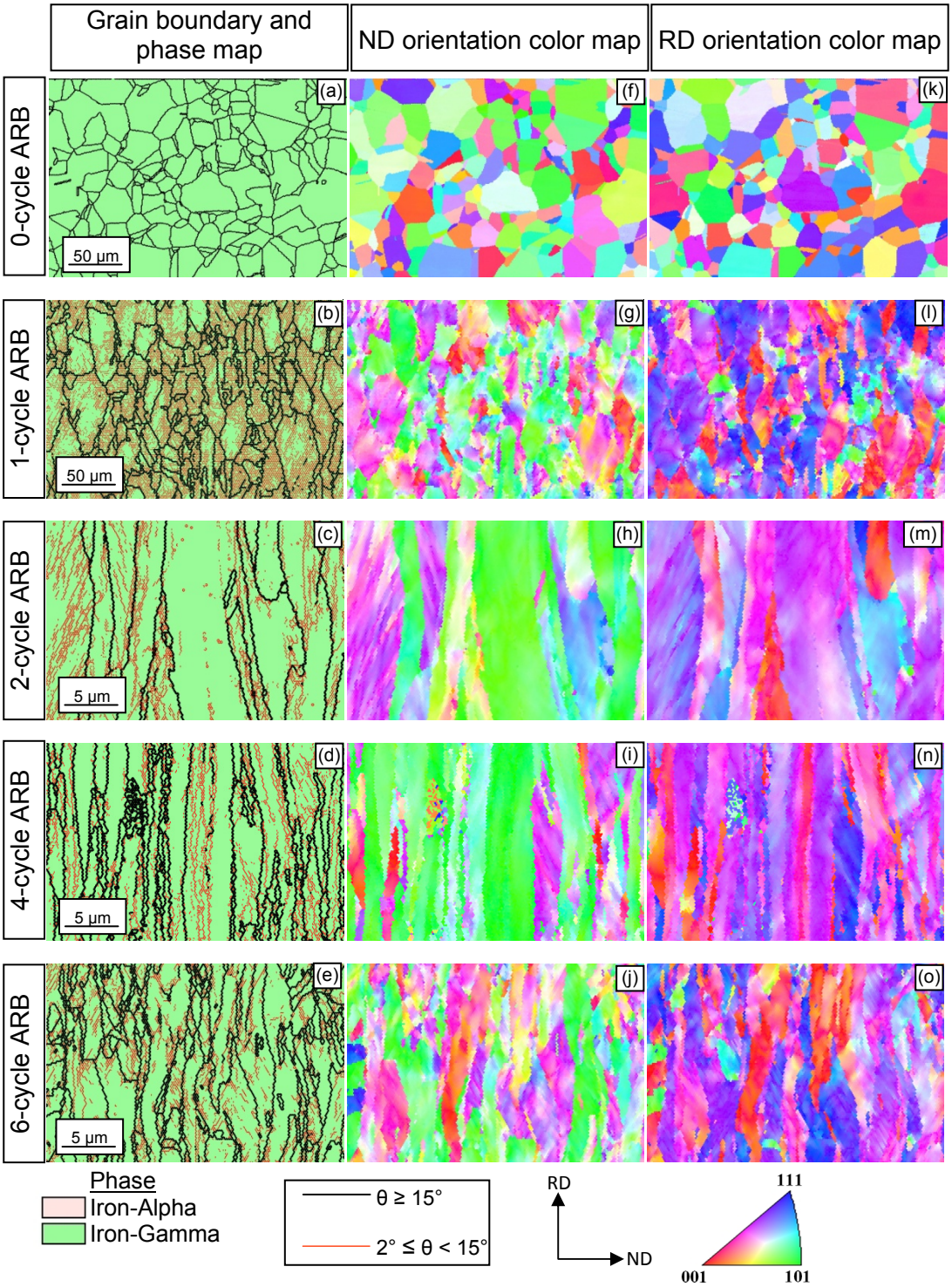

Fig. 2.2. (a)-(e): Grain boundary and phase maps of the starting material, 1-cycle, 2-cycle, 4-cycle and 6-cycle ARB processed specimens. (f)-(j) ND orientation color maps of the starting material, 1-cycle, 2-cycle, 4-cycle and 6-cycle ARB processed specimens. (k)-(o) RD orientation color maps of the starting material, 1-cycle, 2-cycle, 4-cycle and 6-cycle ARB processed specimens.

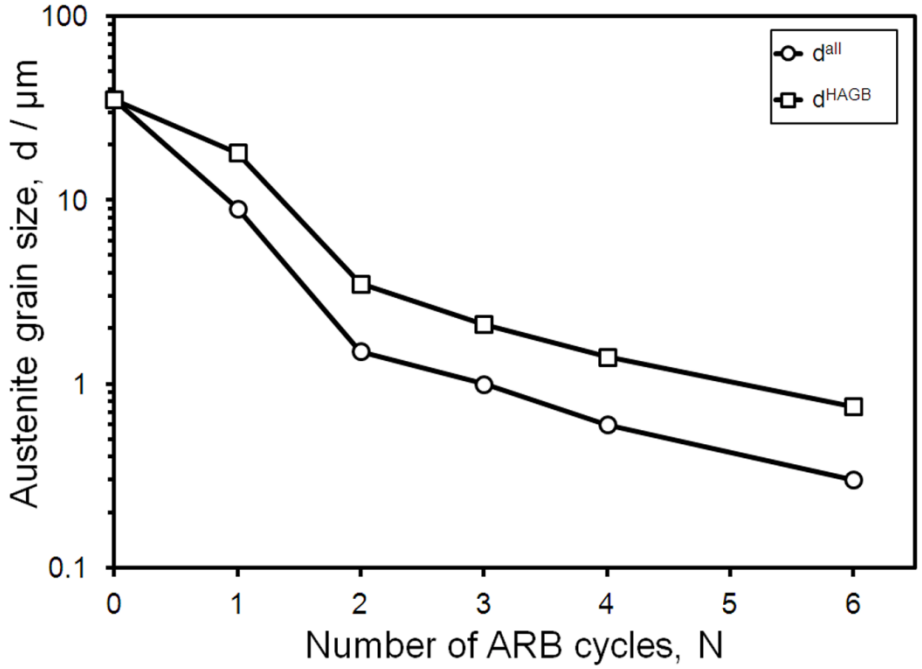

Fig. 2.3. Change in austenite grain size (boundary interval along ND) with the number of the ARB cycles.

The ND and RD orientation color map of the starting material, and those of the 1-cycle, 2-cycle, 4-cycle and 6-cycle ARB processed specimens are shown in **Fig. 2.2(f)-(o)**. The fully recrystallized austenite in the starting specimen does not show any tendency in colors, which indicates that the specimen does not have particular texture. The color maps of the ARB processed specimens indicate that preferred orientation (texture) develops during the ARB process, as particular colors become dominant in the maps. Other studies on Al alloys [14-15] also reported that ARB process resulted in formation of texture. The details of texture development during the ARB process in the present material will be described later in this chapter.

Figure 2.4(a)-(e) shows misorientation distribution profiles of the starting material, 1-cycle, 2-cycle, 4-cycle and 6-cycle ARB processed specimens obtained by EBSD measurement. The misorientation profile of the starting material indicates that the

microstructure mostly consists of high angle boundaries. Relatively higher fraction of the boundaries with misorientation of 60 degree corresponds to annealing twin boundaries frequently found in Fig. 2.1.

Figure 2.4(f) shows the change in the fraction of high angle boundaries as a function of the number of ARB cycle. The 1-cycle ARB process greatly decreases the average misorientation angle from 45.3° to 13.3°, because a large amount of low angle boundaries were introduced in the materials by the deformation. With increasing the number of ARB cycles, the average misorientation angle increases gradually and it reaches to 28.8° by 6-cycle ARB. According to the previous works [10-13], the main mechanism for grain refinement during severe plastic deformation is *grain subdivision* [10] caused by plastic deformation. The original grains are subdivided into fine crystals (domains) with submicron sizes by deformation-induced boundaries. The misorientation of the deformation-induced boundaries which subdivide the original grains, especially that of so-called geometrically necessary boundaries (GNBs), increases with increasing strain, and most of the deformation-induced boundaries become high angle ones at very high strain. The changes in microstructure and boundary misorientation in the present investigation can be also explained in terms of grain subdivision mechanism. It should be noted that there are significant amount of low angle boundaries even in the 6-cycle ARB processed specimens, which indicates that the elongated UFG structures obtained by the ARB process are essentially deformation microstructures.

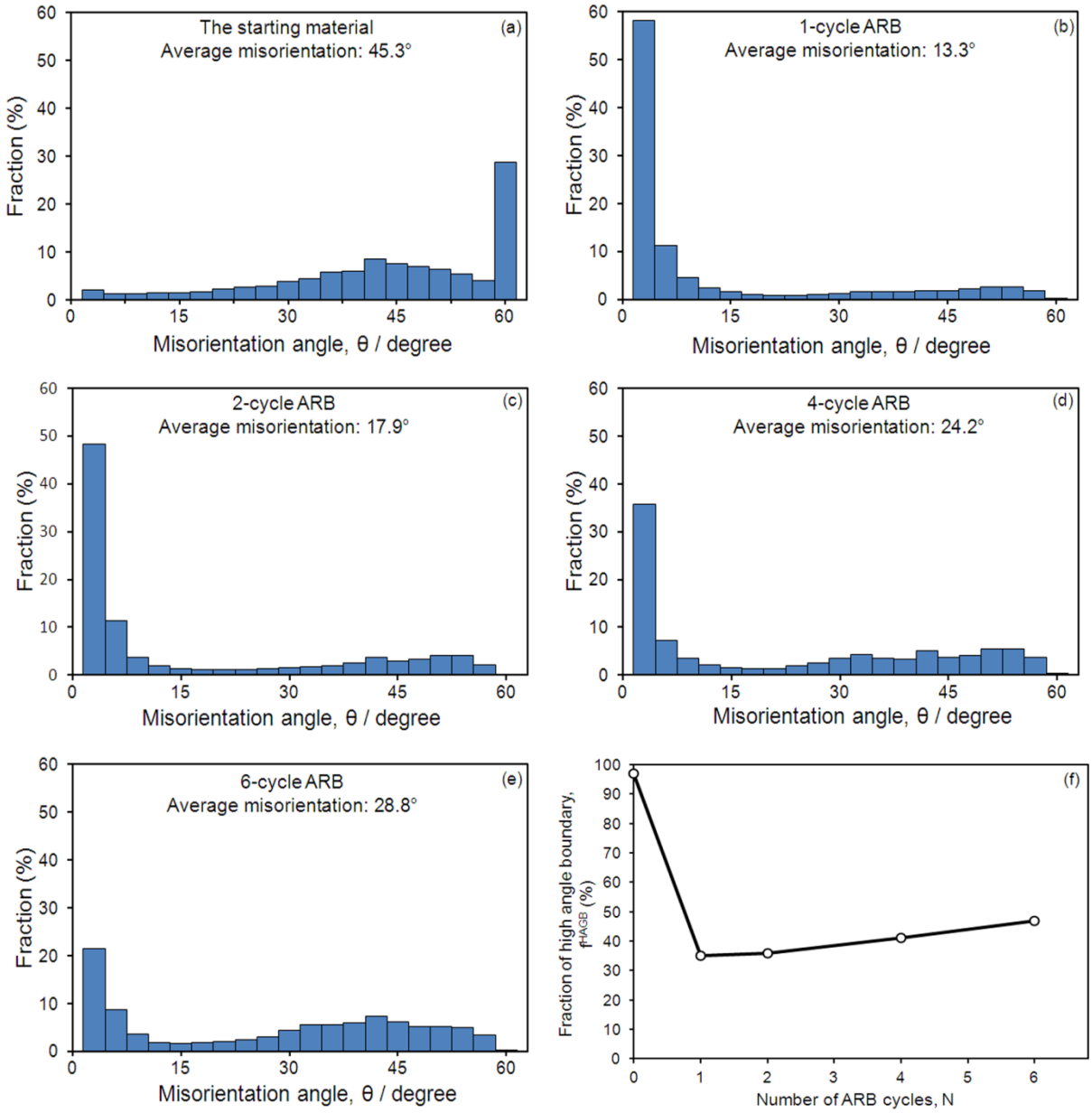

Fig. 2.4. (a)-(e) Boundary misorientation profiles obtained from EBSD analysis of the starting material, 1-cycle, 2-cycle, 4-cycle and 6-cycle ARB processed specimens. (f) Relationship between the number of the ARB cycles and fraction of high angle boundaries in the specimens.

A TEM image and corresponding grain boundary map obtained by Kikuchi-line diffraction pattern analysis of the 6-cycle ARB processed austenite are shown in **Fig. 2.5(a) and (b)**. In the boundary map, boundaries with misorientation larger than 15° and below 15° are indicated by bold and dotted lines, respectively. The TEM image of

Fig. 2.5(a) shows that the austenite grains after 6-cycle ARB exhibit lamellar morphology elongated along RD, and the microstructure contains high density of dislocations. The grain boundary map of Fig. 2.5(b) indicates that a large number of low angle boundaries exist between the high angle boundaries. This result is consistent with the result by EBSD which has been shown in Fig. 2.2(e).

XRD method was used to measure the change in dislocation density in austenite during the ARB process. The XRD patterns of the starting material, 1-cycle, 2-cycle, 4-cycle and 6-cycle ARB processed specimens are shown in **Fig. 2.6(a)**. The XRD pattern consists of three peaks of (111), (200) and (220) austenite planes. The peaks indicated by asterisk (*) are unknown ones which may come from the specimen holder. The XRD patterns confirm no occurrence of phase transformation during the ARB process, as no diffraction peaks of bcc phase (martensite) are found. These XRD results are consistent with the results of EBSD phase maps as shown in Fig. 2.2(a)-(e).

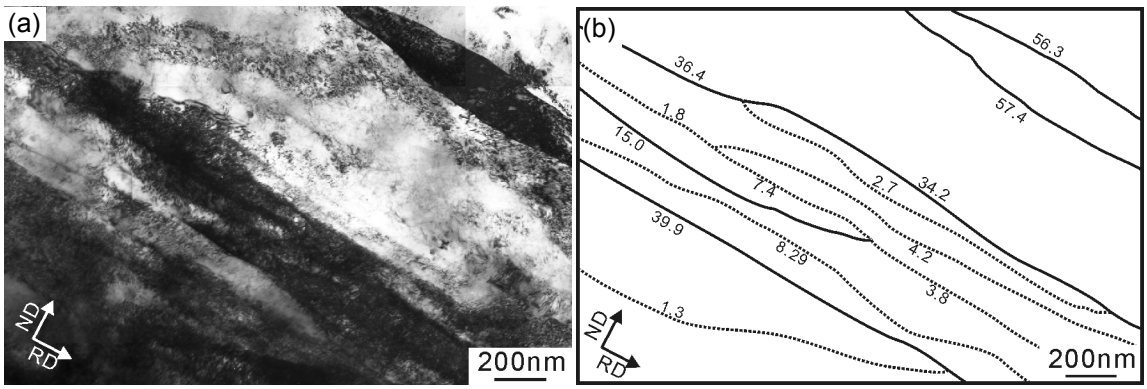

Fig. 2.5. (a) TEM image and (b) corresponding grain boundary map obtained by Kikuchi-line diffraction pattern analysis of the 6-cycle ARB processed specimen.

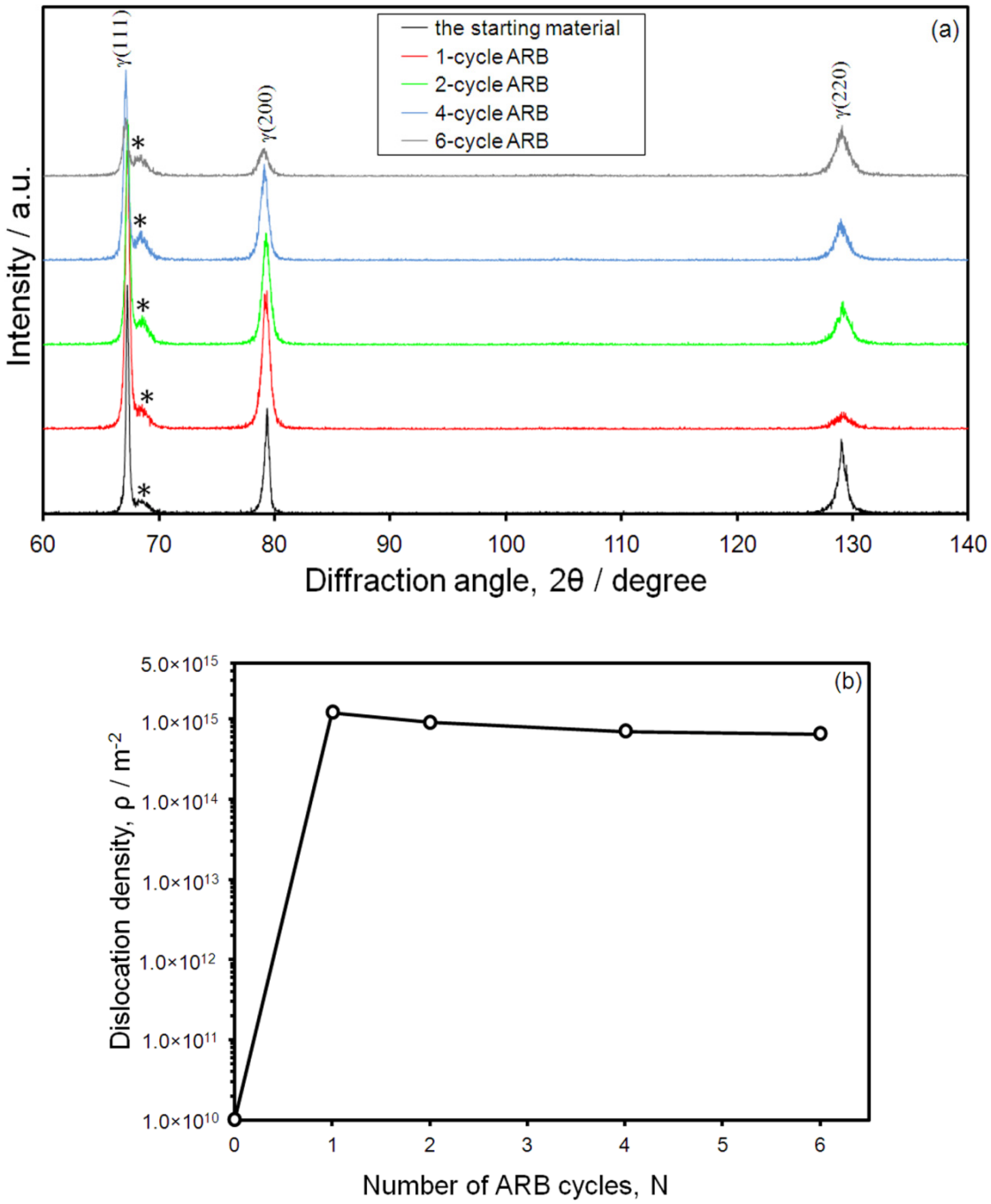

Fig. 2.6. (a) X-ray diffraction patterns and (b) dislocation density obtained from X-ray diffraction results of the 1-cycle, 2-cycle, 4-cycle and 6-cycle ARB processed specimens.

The calculated dislocation densities according to Williamson-Hall method [9] of the 1-cycle, 2-cycle, 4-cycle and 6-cycle ARB processed austenites are shown in **Fig. 2.6(b)**. It should be noted that the Williamson-Hall method was not applicable for the starting

material, because the XRD peak of the starting material was quite sharp. However, it can be easily considered that the starting specimen had very low dislocation density probably in the order of 10^{10} m^{-2}, since it showed a fully recrystallized microstructure (Fig. 2.1 and Fig. 2.2(a)). Figure 2.6(b) indicates that dislocation density of the 1-cycle ARB processed austenite is relatively high (1.2×10^{15} m^{-2}) and dislocation density gradually decreases with increasing the number of ARB cycles, and reaches to 0.65×10^{15} m^{-2} at 6-cycle.

Annealing treatments were applied to the 6-cycle ARB specimens, in order to change the microstructures of austenite for subsequent studies on martensitic transformation. The phase and grain boundary maps, ND orientation color maps and RD orientation color maps of austenite ARB processed by 6-cycle and then annealed at 773, 823 or 873 K for 1.8 ks are shown in **Fig. 2.7**. The grain boundary map of the specimen annealed at 773K (Fig. 2.7(a)) shows that the microstructure still consists of UFG lamellar structure, indicating that annealing at 773 K does not cause recrystallization of austenite. Grain boundary map of Fig. 2.7(b) indicates that recrystallization occurs partly by increasing the annealing temperature to 823 K. The recrystallized regions are free of low angle boundaries. Annealing treatment at 873 K results in fully recrystallized and equiaxed austenite with mean grain size of 2.5 μm, as shown in Fig. 2.7(c). Moreover, phase maps superimposed on grain boundary maps show that no phase transformation occurs during annealing treatments.

The ND and RD orientation color maps of the ARB processed and annealed specimens suggest that annealing treatment at 773 K does not have an influence on texture of austenite, because ND and RD orientation color maps of Fig. 2.7(d),(g) are almost the same as that of Fig. 2.2(j),(o) (the 6-cycle ARB processed specimen).

However, annealing treatment at 873 K significantly changes the texture as shown in Fig. 2.7(f),(i), which is attributed to the occurrence of recrystallization by annealing. Details of textures are shown in the section 2.3.2 of this chapter.

The XRD patterns and corresponding calculated dislocation density of the specimens ARB processed by 6-cycle and annealed at 773, 823 and 873 K are shown in **Fig. 2.8(a) and (b)**. It reveals that by annealing treatment dislocation density decreases monotonously and reaches to the order of 10^{14} m^{-2}, 10^{12} m^{-2}, and 10^{10} m^{-2} for the 6-cycle ARB processed specimens which annealed at 773, 823 and 873 K, respectively.

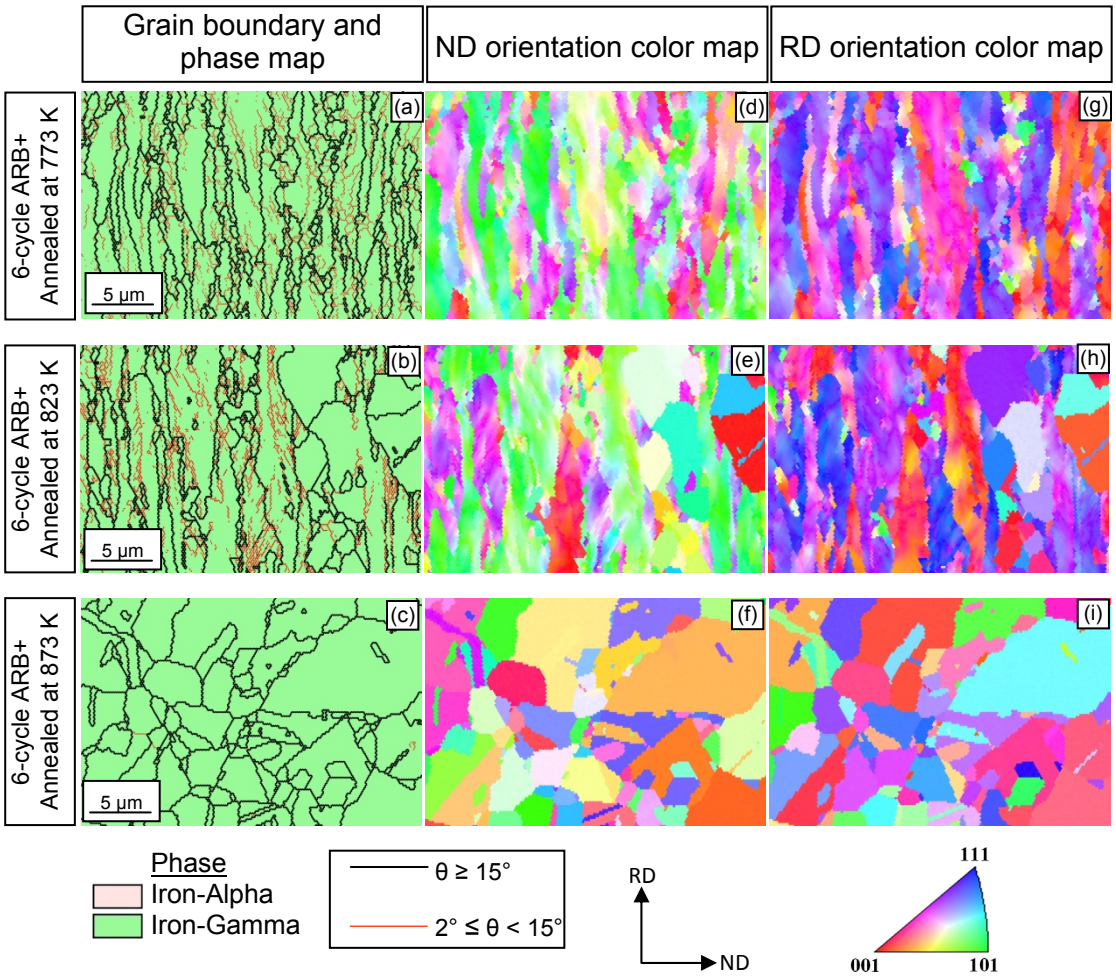

Fig. 2.7. (a)-(c) Grain boundary and phase maps of the specimens ARB processed by 6-cycle and annealed at 773, 823 and 873 K. (d)-(i) ND and RD orientation color maps of the specimens ARB processed by 6-cycle and annealed at 773, 823 and 873 K.

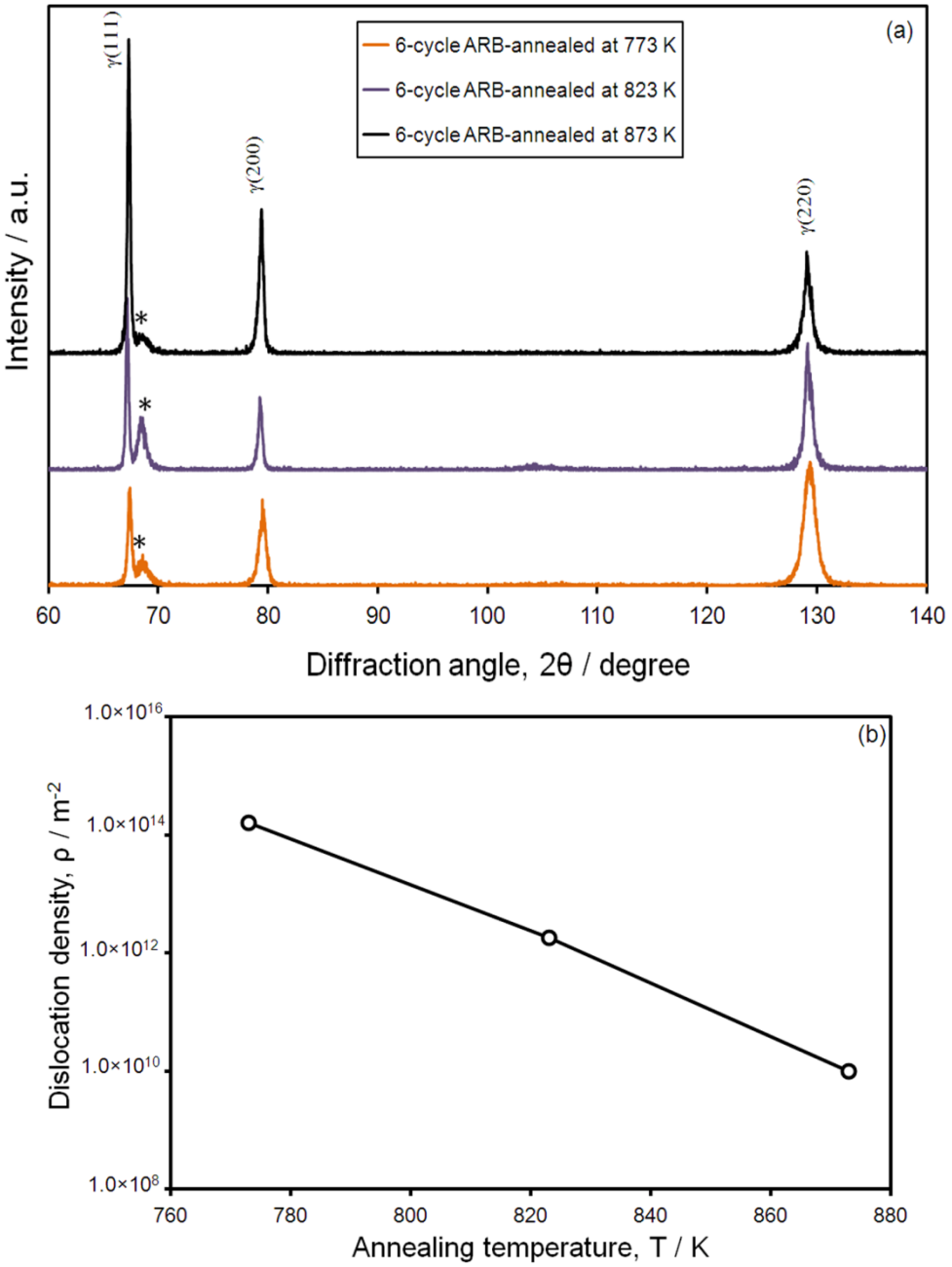

Fig. 2.8. (a) X-ray diffraction patterns and (b) dislocation density obtained from X-ray diffraction results of the 6-cycle ARB processed specimen annealed at 773, 823 and 873 K for 1.8 ks.

2.3.2. Change in texture of austenite during ARB process and subsequent annealing treatment

In this section, the change in texture during the ARB process is studied. For rolled

sheet materials with cubic crystal structures, the orientation and texture are represented by the expression of {hkl}<uvw>, where {hkl} represents the Miller indices of the crystallographic plane parallel to the rolling plane and <uvw> represents the Miller indices of the crystallographic direction parallel to RD. **Figure 2.9(a)-(d)** shows {100} pole figures obtained from EBSD analysis of the starting material, 1-cycle, 2-cycle and 6-cycle ARB processed specimens, respectively. The positions of ideal orientation for typical texture components of fcc crystal, i.e., Brass orientation ({110}<112>), Copper orientation ({112}<111>), S orientation ({123}<634>) and Cube orientation ({100}<001>), are also indicated in the pole figures of Fig. 2.9. As shown in Fig. 2.9(a), the austenite of starting material has nearly a random texture. On the other hand, the (100) pole figure of Fig. 2.9(b) indicates that Copper component ({112}<111>) developed by 1-cycle ARB processing. As shown in Fig. 2.9(c) and (d), the texture changes with increasing the number of ARB cycles, and finally reaches to Brass component ({110}<112>) in the 6-cycle ARB processed specimen.

To have a better and quantitative understanding about the change in texture during the ARB process, orientation distribution functions (ODFs) for the specimens ARB processed by various number of ARB cycles were analyzed using the EBSD data. **Figure 2.10** represents the change in orientation intensity of each texture component with increasing the number of ARB cycles. After the 1-cycle of ARB processing, as shown in Fig. 2.10, Copper orientation ({112}<111>) is the main texture component. After 2-cycle ARB process, however, Copper component ({112}<111>) is weakened, and the texture consisting of strong S component ({123}<634>) and weak Brass component ({110}<112>) are developed. Increasing the number of ARB cycles up to 6-cycle caused strengthening of Brass component ({110}<112>) as the main texture in the austenite.

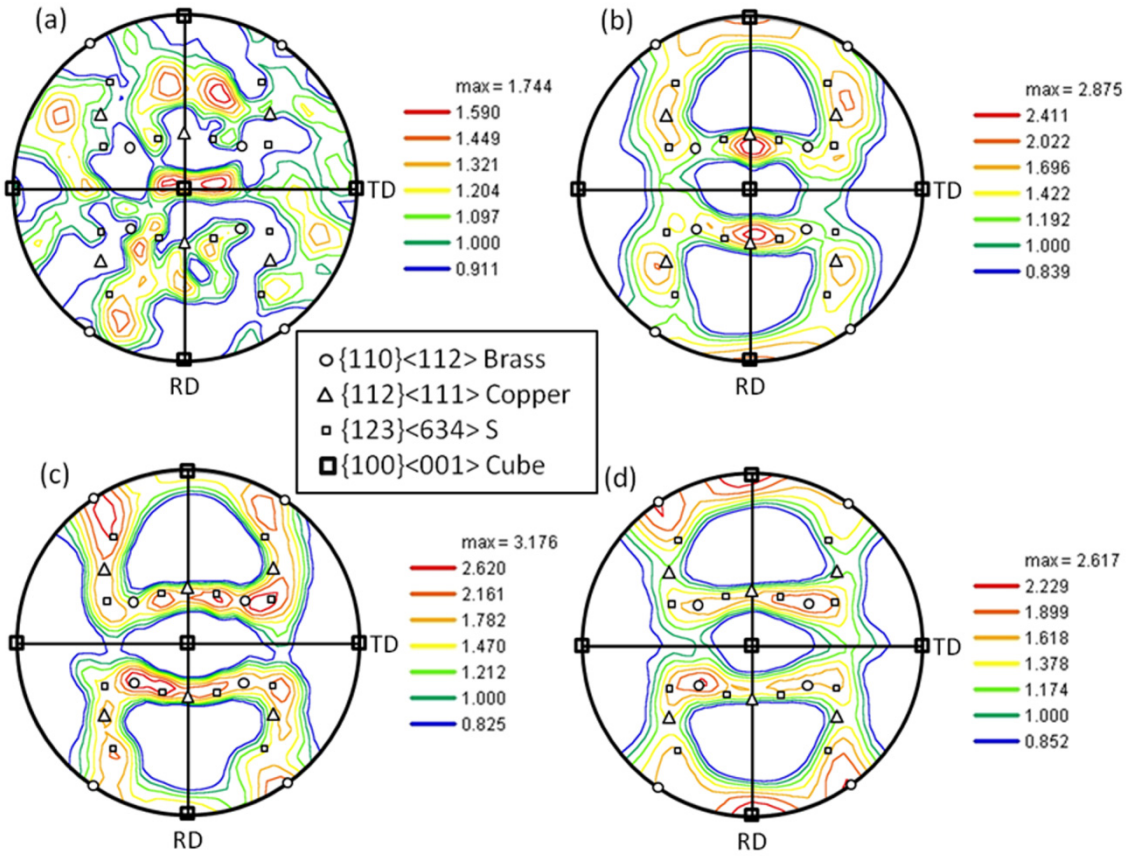

Fig. 2.9. {100} pole figures of austenite in (a) the starting material, (b) 1-cycle, (c) 2-cycle and (d) 6-cycle ARB processed specimens.

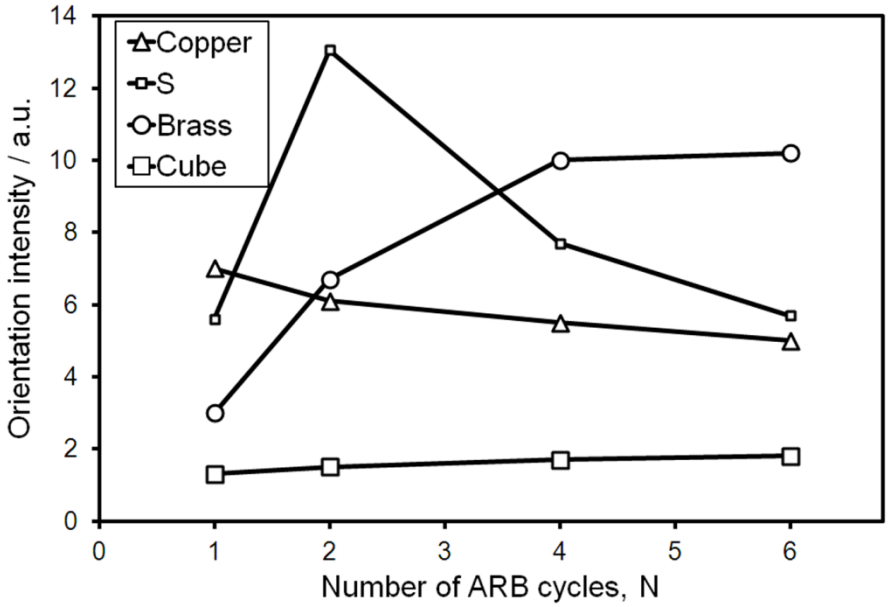

Fig. 2.10. Change in intensity of each texture component as a function of the number of ARB cycles.

The effect of annealing treatment on texture of the 6-cycle ARB processed specimen was also studied. **Figure 2.11(a)-(c)** shows the {100} pole figures of austenite ARB processed by 6-cycle and then annealed at 773 K, 823 K or 873 K for 1.8 ks, respectively. In addition, the change in orientation density of those specimens obtained by ODF analysis is represented in **Fig. 2.12**.

As shown in Fig. 2.11(a) and 2.12, the specimen annealed at 773 K maintains the Brass texture ({110}<112>). This is because annealing at 773 K causes no recrystallization but only recovery happens, as shown in Fig. 2.7(a). By increasing the annealing temperature to 823 K, however, the texture consisting of Cube component ({100}<001>) and Brass component ({110}<112>) develop. After annealing at 873 K, Brass component ({110}<112>) is weakened significantly and strong Cube component ({100}<001>) is observed. As a result, it can be concluded that texture transition was occurred during the ARB process and subsequent annealing in this material. This transition of texture can influence variant selection during martensitic transformation. Previous studies [16-17] demonstrated that texture of austenite was inherited in martensite through transformation. The detailed investigation of transformation texture and martensite variant selection will be described in chapter 5.

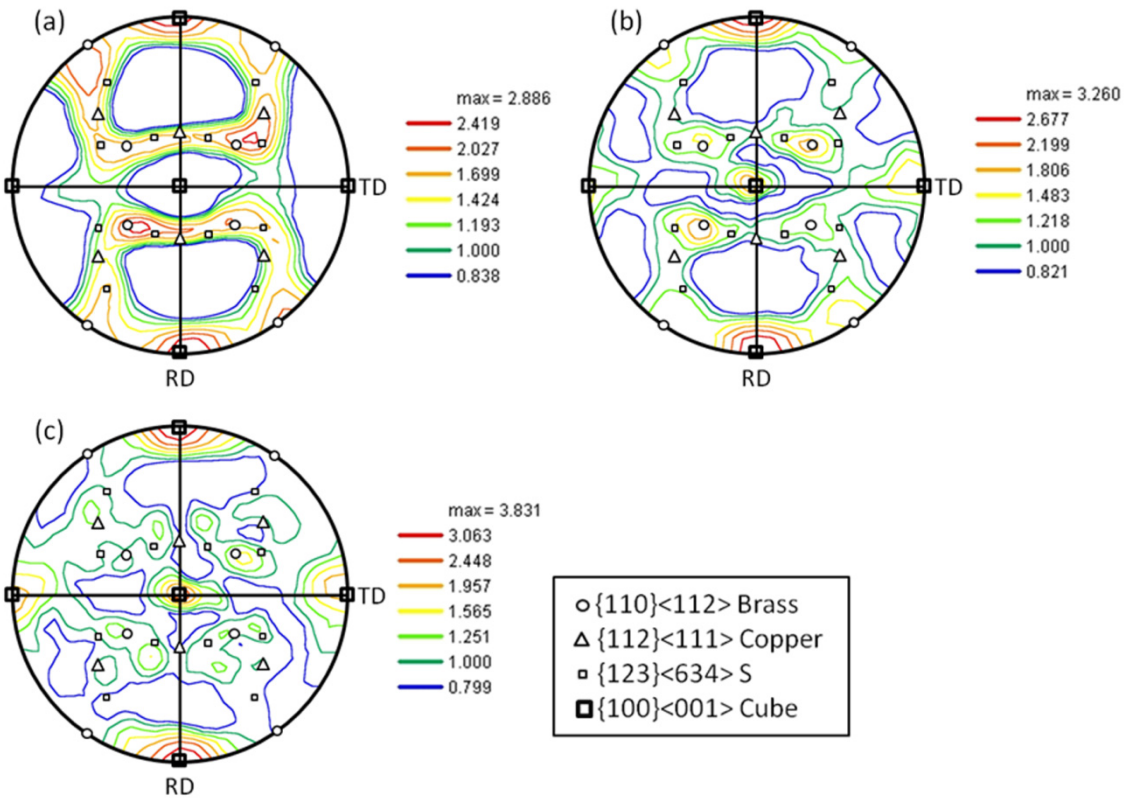

Fig. 2.11. {100} pole figures of austenite ARB processed by 6-cycle and then annealed at (a) 773 K for 1.8 ks, (b) 823 K for 1.8 ks and (c) 873 K for 1.8 ks.

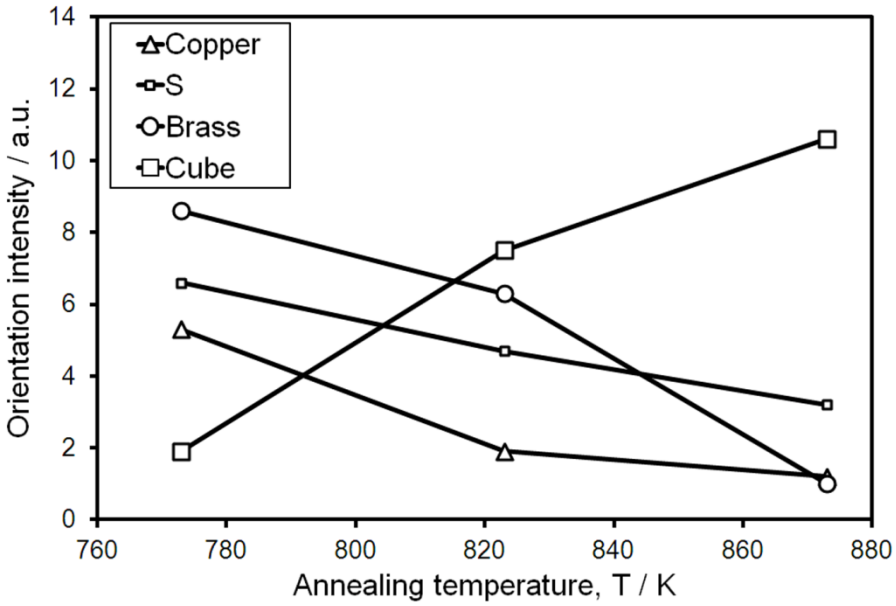

Fig. 2.12. Change in orientation intensity of each texture component of austenite ARB processed by 6-cycle and annealed, as a function of annealing temperature.

2.3.3. Change in mechanical properties during ARB process and subsequent annealing treatment

Nominal stress-strain curves of the ARB processed specimens are shown in **Fig. 2.13**. The starting material has the relatively low yield strength, but a very large uniform elongation over 130% and tensile strength of approximately 1000 MPa are achieved. The stress-strain curve of the starting material exhibits serrated flow and increase in strain-hardening rate at around 30-40% tensile strain, which suggests the occurrence of deformation-induced martensitic transformation during tensile deformation. The large uniform elongation and high tensile strength of the starting material could be attributed to the deformation-induced martensitic transformation (or transformation induced plasticity (TRIP phenomenon) that has been explained in section 1.3.1 of chapter 1) [18-22]. On the other hand, discontinuous yielding accompanied with nearly constant flow stress, which was similar to yield-drop phenomena with Lüders band deformation usually observed in carbon steels, appeared in the stress-strain curves of the ARB processed specimens. The previous master thesis by Maekawa in our group [23] suggested that such peculiar tensile deformation behavior in the ARB processed metastable austenite in Fe-Ni-C alloys could be attributed to the propagation of the region where deformation-induced martensitic transformation occurred across the gage part of the specimen.

The optical microscopy image of the 6-cycle ARB processed specimen after 10% tensile strain is shown in **Fig. 2.14(a)**. It clearly shows the formation of Lüders band at right side of the gage part of the specimen in tensile deformation. **Fig. 2.14(b) and (c)** is the phase map and grain boundary map of the areas inside the Lüders band (b) and outside the Lüders band (c) in the 6-cycle ARB processed specimen. The phase maps

indicate that volume fraction of deformation-induced martensite inside the Lüders band is 35.3% and significantly higher than that outside the Lüders band (3.3%). This clearly demonstrates that the Lüders band propagation corresponds to the propagation of the region where deformation-induced martensitic transformation occurred. In addition, the Lüders strain increases from 8% to 14% with increasing the number of ARB cycles from 1-cycle to 6-cycle ARB process as shown in Fig. 2.13.

The change in mechanical properties, i.e., (a) 0.2% proof strength and tensile strength, (b) uniform elongation and total elongation, obtained from the stress-strain curves are summarized as a function of the number of ARB cycles in **Fig. 2.15(a),(b)**. Figure 2.15(a) shows that the proof strength of austenite increases significantly from 145 MPa to 710 MPa only by 1-cycle ARB process. It furthermore increases with increasing the number of ARB cycles and reaches to 1050 MPa after 6-cycle ARB. The large increase in the proof strength after 1-cycle ARB process results from the drastic

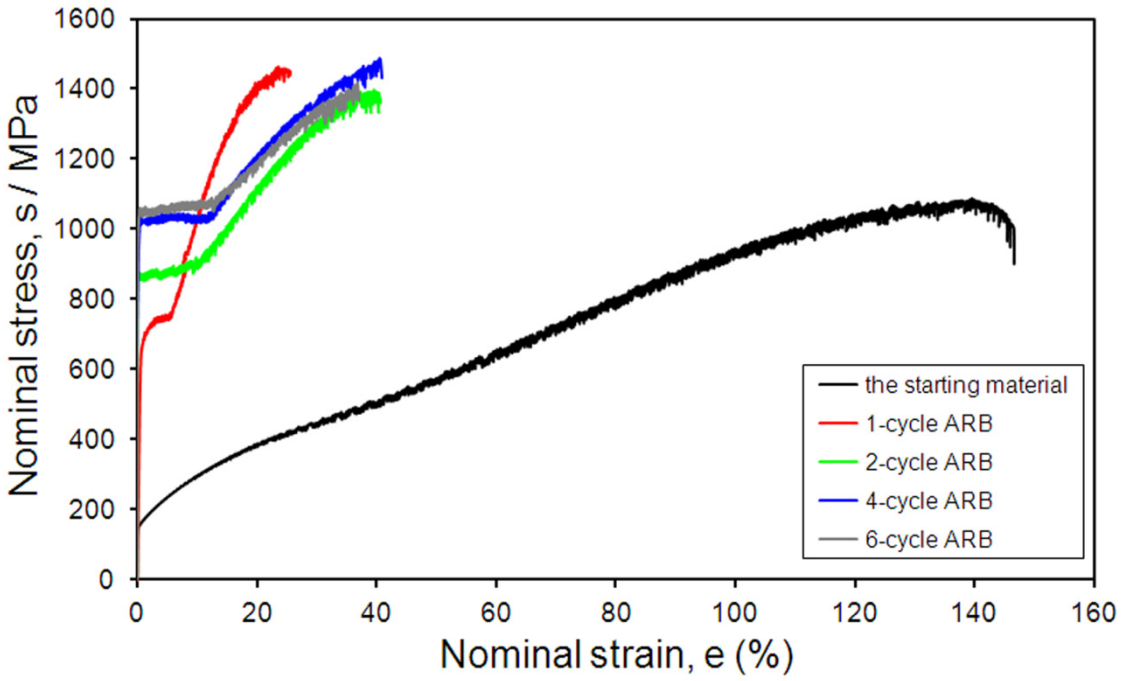

Fig. 2.13. Nominal stress-strain curves of the starting material, 1-cycle, 2-cycle, 4-cycle and 6-cycle ARB processed specimens.

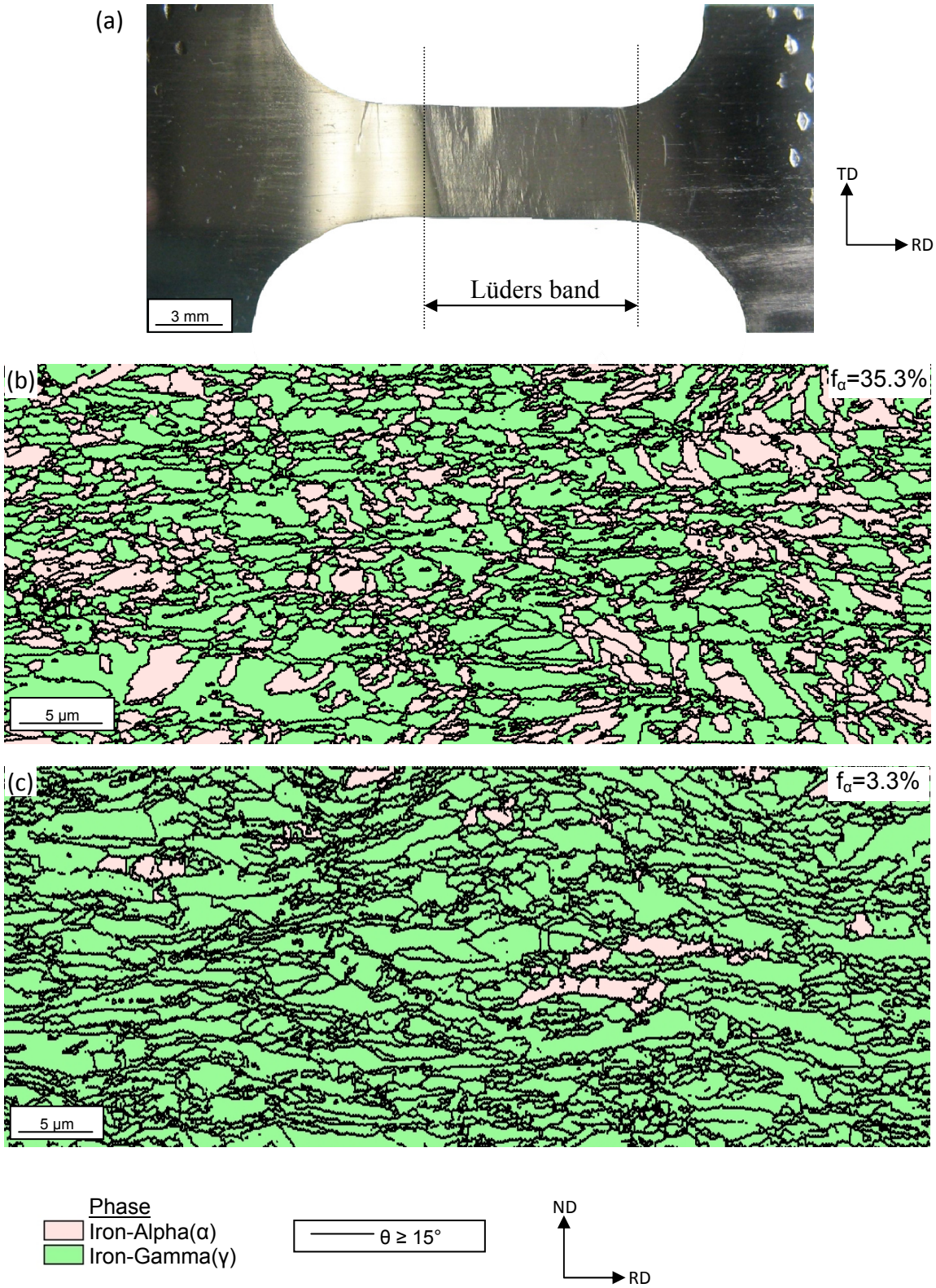

Fig. 2.14. (a) Optical microscope image showing Lüders band appeared in tensile test of the specimen ARB processed by 6-cycle, (b) phase and grain boundary map inside the Lüders band and (c) phase and grain boundary map outside the Lüders band in the 6-cycle ARB processed specimen after 10% tensile deformation.

increase in dislocation density as shown in Fig. 2.6(b). With increasing the number of ARB cycle, dislocation density rather decreases but austenite grains are significantly refined. Decrease of dislocation density lowers the proof strength, while grain refinement of austenite increases the proof strength, resulting in the gradual increase in proof strength eventually. As shown in Fig. 2.15(a), the tensile strength also increases significantly from 1030 MPa to 1475 MPa by 1-cycle ARB process, but it does not change so much with further increase of ARB cycles. **Figure 2.16** shows the change in volume fraction of deformation-induced martensite after fracture in the tensile test as a function of the number of ARB cycles. The volume fraction of deformation-induced martensite was measured by EBSD in the areas of 850 μm × 400 μm for the starting material (0-cycle ARB) and 150 μm × 50 μm for 1-cycle, 2-cycle, 4-cycle and 6-cycle ARB processed specimens. The measured areas are large enough to obtain the volume fraction of deformation-induced martensite statistically. Figure 2.16 indicates that volume fraction of deformation-induced martensite increases by 1-cycle ARB process from 73.4% to 87.6%. Further increase in ARB cycles does not change the volume fraction of deformation-induced martensite significantly. This tendency of the change in volume fraction of deformation-induced martensite with increasing the number of ARB cycles is quite similar to that of the change in tensile strength. This suggests that tensile strength of the ARB processed austenite depends on the volume fraction of deformation-induced martensite.

Figure 2.15(b) indicates that the uniform elongation and total elongation drastically decrease by 1-cycle ARB process from 134% to 28% and from 152% to 30%, respectively. The uniform elongation keeps nearly the same value of about 36% with increasing the number of ARB cycle. In addition, the amount of uniform elongation and total elongation in the ARB processed samples are nearly the same as that shown in Fig.

2.15(b). Such a tendency including large drop of tensile elongation at early stage of ARB process is a typical feature reported in the ARB processed Al and IF steel (ferritic steel) [24]. Compared with the ARB processed Al and IF steel, however, uniform elongation and total elongation of the present austenite are very large. Such a large elongation of the ARB processed austenite presumably originates from deformation-induced martensitic transformation.

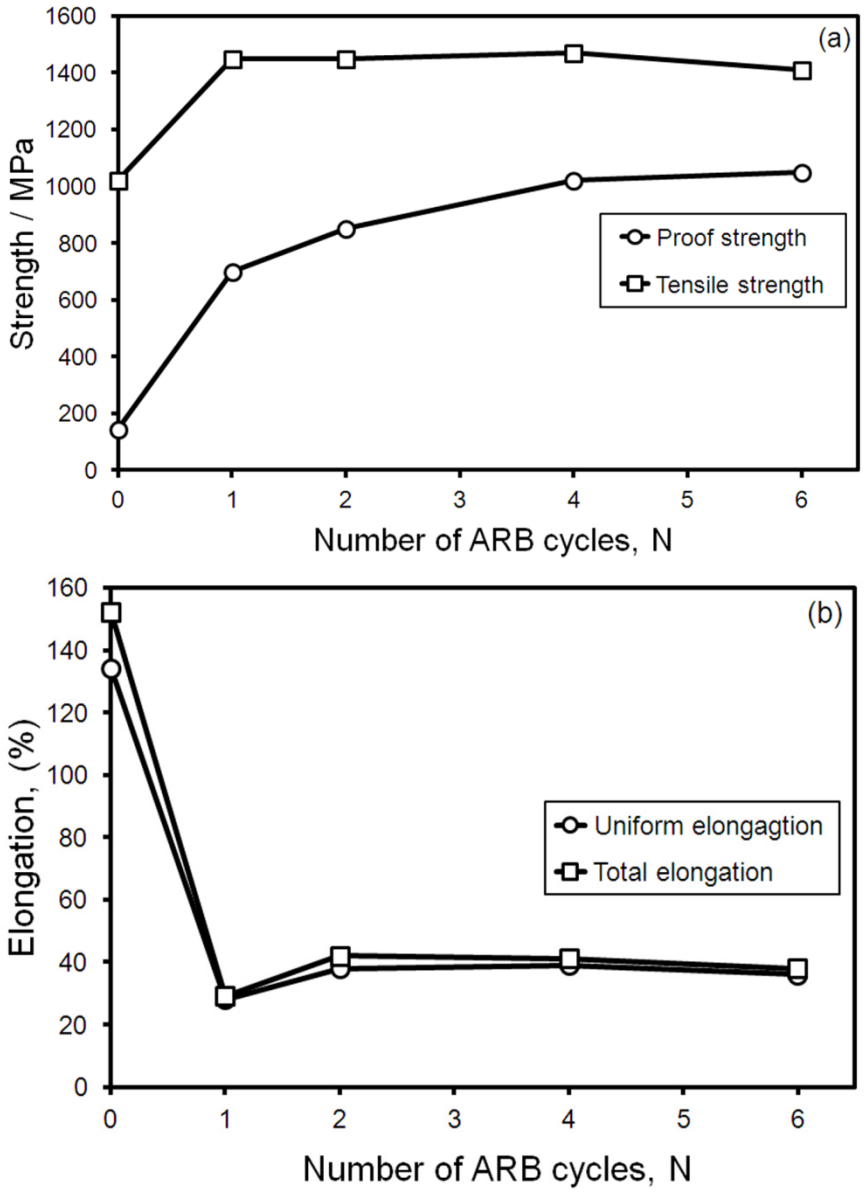

Fig. 2.15. Relationship between the number of the ARB cycles and (a) 0.2% proof and tensile strength, and (b) uniform and total elongation of the ARB processed specimens.

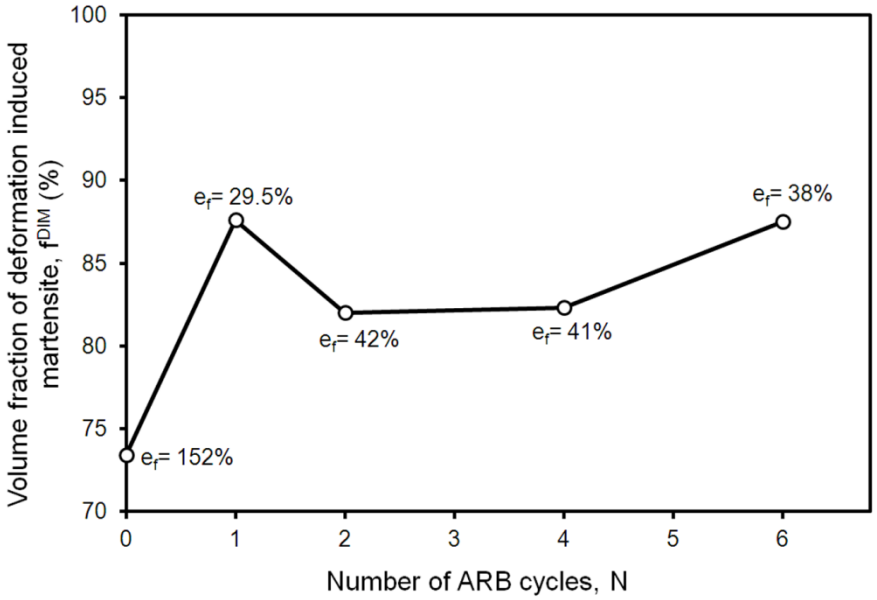

Fig. 2.16. Relationship between the number of the ARB cycles and volume fraction of deformation-induced martensite after fracture in tensile tests. (The e_f indicates the failure or total elongation)

The nominal stress-strain curves of austenite ARB processed by 6-cycle and then annealed at 773, 823 or 873 K for 1.8 ks are shown in **Fig. 2.17**. From Fig. 2.17, it is clear that both proof strength and tensile strength decrease with increase of annealing temperature. It should be noted that the characteristic yielding behavior accompanied with Lüders band-like phenomenon still appears in the stress-strain curve of austenite annealed at 773 K, but it disappears in the specimens annealed at 823 K and 873 K. As was shown in Fig. 2.7(a), the microstructure of austenite annealed at 773 K consists of ultrafine-lamellar grains. On the other hand, recrystallization has started in austenite annealed at 823 K and has completed at 873 K, as shown in Fig. 2.7(b),(c). It is noteworthy that the characteristic yielding behavior disappears even in the partly recrystallized microstructure (823 K annealed specimen). It can be concluded that the characteristic yielding behavior happens only when the austenite has elongated UFG structures, i.e., a kind of deformed structure.

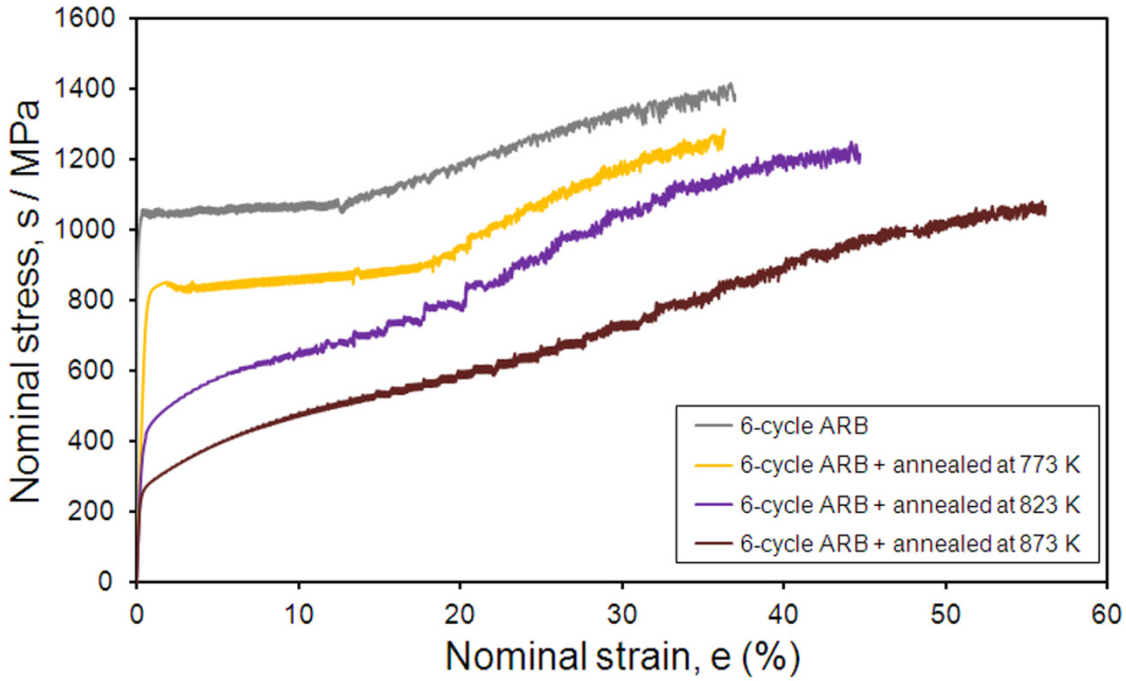

Fig. 2.17. Nominal stress-strain curves of the specimens ARB processed by 6-cycle and then annealed at 773 K, 823 K or 873 K for 1.8 ks.

The 0.2% proof strength, tensile strength, uniform and total elongations, obtained from the stress-strain curves of the specimens ARB processed by 6-cycle and annealed at 773, 823 and 873 K are summarized in **Fig. 2.18(a),(b)**. Figure 2.18(a) shows that the proof strength of austenite decreases significantly from 1050 MPa to 780 MPa after annealing at 773 K. It furthermore decreases with increasing the annealing temperature and reaches to 240 MPa after annealing at 873 K. Decrease in proof strength results from the drastic decrease in dislocation density and recrystallization by annealing treatment. Figure 2.18(a) also indicates that tensile strength also decreases from 1410 MPa to 1030 MPa by increasing the annealing temperature to 873 K. Surprisingly, the tensile strength of the starting material and the specimen ARB processed by 6-cycle and annealed at 873 K are almost the same, despite the fact that both of those specimens are equiaxed and fully recrystallized. The austenite grain sizes of those specimens are 35 μm and 2.5 μm, respectively.

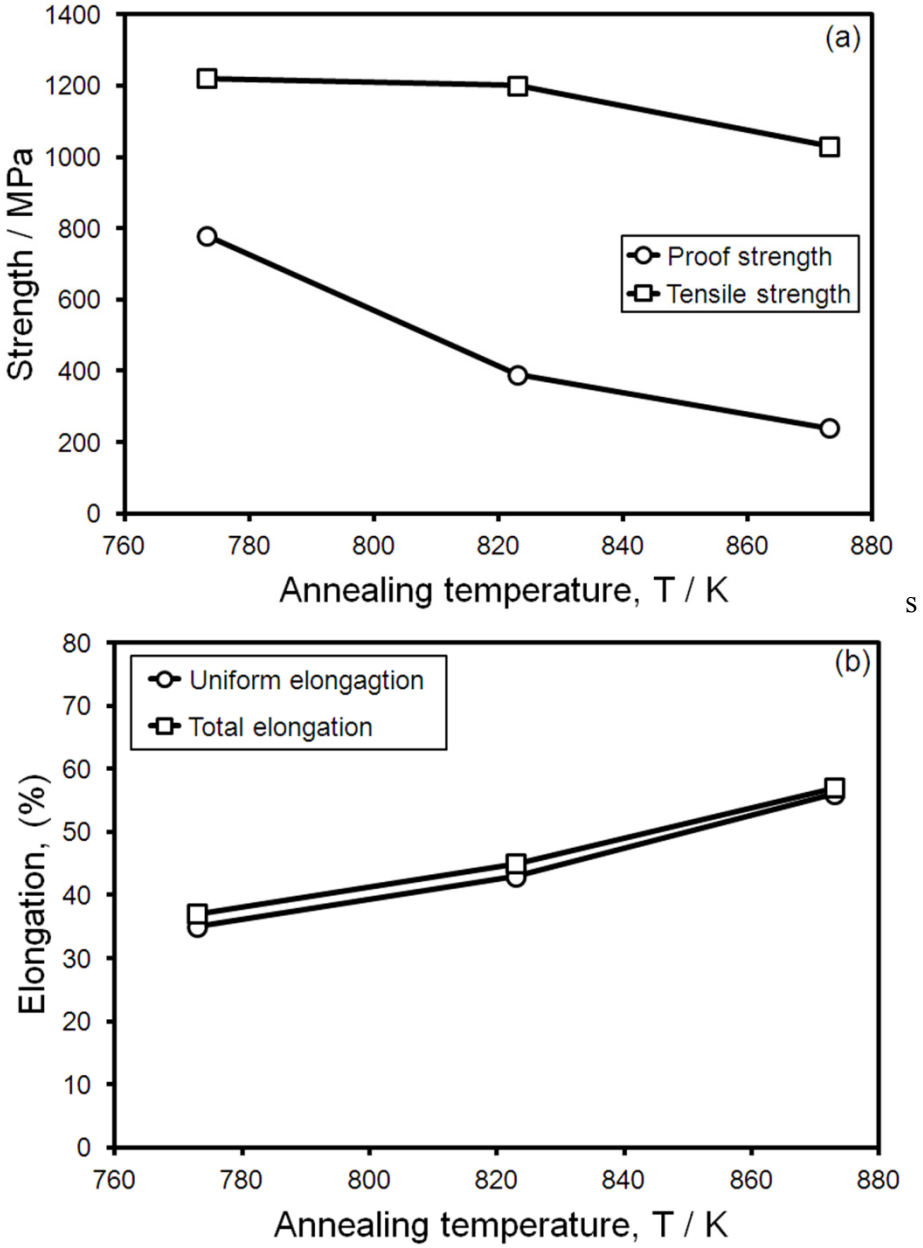

Fig. 2.18. Relationship between annealing temperature for the 6-cycle ARB processed sample and (a) 0.2% proof and tensile strength, or (b) uniform and total elongation.

Figure 2.18(b) indicates that the uniform elongation does not change significantly after annealing at 773 K, however, it slightly increases by annealing treatment at 823 and 873 K. Figure 2.18(b) also shows that the total elongation is almost the same as uniform elongation. By comparing the stress-strain curves of the starting material with that of the specimen ARB processed by 6-cycle and then annealed at 873 K for 1.8 ks,

the total elongation decreases from 152% to 57%. As a result, it can be concluded that grain refinement of fully recrystallized equiaxed austenite causes significant decrease in elongation, while tensile strength does not change greatly.

2.4. Conclusion

In this chapter, microstructure, texture and mechanical properties of the ultrafine-grained (UFG) austenite in Fe-24Ni-0.3C (wt.%) fabricated by accumulative roll bonding (ARB) process were studied. In addition, the effect of annealing treatment on the UFG austenite was investigated. The main results obtained in this chapter are summarized as follows:

(i) The ARB process resulted in grain refinement of austenite. The obtained UFG austenite consisted of the lamellar grains elongated along the rolling direction (RD) with mean grain thickness of 300 nm after 6-cycle of the ARB process. Annealing treatment at 773 K for 1.8 ks did not change the microstructure of the 6-cycle ARB processed austenite so much. By increasing the annealing temperature to 823 K, however, recrystallization occurred partly. An equiaxed and fully recrystallized austenite with mean grain size of 2.5 μm was obtained by annealing of the 6-cycle ARB processed austenite at 873 K for 1.8 ks.

(ii) Dislocation density measurement showed that 1-cycle of ARB caused a significant increase in dislocation density in austenite up to 1.2×10^{15} m^{-2}, while further ARB processing resulted in a gradual decrease in dislocation density and it reached to 0.65×10^{15} m^{-2} at 6-cycle.

(iii) Texture components of austenite changed during the ARB process. After 1-cycle ARB process, Copper orientation was the main texture component. After 2-cycle

ARB process, Copper component was weakened and a texture consisting of strong S component and weak Brass component developed. Increasing ARB cycle up to 6-cycle resulted in the development of strong Brass component. By annealing at 773 K for 1.8 ks, texture did not change. However, increase of annealing temperature to 823 ~ 873 K weakened the Brass component but strengthened the Cube component considerably.

(iv) Characteristic yielding behaviors with Lüders-like deformation appeared in the stress-strain curves of the ARB processed austenite. The Lüders band propagation corresponded to deformation-induced martensitic transformation. The proof strength and tensile strength of austenite increased significantly only after 1-cycle ARB process. With increasing the number of ARB cycles, proof strength increased gradually while tensile strength did not change. The tensile strength of the ARB processed specimen depended on the volume fraction of deformation-induced martensitic transformation. The uniform elongation drastically decreased after 1-cycle ARB process, but the ARB processed austenite in the present alloy maintained relatively large tensile deformation compared with other materials ARB processed. Annealing treatment at 773-873 K for 1.8 ks of the 6-cycle ARB processed austenite resulted in significant decrease in proof strength and tensile strength, while uniform elongation did not change.

References

[1] R.Z. Valiev, M.J. Zehetbauer, Y. Estrin, H.W. Höppel, Y. Ivanisenko, H. Hahn, G. Wilde, H.J. Roven, X. Sauvage, T.G. Langdon, Adv. Eng. Mater. 9 (2007), p. 527-533.

[2] N. Tsuji, J. of Nanosci. and Nanotech. 7 (2007), pp. 3765-3770.

[3] Y. Saito, N. Tsuji, H. Utsunomiya, T. Sakai, Acta Mater. 47 (1999), pp. 579-583.

[4] R.Z. Valiev, N.A. Krasilnikov, N.K. Tsenev, Mater. Sci. and Eng. A 137 (1991), pp. 35-40.

[5] Z. Horita, D.J. Smith, M. Furukawa, N. Nemoto, R.Z. Valiev, T.G. Langdon, Mater. Res. 11 (1996), pp. 1880-1890.

[6] M. Richert, Q. Liu, N. Hansen, Mater. Sci. Eng. A 260 (1999), pp. 275-283.

[7] K.T. Park, H.J. Kwon, W.J. Kim and Y.S. Kim, Mater. Sci. and Eng. A 316 (2001), pp. 145-152.

[8] M. Slamova, P. Homola, M. Karlik, Mater. Sci. and Eng. A Vol. 462 (2007), p. 106-110.

[9] G.K. Willamson, W.H. Hall, Acta Metall. 1 (1953), pp. 22-31.

[10] N. Hansen, D. Juul Jensen, Mater. Sci. Forum 156-157 (1994), pp. 1211.

[11] N. Tsuji, Y. Saito, H. Utsunomiya, S. Tanigawa, Scripta Mater. 40 (1999), pp. 795-800.

[12] N. Hansen, Metall. Mater. Trans. A, 32A (2001), pp. 2917-2935.

[13] N. Hansen, D. Juul Jensen, Phil. Trans. R. Soc. Lond. A, 357 (1999), pp. 1447-1469.

[14] M. Raei, M.R. Toroghinejad, R. Jamaati, J.A. Szpunar, Mater. Sci. and Eng. A 527 (2010), pp. 7068-7073.

[15] H.W. Kim, S.B. Kang, N. Tsuji, Y. Minamino, Metall. Mater. Trans. A 36 (2005), pp. 3151-3163.

[16] R. K. Ray, J. J. Jonas, International Materials Reviews, 35 (1990), pp.1-36.

[17] R.K. Ray, M.P. Butron-Guillen, J.J. Jonas, Textures and Microstructures 14-18 (1991), pp. 471-483.

[18] M. Dejong, G.W. Rathenau, Acta Metall. 7 (1959), pp. 246-253.

[19] F. Lecroisey, A. Pineau, Metall. Trans. 3 (1972), pp. 387-396.

[20] P.C. Maxwell, A. Goldberg, J.C. Shyne, Metall. Trans. 5 (1974), pp. 1305-1318.

[21] G.B. Olson, M. Azrin, Metall. Trans. A 9 (1978), pp. 713-721

[22] B. Eghbali, A. Abdollah-zadeh, Scripta Mater. 54 (2006), pp. 1205-1209.

[23] T. Maekawa, Master thesis, Osaka University, (2008).

[24] N. Tsuji, Y. Ito, Y. Saito, Y. Minamino, Scripta Mater. 47 (2002), p. 893-899.

Chapter 3. Characteristics of martensite transformed from ultrafine-grained (UFG) austenite fabricated by accumulative roll bonding (ARB) process and subsequent annealing

3.1. Introduction

As the author demonstrated in chapter 2, severe plastic deformation (ARB process) of metastable austenitic steel can fabricate ultrafine-grained (UFG) structure which exhibits excellent mechanical properties. Besides severe plastic deformation, martensitic transformation can also induce fine microstructure and high strength even though the grain size of mother austenite phase is coarse. Accordingly, the combination of UFG austenite structure and martensitic transformation is expected to achieve finer microstructure and more superior mechanical properties. Tadaki et al. [1] studied martensitic transformation of nanometer scale particles (powders) in Fe-Ni alloys. They found that austenite was stabilized significantly in the nano-powders. Han and Xu [2] reported that martensite plate transformed from UFG austenite fabricated by severe plastic deformation exhibited fragmented shape, which was somewhat different from that transformed from coarse-grained austenite. So far, however, there have been no deep understanding and systematic study about martensitic transformation from UFG mother phases.

The aim of this chapter is to clarify the characteristics of martensite transformed from UFG austenite and to compare them with those transformed from conventionally coarse-grained austenite. In addition, effect of austenite microstructure on the martensite transformation starting temperature (M_s) is investigated.

3.2. Experimental procedure

Fe–24Ni-0.3C (wt.%) metastable austenitic alloy sheets with mean grain size of 35 μm were used as a starting material in this study. **Table 1.2** (in chapter 1) represents chemical composition of the alloy. The starting material was annealed at 1273-1473 K for 1.8 ks to obtain austenite structures with much coarser grains. To fabricate UFG austenite structures, the sheets were provided to accumulative roll bonding (ARB) process. The details of the ARB process was explained in chapters 1 and 2. The specimens ARB processed by 6-cycle were annealed at 773-873 K for 1.8 ks to obtain recovered or recrystallized austenite with UFG or fine-grained structures.

The sheets subjected to the above mentioned treatment were cooled down to 77 K (in liq. N_2) to obtain thermally induced martensite. The M_s was measured by a differential scanning calorimetry (DSC) machine at cooling rate of 4 K/min. The microstructures of martensite were characterized by scanning electron microscopy (SEM) using a field-emission type SEM (Philips XL30S-FEG) equipped with electron backscatter diffraction (EBSD) system operated at 15 kV. The sections parallel to the transverse direction (TD) of the specimens for EBSD observation were polished mechanically and then electrolytically in a 900 ml CH_3COOH + 100 ml $HClO_4$ solution at approximately 284 K with a voltage of 20 V. The obtained EBSD data were analyzed by TSL-OIM Analysis software.

3.3. Results and discussion

3.3.1. Microstructure of martensite transformed from austenite ARB processed and subsequently annealed

Change in microstructure of martensite transformed from austenite of the starting

material, 1-cycle, 2-cycle, 4-cycle and 6-cycle ARB processed specimens are shown in **Fig. 3.1**. Figure 3.1(a)-(e) shows grain boundary maps together with phase maps. In the grain boundary maps, high angle boundaries with misorientation more than 15° are drawn in black lines and low angle boundaries with misorientation between 2° and 15° are drawn in red lines. In addition, martensite and austenite phases are shown in pink and green colors, respectively. The martensite plates transformed from the starting material exhibit a zigzag array. Almost all of the martensite plates are surrounded by high angle boundaries and do not contain low angle boundaries inside. On the other hand, the martensite plates transformed from ARB processed austenite contain low angle boundaries as shown in Fig. 3.1(b)-(e). These low angle boundaries inside the martensite plates were originated from the ARB processed austenite because the ARB process introduces large amount of dislocations and low angle boundaries in austenite as demonstrated in chapter 2.

The normal direction (ND) and rolling direction (RD) orientation color maps of martensite crystals are shown in Fig. 3.1(f)-(o). The martensite transformed from the starting material having coarse-grained austenite does not have any tendency in color, indicating that martensite plates have random orientation distribution. The ND and RD orientation color maps of Fig. 3.1(f)-(o), however, indicate that martensitic transformation from ARB processed austenite develops preferred orientation (transformation texture). This is probably because texture developed in austenite during the ARB process was inherited by martensite. The details of transformation texture and variant selection in martensitic transformation will be investigated in chapter 5.

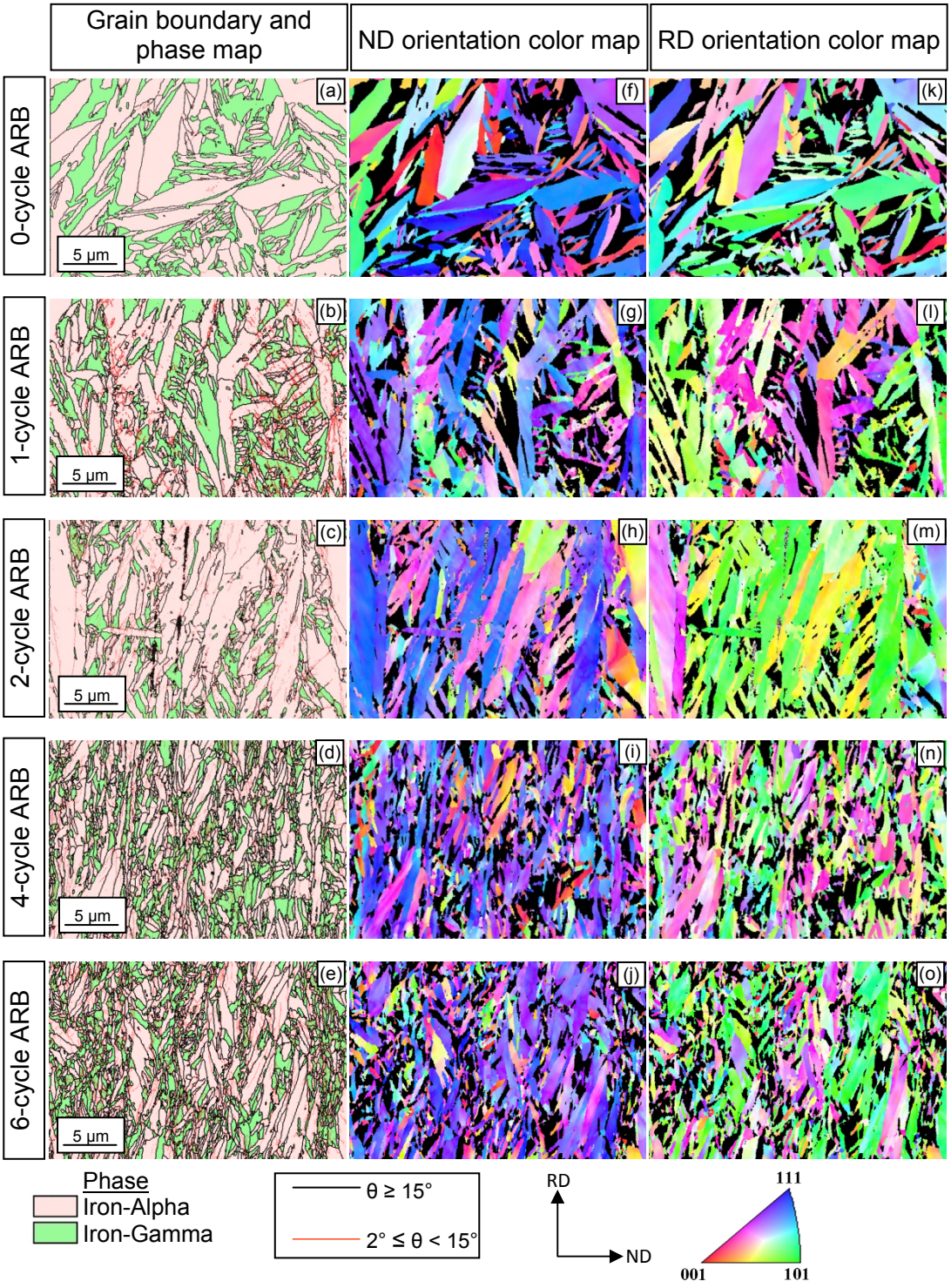

Fig. 3.1. (a)-(e) Grain boundary and phase maps of the starting material, 1-cycle, 2-cycle, 4-cycle and 6-cycle ARB processed specimens after martensitic transformation. (f)-(j) ND orientation color maps of martensite transformed from the starting material, 1-cycle, 2-cycle, 4-cycle and 6-cycle ARB processed specimens. (k)-(o) RD orientation color maps of martensite transformed from the starting material, 1-cycle, 2-cycle, 4-cycle and 6-cycle ARB processed specimens.

An optical microscope image of the starting material after martensitic transformation is shown in **Fig. 3.2(a)**. The martensite structure exhibits plate type morphology with smoothly curved interphase boundary. Midrib is recognized as traced by white dotted lines. An EBSD orientation color map of martensite transformed from austenite of the starting material is also shown in **Fig. 3.2(b)**. The trace of martensite in the middle part (midrib) corresponds to $(3\ 15\ 10)_A$ plane. It is well known that the lenticular martensite has the smoothly curved interphase boundary and its habit plane (midrib plane) is close to $(3\ 15\ 10)_A$ plane [3-6]. On this basis, it can be concluded that the martensite transformed from coarse-grained austenite (the starting material) is classified as lenticular type martensite.

A SEM image and EBSD orientation color map of martensite plate transformed from the 6-cycle ARB processed austenite are shown in **Fig. 3.3**. In Fig. 3.3(a), the martensite exhibits plate type morphology with smoothly curved interphase boundary and contains midrib inside the martensite plate. The EBSD orientation color map indicates that habit plane of martensite is also close to $(3\ 15\ 10)_A$ plane. From these observations, it can be said that the morphology of martensite transformed from UFG austenite (the 6-cycle ARB processed specimen) is almost the same as martensite transformed from coarse-grained austenite. However, some martensite plates transformed from UFG austenite are broken and fragmented. Han and Xu [2] also observed that the martensite plates transformed from UFG austenite fabricated by severe plastic deformation in Fe–32%Ni alloy were broken and fragmented.

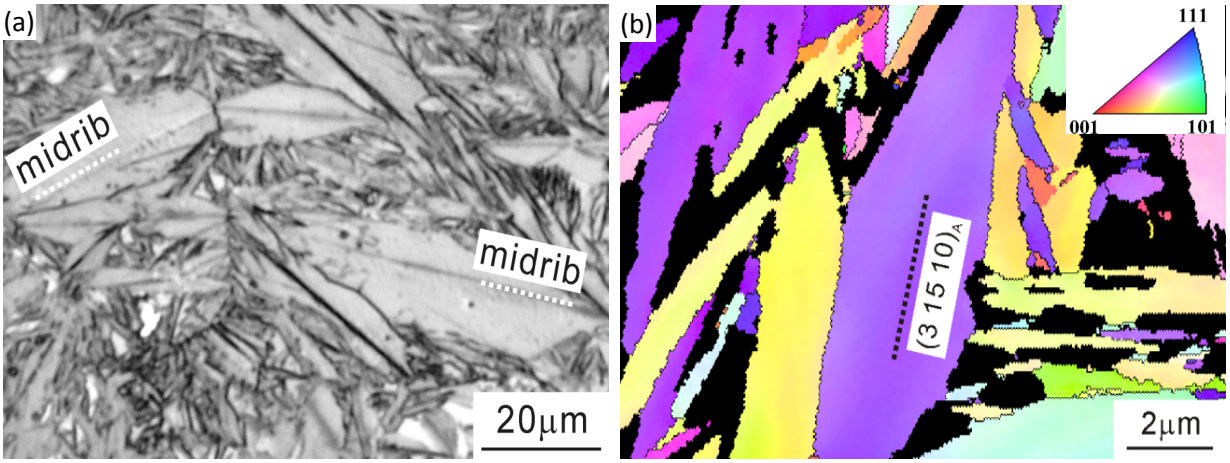

Fig. 3.2. (a) An optical microscope image, and (b) EBSD orientation map of martensite transformed from the starting material with coarse-grained austenite.

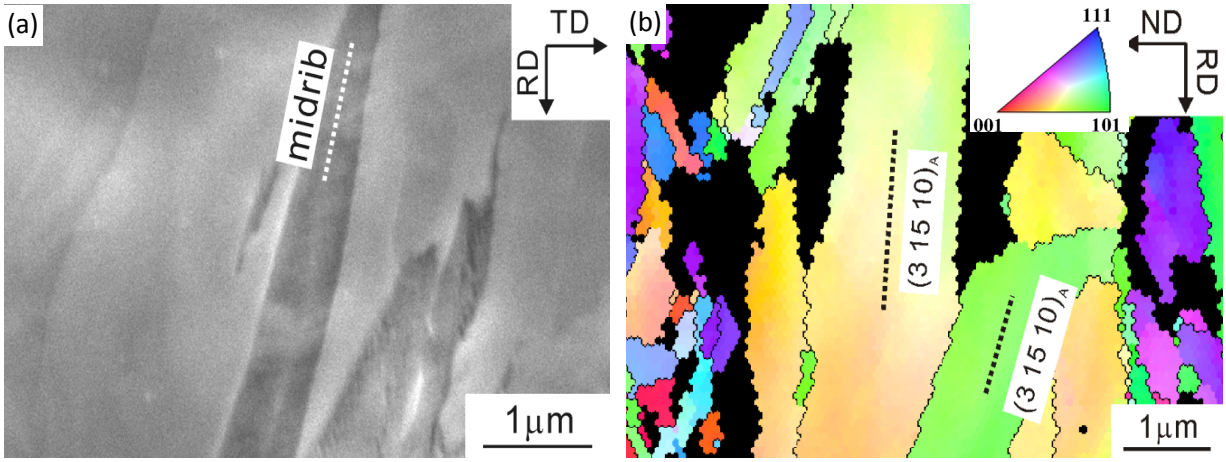

Fig. 3.3. (a) A SEM image, and (b) EBSD orientation map of martensite transformed from the 6-cycle ARB processed specimen with elongated ultrafine-grained austenite.

The grain boundary and phase maps, ND orientation maps and RD orientation maps of martensite transformed from austenite ARB processed by 6-cycle and subsequently annealed at 773, 823 or 873 K for 1.8 ks are shown in **Fig. 3.4**. The grain boundary and phase maps of Fig. 3.4(a) show that martensite plate still contains low angle boundaries. The presence of low angle boundaries inside the martensite plate is consistent with the result that annealing at 773 K for 1.8 ks does not cause recrystallization of austenite as described in chapter 2. In contrast, martensite plates transformed from the austenite

ARB processed by 6-cycle and subsequently annealed at 823 K indicate two kinds of morphologies, i.e., some of them consist of low angle boundaries that transformed from elongated UFG austenite, and some of them are free of low angle boundaries that transformed from recrystallized grains of austenite. These results are consistent with the fact that annealing at 823 K for 1.8 ks caused partial recrystallization as explained in chapter 2. On the other hand, martensite plates transformed from austenite annealed at 873 K are free of low angle boundaries as shown in Fig. 3.4(c). This corresponds to the fact that the austenite phase annealed at 873 K after 6-cycle ARB process is fully recrystallized and free of low angle boundaries as shown in Fig. 2.7(c) of chapter 2.

Relationship between the austenite grain size (d^{HAGB}) and martensite plate size is summarized in **Fig. 3.5**. Both austenite grain size (The average interval of high angle boundaries along ND) and martensite plate size (The average interval along ND of high angle boundaries surrounding each martensite plate) were measured by line interception method. The graph shows that martensite plate size is significantly small compared to the austenite grain size when the austenite is coarse (more than 10 μm), indicating that martensitic transformation leads to grain refinement. This is because each martensite plate can not grow across austenite grain boundary. However, when the austenite grain size becomes smaller than 2~3 μm, the martensite plate size becomes almost the same as the austenite grain size. This means that martensitic transformation does not make grain refinement efficiently when the austenite grain size is very fine or ultrafine.

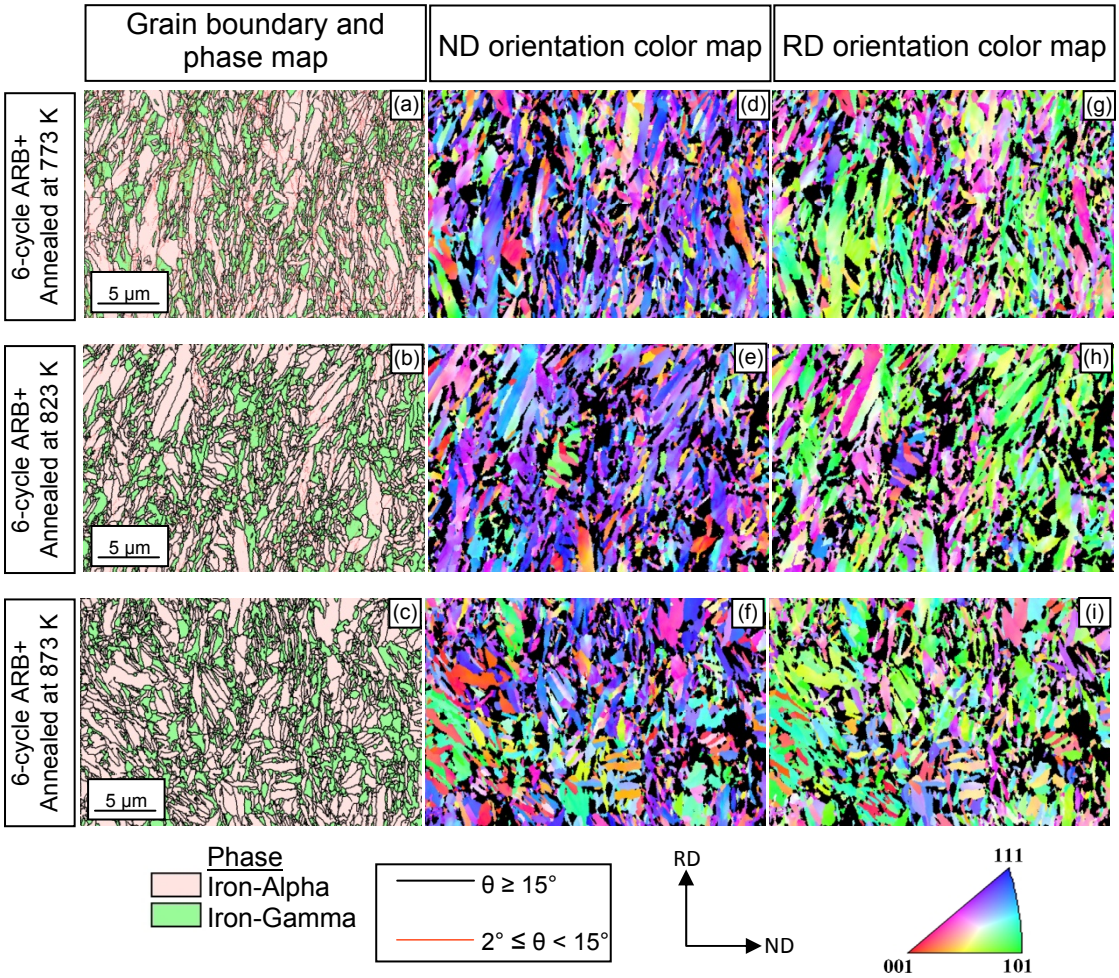

Fig. 3.4. (a)-(c) Grain boundary and phase maps after martensitic transformation of the specimens 6-cycle ARB processed and annealed at 773, 823 and 873 K, respectively. (d)-(i) ND and RD orientation color maps of martensite transformed from the 6-cycle ARB processed specimens annealed at 773, 823 and 873 K, respectively.

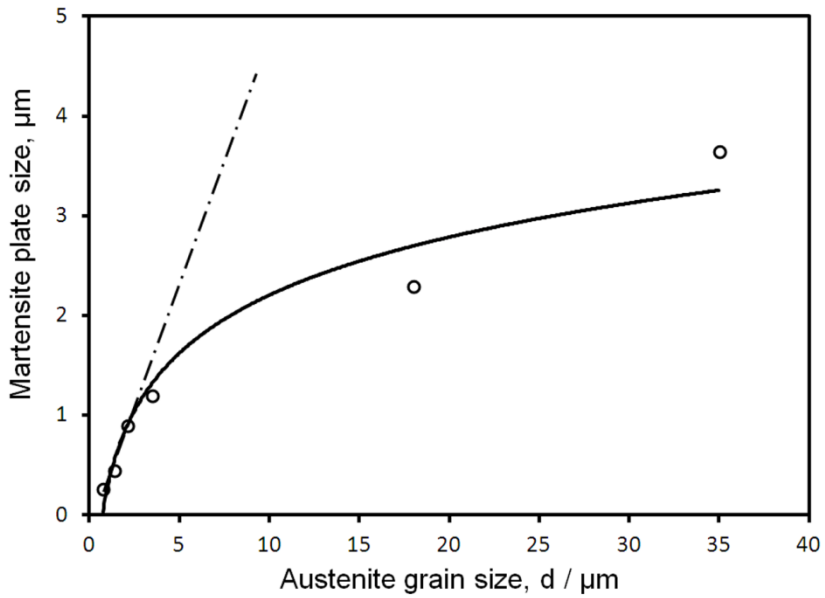

Fig. 3.5. Relationship between the martensite plate size and the austenite grain size.

3.3.2. Effect of ARB process and subsequent annealing on martensite starting (M_s) temperature

M_s temperature is one of an important characteristic in martensitic transformation, because M_s temperature has a great influence on morphology and substructure of martensite. It is well known that M_s temperature strongly depends on microstructure of austenite as well as its chemical composition [7-18]. The DSC curves of the ARB processed specimens are shown in **Fig. 3.6(a)**. The DSC curve of the starting material with mean grain size of 35 μm exhibits a sudden increase of heat flow corresponding to the occurrence of burst transformation. The burst transformation accommodates with a significant increase in temperature as shown in the DSC curve of the starting material in Fig. 3.6(a). In contrast, there is no sudden change in the DSC curves of the ARB processed specimens, indicating that the burst transformation does not appear in the ARB processed specimens.

Change in M_s temperature as a function of the number of ARB cycles is shown in **Fig. 3.6(b)**. After 1-cycle ARB process, the M_s temperature significantly increases and then decreases with increasing the number of ARB cycles. Previous studies [8-9,17] reported that M_s temperature decreases significantly and monotonously with decreasing the austenite grain size, because austenite grain boundary suppress the growth of martenite plate. However, it should be noted that the starting material and the 6-cycle ARB processed specimen have almost the same M_s temperature, despite the fact that 6-cycle ARB process decreases the austenite grain size from 35 μm to 750 nm as depicted in **Fig. 2.3** (chapter 2). Here, the present UFG austenite structures were fabricated by severe plastic deformation process and they contain high density of dislocations and low angle boundaries as shown in chapter 2. The change in dislocation density with

increasing the number of ARB cycles has been shown in **Fig. 2.6(b)** of chapter 2. It reveals that dislocation density reaches to the maximum value just after 1-cycle ARB process, and then decreases gradually with increasing the number of ARB cycles. This corresponds to the fact that deformation-induced boundaries with small misorientation formed by the arrangement of dislocations changed to high angle boundaries by the accumulation of plastic deformation. Olson and Cohen [18-21] proposed that nucleation in martensitic transformation is associated with the dissociation of existing dislocations in austenite. Their model implies that dislocations or low angle boundaries in austenite raise M_s temperature, because they act as nucleation sites for martensitic transformation. Supposing that dislocations act as nucleation sites for martensite transformation and high angle boundaries are obstacles for martensitic transformation, the present change in M_s temperature with increasing the number of ARB cycles can be well explained. The 1-cycle ARB process introduces high density of dislocations, i.e., nucleation sites of martensite, resulting in the increase of M_s temperature. The slight decrease in dislocation density and formation of large density of high angle boundaries by further ARB process cause the decrease of M_s temperature. Because the 6-cycle ARB processed specimen still contains high density of dislocations, M_s of the 6-cycle ARB processed specimen is almost the same as that of the starting material in spite of the fact that 6-cycle ARB process causes significant decrease of the austenite grain size from 35 μm to 750 nm.

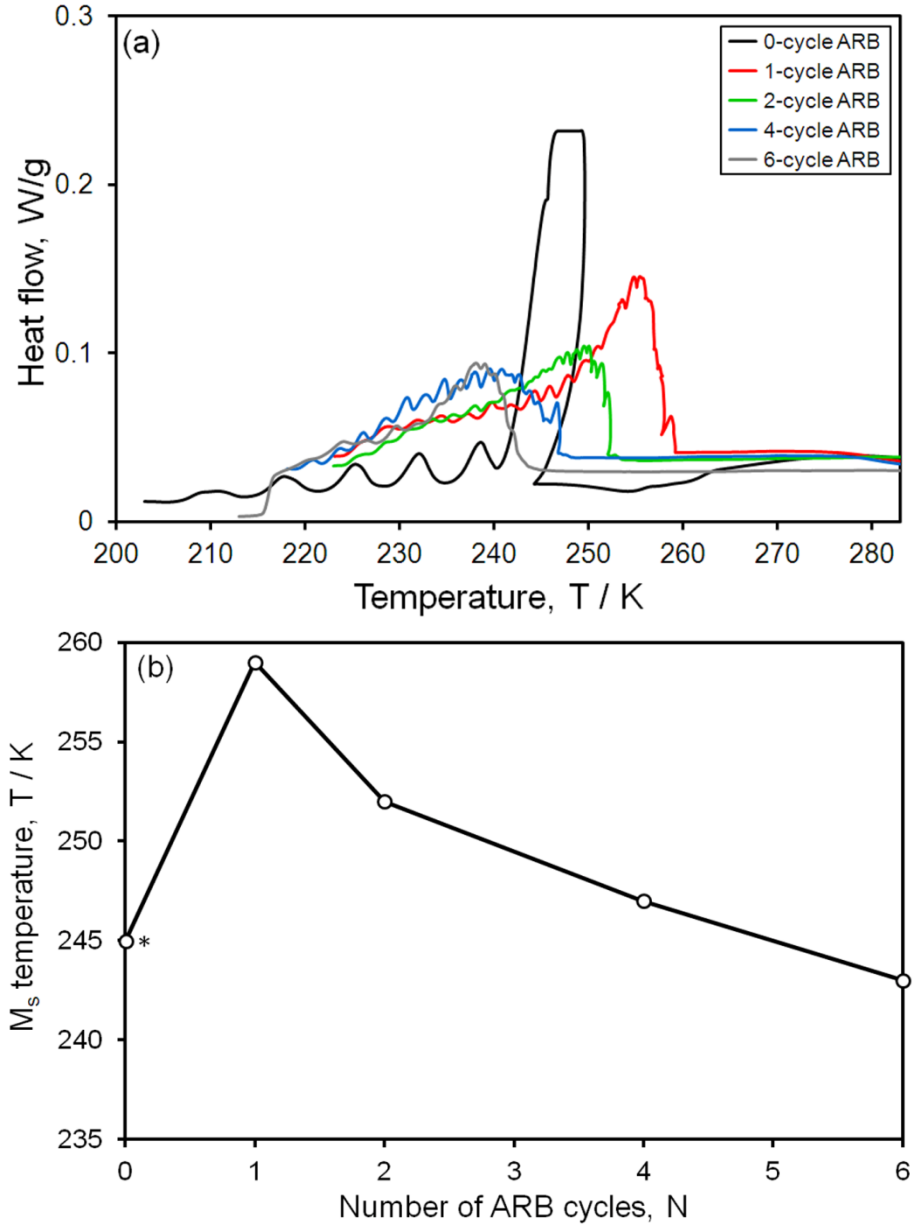

Fig. 3.6. (a) DSC curves, and (b) corresponding M_s temperature of the specimens ARB processed by various cycles. The occurrence of burst transformation is indicated by asterisk symbol (*).

Change in the yield strength of austenite (0.2% proof stress) is shown as a function of the number of ARB cycles in **Fig. 2.15(a)**. By comparison with Fig. 3.6(b) and Fig. 2.15(a), it seems that there is no any direct correlation between M_s temperature and austenite strength. **Figure 3.7** illustrates the change in M_s temperature as a function of yield strength of austenite for the starting material, 1-cycle, 2-cycle, 4-cycle and 6-cycle

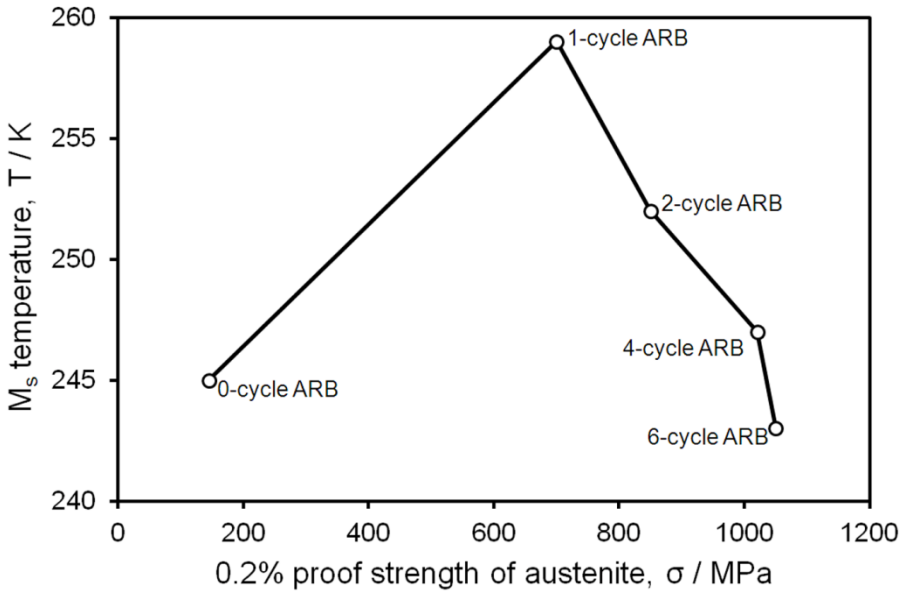

Fig. 3.7. Relationship between 0.2% proof stress and M_s temperature for the starting material, 1-cycle, 2-cycle, 4-cycle and 6-cycle ARB processed specimens.

ARB processed specimens. By comparing the yield strength of the ARB processed austenite with Fig. 3.6(b), it is possible to say that the yield strength of the ARB processed austenite does not correspond with the change in M_s temperature of the ARB processed specimens.

Figure 3.8 illustrates the change in M_s temperature as a function of austenite grain size for fully recrystallized, partially recrystallized and as ARB processed specimens. Annealing treatments at temperatures from 773 to 873 K for 1.8 ks for the 6-cycle ARB processed specimen result in significant decrease in M_s temperature as shown in Fig. 3.8. As shown in the austenite grain boundary maps of the 6-cycle ARB processed specimen after annealing (Fig. 2.7(a)-(c)), the microstructure does not change significantly and only recovery occurred by annealing at 773 K (Fig. 2.7(a)). On the other hand, annealing treatment at 823 K resulted in partial recrystallization, but the microstructure was still composed of elongated ultrafine grains (Fig. 2.7(b)). The austenite after 873 K annealing treatment exhibited fully recrystallized microstructure (Fig. 2.7(c)). Figure

2.8(b) (in chapter 2) showed the change in dislocation density by annealing treatment at 773~873 K in the 6-cycle ARB processed austenite. It revealed that the dislocation density gradually decreased by annealing treatment. The decrease of M_s temperature for the 6-cycle ARB processed austenite by annealing treatment is consistent with the decrease in dislocation density. These results clearly indicate that dislocations are basically nucleation sites for martensitic transformation. However, for fully recrystallized specimens that are free of dislocations and low angle boundaries, M_s temperature essentially depends on austenite grain size as shown in Fig. 3.8 and also reported by Umemoto and Owen [9]. For the specimens with the austenite grain size below 100 μm, M_s temperature decreases significantly with decrease in austenite grain size. In contrast, dependency of M_s temperature with austenite grain size is not noticeable when the austenite grain size is more than 100 μm.

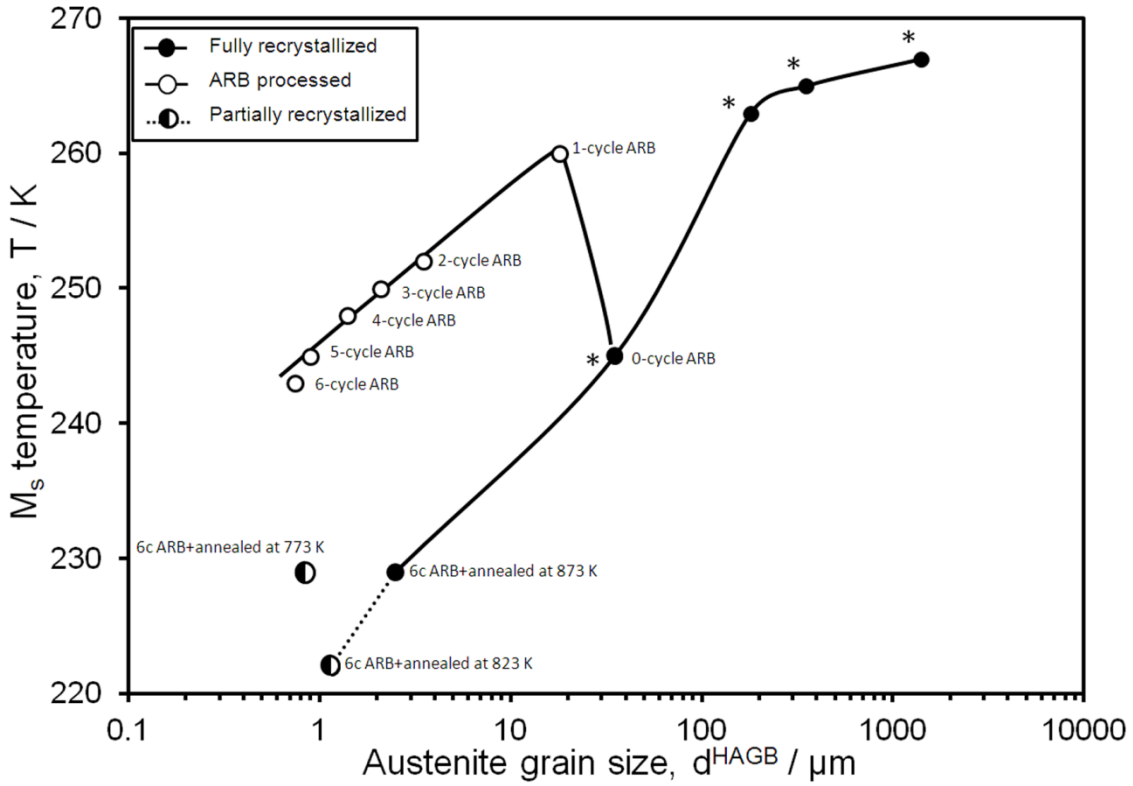

Fig. 3.8. Relationship between austenite grain size and M_s temperature for the fully recrystallized, partially recrystallized and as ARB processed specimens. The occurrence of burst transformation is indicated by asterisk symbol (*).

Figure 3.9 shows the DSC curves of the fully recrystallized specimens. Only the DSC curve of the specimen ARB processed by 6-cycle and subsequently annealed at 873 K does not exhibit burst transformation, indicating that burst transformation is suppressed by grain refinement of austenite. Decrease of M_s temperature and suppression of burst transformation by grain refinement suggest that high angle boundaries can act as obstacles for martensitic transformation.

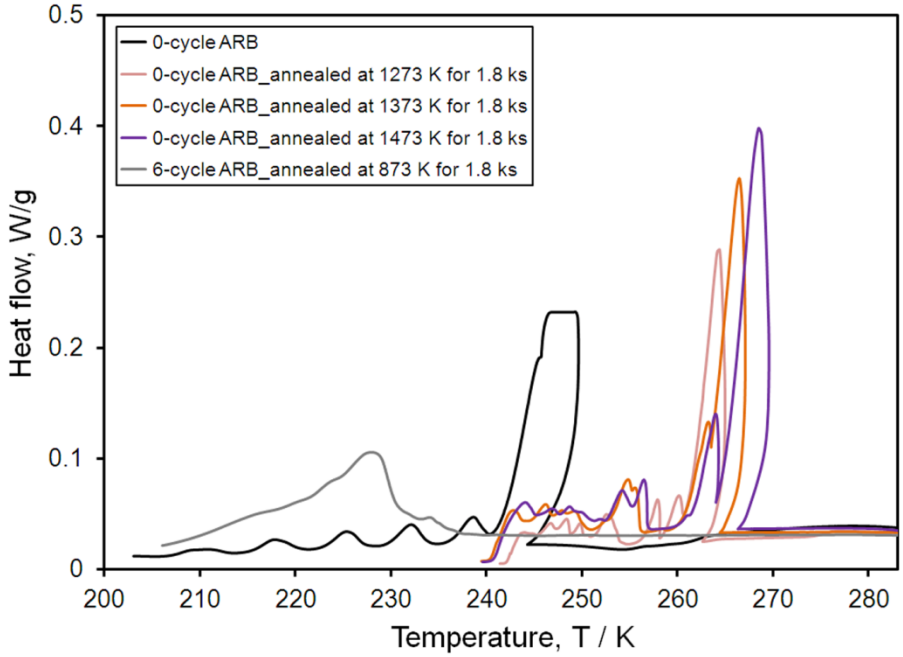

Fig. 3.9. DSC curves of fully recrystallized specimens with various austenite grain sizes.

3.4. Conclusion

In this chapter, microstructure of martensite transformed from ultrafine-grained (UFG) austenite fabricated by accumulative roll bonding (ARB) process and subsequent annealing has been studied in details. In addition, change in martensite transformation starting (M_s) temperature with respect to austenite microstructure has been discussed. The main results obtained in this chapter can be summarized as follows:

(i) Morphologies of martensite transformed from the coarse-grained austenite and UFG austenite were both lenticular types. However, some martensite plates transformed from UFG austenite contained low angle boundaries and exhibited broken and fragmented shapes. The size of martensite plates decreased with decrease in austenite grain size. However, the ratio of the austenite grain size to martensite plate size decreased when the austenite grain size was smaller than 2~3 μm. Moreover, the presence of low angle boundaries inside the martensite plates transformed from ARB processed austenite indicated that the low angle boundaries were not effective for grain refinement through martensitic transformation.

(ii) Although the austenite grain size decreased greatly from 35 μm to 750 nm by ARB process, the M_s temperature did not change so much. In contrast, annealing treatment after 6-cycle ARB process decreased the M_s temperature significantly. The change in the M_s temperature by the ARB process and subsequent annealing treatment was consistent with the change in the dislocation density and austenite grain size.

(iii) On the basis of experimental results, it is possible to conclude that the low angle boundaries or dislocations can act as nucleation sites for martensitic transformation while high angle boundaries suppress martensitic transformation.

References

[1] T. Tadaki, Y. Murai, A. Koreeda, Y. Nakata, Y. Hirotsu, Mater. Sci. and Eng. A 217–218 (1996), pp. 235-240.

[2] B. Han, Z. Xu, Mater. Sci. and Eng. A 487 (2008), pp. 64-67.

[3] A. Shibata, S. Morito, T. Furuhara, T. Maki, Acta Mater. 57 (2009), pp. 483-492.

[4] A. Shibata, S. Morito, T. Furuhara, T. Maki, Scripta Mater. 53 (2005), pp. 597-602.

[5] A. Shibata, PhD thesis, Kyoto University, (2005).

[6] A. Shibata, T. Murakami, S. Morito, T. Furuhara, T. Maki, Mater. Trans. 49 (2008), pp. 1242-1248.

[7] A.S. Sastri, D.R.F. West, J. Iron Steel Inst. 203 (1965), pp. 138-145.

[8] T. Maki, S. Shimooka, I. Tamura, Metall. Trans. 2 (1971), pp. 2944-2955.

[9] M. Umemoto, W.S. Owen, Metall. Trans. 5 (1974), pp. 2041-2046.

[10] P.J. Brofman, G.S. Ansell, Metall. Trans. A 14A (1983), pp. 1929-1931.

[11] C. Hayzelden, B. Cantor, Acta Metall. 34 (1986), pp. 233-242.

[12] S.A. Mujahid, H.K.D.H. Bhadeshia, Acta Metall. 41 (1993), pp. 967-973.

[13] J.H. Jun, C.S. Choi, Mat. Sci. and Eng. A 257 (1998), pp. 353-356.

[14] C. Capdevila, F.G. Caballero, C. García de Andrés, Mat. Sci. and Tech. 19 (2003), pp. 581-588.

[15] S.J. Lee, Y.K. Lee, Mater. Sci. Forum 475–479 (2005), pp. 3169-3172.

[16] J. Huang, Z. Xu, Mater. Sci. and Eng. A 438–440 (2006), pp. 254-257.

[17] A. Garcia-Junceda, C. Capdevila, F.G. Caballero, C. Garcia de Andres, Scripta Mater. 58 (2008), pp. 134-137.

[18] H.S. Yanga, H.K.D.H. Bhadeshia, Scripta Mater. 60 (2009), pp. 493-495.

[19] G.B. Olson, M. Cohen, Metall. Mater. A. 7A (1976), pp. 1897-1904.

[20] G.B. Olson, M. Cohen, Metall. Mater. A. 7A (1976), pp. 1905-1914.

[21] G.B. Olson, M. Cohen, Metall. Mater. A. 7A (1976), pp. 1915-1923.

Chapter 4. Orientation relationships between martensite and ultrafine-grained (UFG) austenite fabricated by accumulative roll bonding (ARB) process and subsequent annealing

4.1. Introduction

Recently, as described in the previous chapters, a new class of materials having ultrafine-grained (UFG) structures has been developed by severe plastic deformation. In chapters 2 and 3, the author demonstrated that the 6-cycle ARB processed austenite exhibited elongated ultrafine grains containing high density of low angle boundaries and dislocations that influenced martensitic transformation behaviors, i.e., plate size and starting temperature (M_s) of martensite.

Crystallographic feature of martensite, especially orientation relationship between martensite and austenite, is one of the characteristics of martensitic transformation involving important information concerning transformation mechanism [1-8]. For martensite transformation in iron-based alloys, three kinds of orientation relationships have been reported [9-12]; Kurdjumov-Sachs (K-S) relationship ($\{111\}_A$ // $\{011\}_M$, $<\bar{1}01>_A$ // $<\bar{1}\bar{1}1>_M$), Nishiyama-Wasserman (N-W) relationship ($\{111\}_A$ // $\{011\}_M$, $<\bar{1}\bar{1}2>_A$ // $<0\bar{1}1>_M$) and Greninger-Troiano (G-T) relationship ($\{111\}_A$ 1° from $\{011\}_M$, $<\bar{1}\bar{1}2>_A$ 2.5° from $<0\bar{1}1>_M$), where subscripts of A and M represent austenite and martensite, respectively. The G-T is the intermediate orientation relationship between the K-S and N-W orientation relationships. Different orientation relationship is observed depending on martensite morphology, such as lath, butterfly, lenticular and thin plate [13]. According to the recent studies, the orientation relationship of martensite and austenite varies even within a given martensite plate [14-15]. Although orientation relationship of martensite transformed from coarse-grained austenite has

been studied well, there is no study about orientation relationship of martensite transformed from UFG austenite.

In this chapter, in order to clarify the crystallographic features of martensite transformed from UFG austenite, the orientation relationship between martensite and UFG austenite is studied in details.

4.2. Experimental procedure

As mentioned in the previous chapters (1, 2 and 3), a Fe–24Ni-0.3C (wt.%) metastable austenitic steel with the mean grain size of 35 μm was used as the starting material. The sheets were provided to the ARB process to obtain UFG austenite structures. The details of the ARB process have been explained in chapters 1 and 2. The ARB was repeated up to 6 cycles with pre-heating at 873 K for 0.6 ks, so that the total equivalent strain accumulated was 4.8. The 6-cycle ARB processed austenite was annealed at 873 K for 1.8 ks to obtain fine-grained austenite having fully recrystallized and equiaxed grains.

The sheets subjected to the above mentioned treatments were cooled down to 77 K (in liq. N_2) to obtain thermally-induced martensite. The microstructures of the specimens were characterized by electron backscatter diffraction (EBSD) in a scanning electron microscope (SEM) equipped with a field-emission electron gun (Philips XL30S-FEG) operated at 15 kV. For EBSD observation, the sections parallel to the transverse direction (TD) of the specimens were polished mechanically and then electrolytically in a 900 mL CH_3COOH + 100 mL $HClO_4$ solution at approximately 284 K with a voltage of 20 V. The obtained EBSD data were analyzed by TSL-OIM Analysis software.

4.3. Results and discussion

4.3.1. Orientation relationship of martensite transformed from coarse-grained austenite (starting material)

Figure 4.1 shows an EBSD orientation image of martensite transformed from the coarse-grained austenite (the starting material). The black areas represent retained austenite. The smoothly curved interfaces between martensite and austenite (M/A interface) indicate that the morphology of the martensite transformed from the coarse-grained austenite is lenticular type, as also shown in chapter 3.

Figure 4.2(a) shows grain boundary and phase maps of the starting material after martensitic transformation. In Fig. 4.2(a), only high angle boundaries with misorientation more than 15° (drawn in black lines) exist, but low angle boundaries with misorientation between 2° and 15° are not observed. In addition, martensite and austenite phases are shown in pink and green colors, respectively.

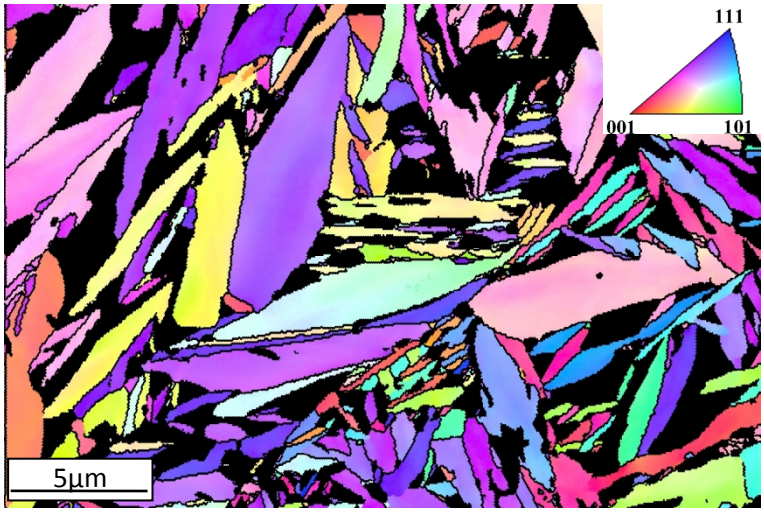

Fig. 4.1. EBSD orientation map of thermally-induced martensite transformed from coarse-grained austenite (the starting material). The black areas represent retained austenite.

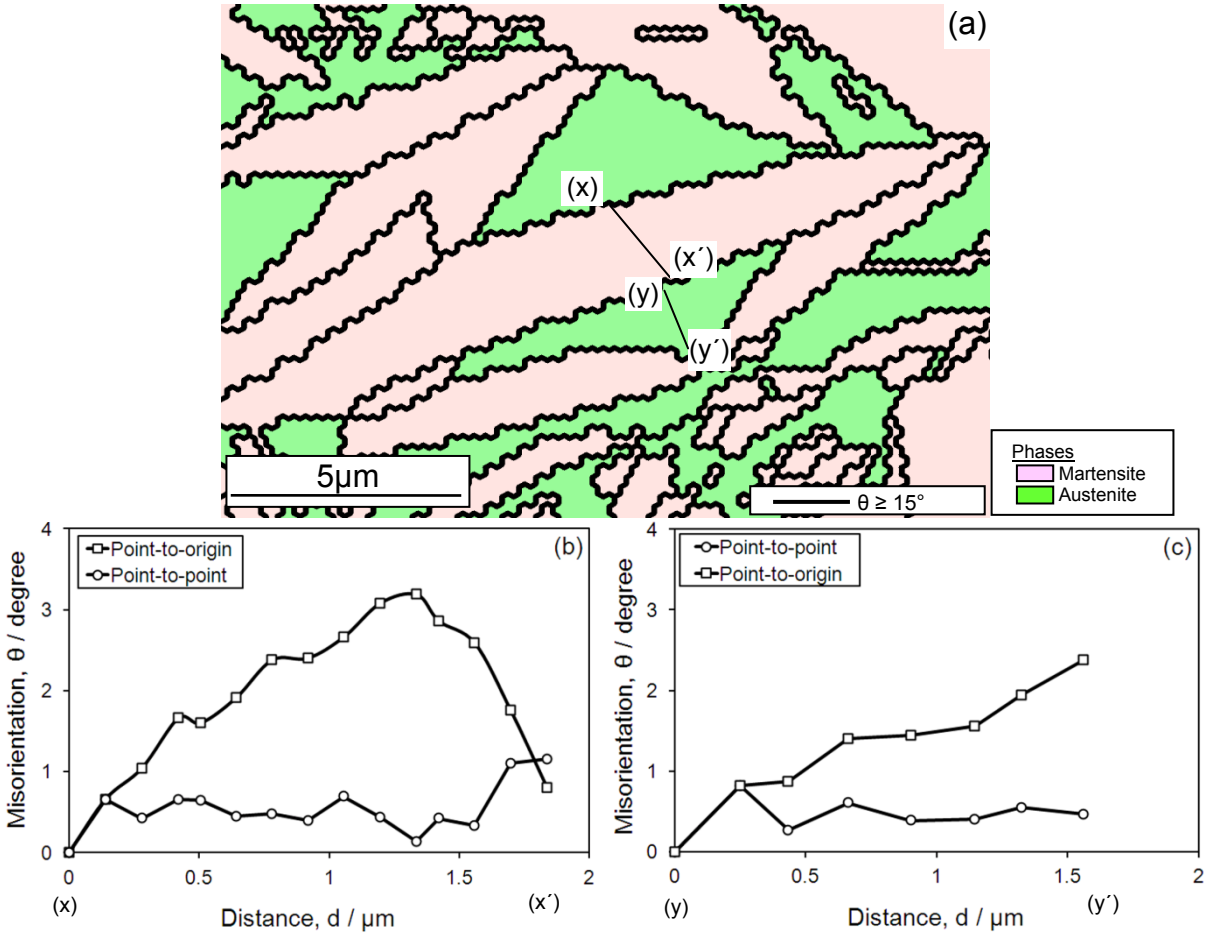

Fig. 4.2. (a) Grain boundary and phase map of the starting material after martensitic transformation, (b) local orientation profile along x-x´ inside the lenticular martensite, and (c) local orientation profile along y-y´ in the surrounding austenite.

Figure 4.2(b) shows the change in the local orientation along x-x´ line inside the martensite in Fig. 4.2(a). "Point-to-origin" in Fig. 4.2(b) represents the misorientation from the point of x (original point), and "point-to-point" represents the misorientation between the neighboring measured points. It is clear that the orientation gradually changes from the center of martensite plate (midrib) to the M/A interfaces, and the regions at both sides of midrib have the same orientation. This suggests that the plate of lenticular martensite nucleates at the midrib region and it grows to both sides, as previously reported by Shibata et al. [14]. **Figure 4.2(c)** shows the change in the local orientation along y-y´ in the surrounding austenite in Fig. 4.2(a). It indicates that the

local orientation of austenite also changes near the vicinity of M/A interface. The change in orientation inside the lenticular martensite plate and surrounding austenite indicates that orientation relationships of martensite with respect to austenite can vary within a given lenticular martensite plate.

In order to investigate the orientation relationship of lenticular martensite, the change in local orientation of martensite plate and the surrounding austenite should be taken into account. Thus, as shown in the schematic illustration of **Fig. 4.3(a)**, the orientation relationships at the middle part of martensite plate were measured using the orientation of austenite far from the M/A interface (blue circles). On the other hand, the orientation relationships in the vicinity of M/A interface were measured using the orientation of austenite just beside the M/A interface (red circles). The enlarged region around $[\bar{1}01]_A$ of standard $[001]_A$ stereographic projection showing the orientation relationship of martensite transformed from the coarse-grained austenite (the starting material) is illustrated in **Fig. 4.3(b)**. The points express the experimentally measured $[\bar{1}\bar{1}1]_M$ directions of martensite picked up from many different martensite plates. The ideal $[\bar{1}\bar{1}1]_M$ directions of martensite for the exact K-S and N-W relationships are also indicated as solid circles as shown in Fig. 4.3(b). The results show that the blue circles are distributed around the area between the K-S and N-W relationships (Fig. 4.3(b)), indicating that the middle part of martensite plate satisfies the G-T relationship with respect to austenite far from M/A interface. On the other hand, the red circles are relatively close to the K-S relationships. This suggests that the orientation relationship of lenticular martensite changes from the G-T relationship to the K-S relationship during growth. The local change of orientation inside the martensite plate and the surrounding austenite (Fig. 4.2(b) and (c)) can well explain the change in orientation relationship in lenticular martensite during the growth of martensite plate. The change

in orientation relationship inside the lenticular type martensite was also reported in the previous work [14].

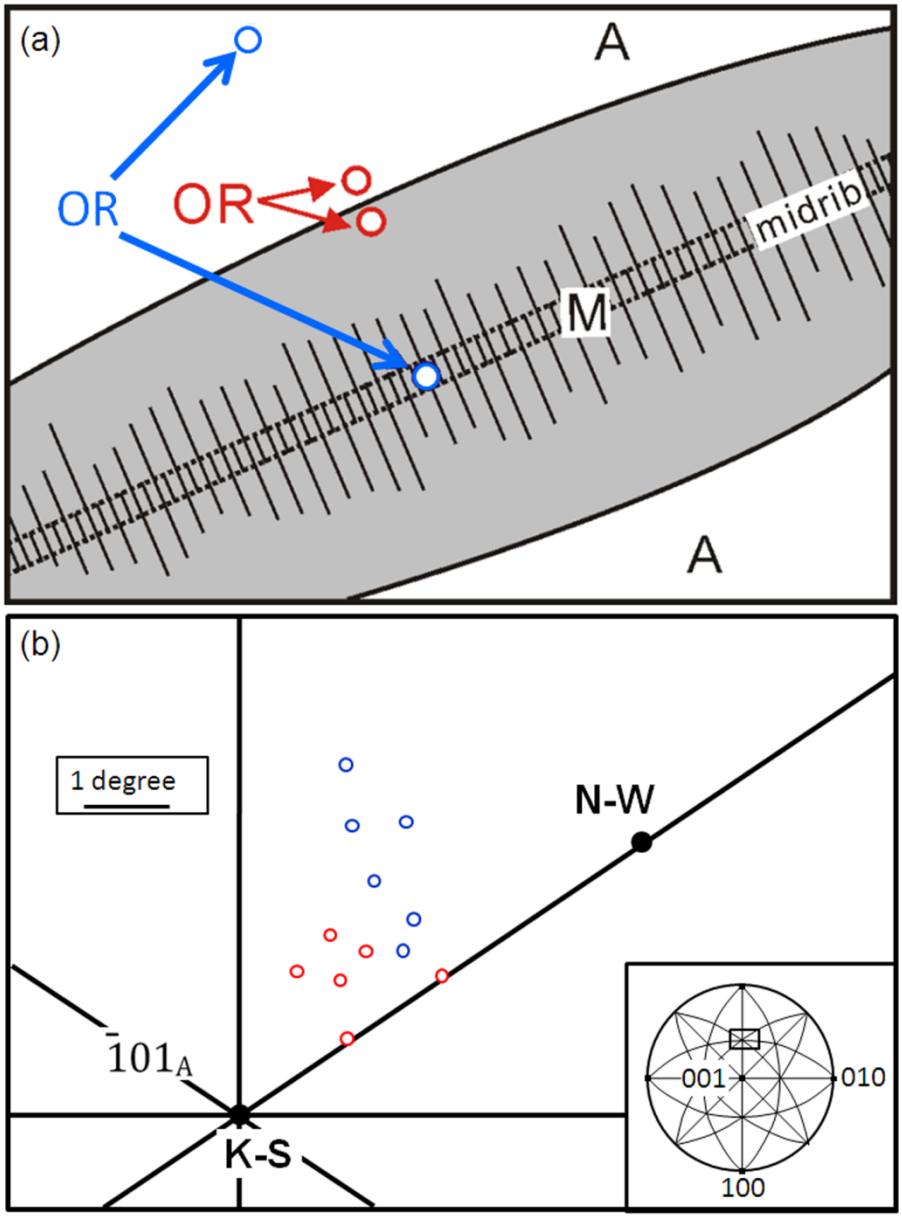

Fig. 4.3. (a) Schematic illustration showing the measured positions of martensite and austenite to obtain orientation relationships. (b) Standard $[001]_A$ stereographic projection around $[\bar{1}01]_A$ axis showing the $[\bar{1}\bar{1}1]_M$ directions of martensite transformed from the coarse-grained austenite. The orientation relationships in the vicinity of M/A interfaces are represented by red circles and for the middle part of martensite plates are represented by blue circles.

4.3.2. Orientation relationship of martensite transformed from ultrafine-grained austenite (6-cycle ARB processed austenite)

Grain boundary and phase maps of the 6-cycle ARB processed specimen (having UFG austenite) after martensitic transformation is shown in **Fig. 4.4(a)**. In Fig. 4.4(a), high angle boundaries with misorientation larger than 15° are drawn in black lines and low angle boundaries with misorientation between 2° and 15° are drawn in gray lines. Again, martensite and austenite phases are shown in pink and green colors, respectively. The size of martensite plate transformed from the UFG austenite is significantly smaller than those transformed from the coarse-grained austenite (Fig. 4.4(a)). The martensite plates in Fig. 4.4(a) contain low angle boundaries that have not observed in the martensite plates transformed from the coarse-grained austenite. These low angle boundaries inside the martensite plates correspond to the presence of low angle boundaries in the 6-cycle ARB processed austenite, which are inherited by martensite.

Figure 4.4(b) and (c) shows the changes in local orientation along x-x′ line inside the martensite plate and along y-y′ in the surrounding austenite in Fig. 4.2(a), respectively. It clearly shows that the change in local orientation for both martensite and austenite are significantly large, although the martensite plate size is very small, compared with the case of coarse-grained austenite (Fig. 4.1 or Fig. 4.2(a)).

Orientation relationships of martensite transformed from the 6-cycle ARB processed austenite are plotted in **Fig. 4.5**. In Fig. 4.5, only the orientation relationships just beside the M/A interface (red circles) are shown, because large local orientation distribution inside the 6-cycle ARB processed specimen (Fig. 4.4(c)) makes it difficult to assume the exact orientation of austenite before transformation. The experimentally measured orientation relationships (red circles) are located between the K-S and N-W

relationships, indicating that the martensite transformed from the 6-cycle ARB processed austenite holds the G-T relationship with respect to austenite. However, the measured orientation relationships in Fig. 4.5 are largely scattered between different martensite plates. The 6-cycle ARB processed austenite contains high density of dislocations and low angle boundaries as explained in chapter 2. These dislocations or low angle boundaries cause the relatively large change in local orientation inside the austenite grains and martensite plates as shown in Fig. 4.4(b) and (c), resulting in the large scatter of observed orientation relationships.

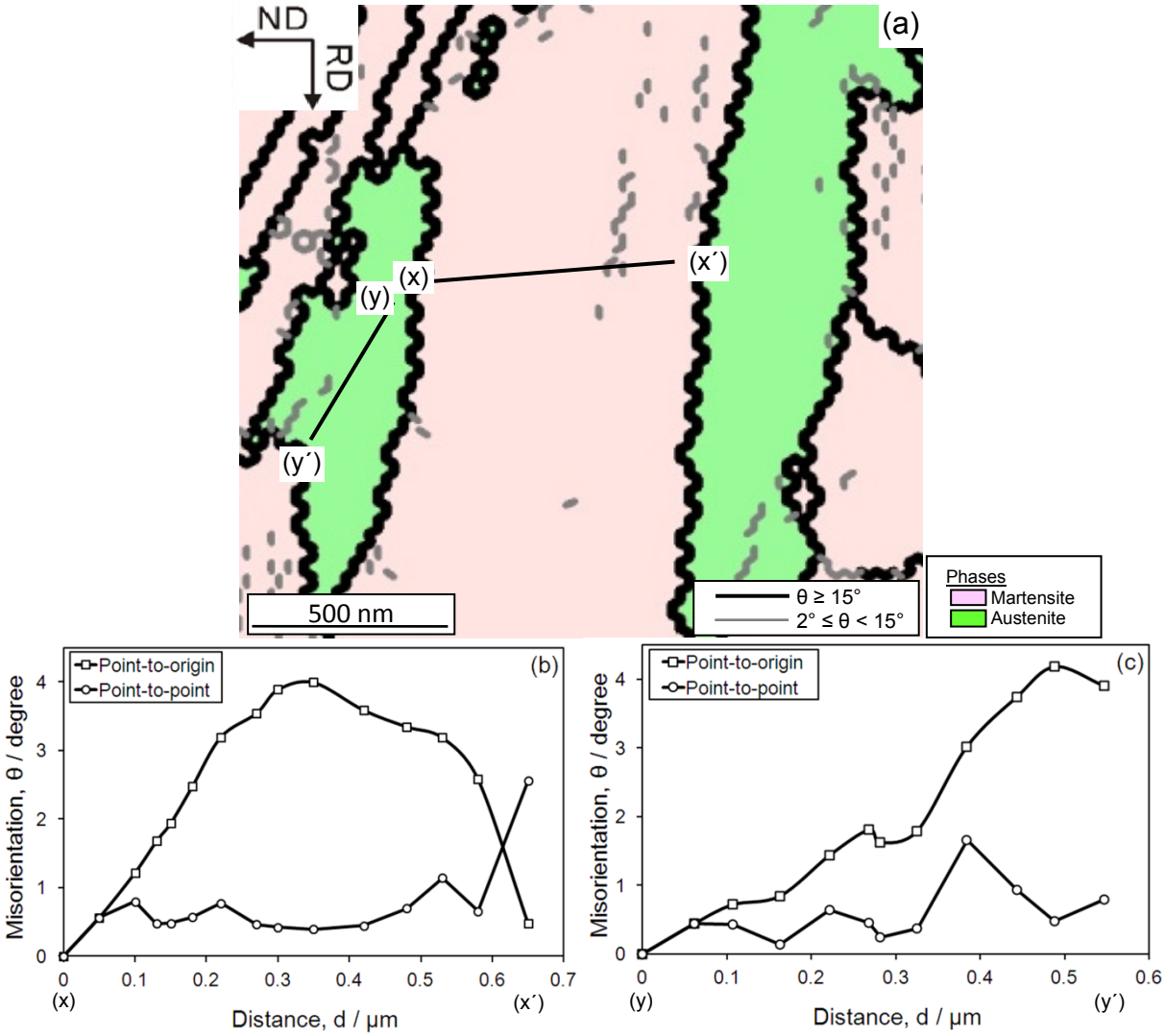

Fig. 4.4. (a) Grain boundary and phase map of the 6-cycle ARB processed specimen after martensitic transformation, (b) local orientation profile along x-x´ inside the lenticular martensite, and (c) local orientation profile along y-y´ in the surrounding austenite.

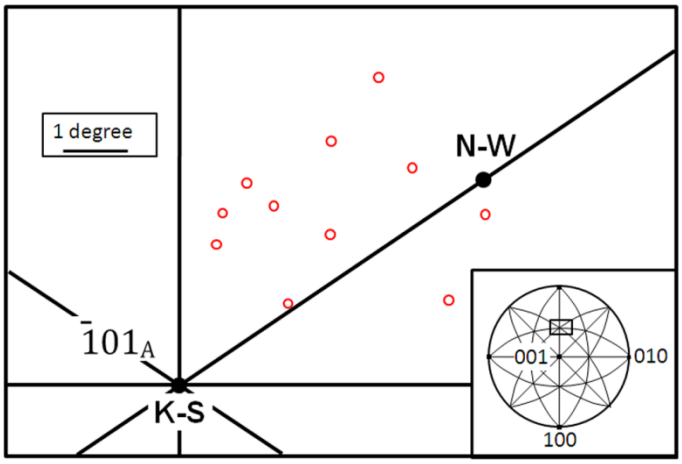

Fig. 4.5. Standard $[001]_A$ stereographic projection around $[\bar{1}01]_A$ axis showing the $[\bar{1}\bar{1}1]_M$ directions of martensite transformed from the 6-cycle ARB processed specimen having elongated ultrafine-grained austenite. The orientation relationships in the vicinity of M/A interfaces are represented by red circles.

4.3.3. Orientation relationship of martensite transformed from fully recrystallized fine-grained austenite (6-cycle ARB processed and 873 K annealed austenite)

Annealing treatment at 873 K for 1.8 ks on the 6-cycle ARB processed specimen results in the formation of the fully-recrystallized austenite having equiaxed and fine grains as described in chapter 2 (Fig. 2.7(c)). **Figure 4.6** shows orientation relationship of martensite transformed from austenite 6-cycle ARB processed and then annealed at 873 K having equiaxed and fine grains with mean grain size of 2.5 μm. The measured orientation relationships at the middle part of martensite plate (blue circles) and at the vicinity of M/A interface (red circles) are distributed around the middle of the exact K-S and N-W relationships. This indicates that the whole area of martensite plate transformed from the equiaxed and fine-grained austenite satisfies the G-T relationship with respect to austenite. In addition, the measured orientation relationships are not scattered between different martensite plates.

As shown in Fig. 4.2(b), the orientation relationship of the lenticular martensite transformed from the coarse-grained austenite holds the G-T orientation relationship at earlier stage of transformation, but the orientation relationship gradually deviates towards the K-S during growth. As has been already denoted in chapter 3 of this thesis, the martensite plate size is decreased by grain refinement of austenite. Accordingly, it can be said that the martensite transformed from the fine-grained austenite does not grow enough to change the orientation relationship from the G-T to K-S relationships, resulting that the whole area in the martensite plate satisfies the G-T relationship. Moreover, annealing treatment at 873 K for 1.8 ks causes fully recrystallized austenite free of dislocations or low angle boundaries as described in chapter 2 (Fig. 2.7(c)). As a result, the measured orientation relationships of martensite in the fine-grained austenite are not scattered between different martensite plates.

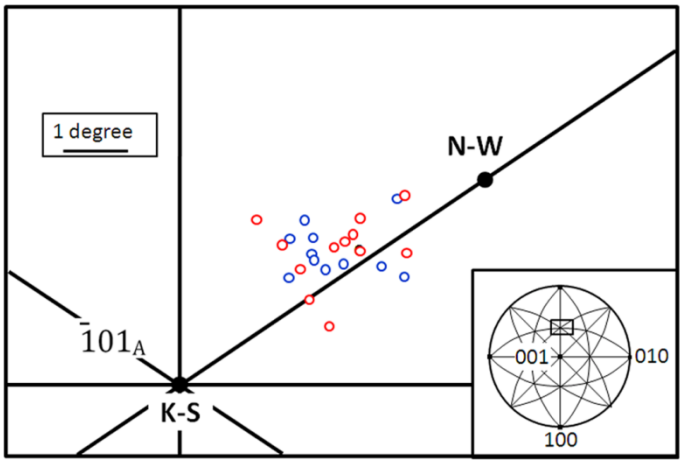

Fig. 4.6. Standard $[001]_A$ stereographic projection around $[\bar{1}01]_A$ axis showing the $[\bar{1}\bar{1}1]_M$ directions of martensite transformed from the fully-recrystallized austenite with equiaxed and fine-grained structure. The orientation relationships in the vicinity of M/A interfaces are represented by red circles and for the middle part of martensite plate are represented by blue circles.

4.4. Conclusion

In this chapter, orientation relationship of martensite with respect to the coarse-grained austenite (the starting material), the elongated ultrafine-grained (UFG) austenite (the 6-cycle ARB processed specimen) and the fully-recrystallized and fine-grained austenite (the specimen 6-cycle ARB processed and annealed at 873 K for 1.8 ks) in a Fe-24Ni-0.3C alloy were studied. The conclusions are summarized as follows:

(i) The martensite transformed from the coarse-grained austenite held the G-T orientation relationship at the middle part of martensite plate, but it shifted to the K-S relationship as approaching the M/A interfaces.

(ii) The martensite transformed from the ultrafine-grained austenite held the G-T orientation relationship with respect to austenite, but the observed orientation relationships were significantly scattered between different martensite plates. The existence of high density of dislocations or low angle boundaries inside the austenite grains resulted in the large scatter of the observed orientation relationships.

(iii) The whole area in the martensite plates transformed from the fully recrystallized fine-grained austenite satisfied the G-T relationship. This is attributed to the smaller size of the martensite plate transformed from fine-grained austenite, of which growth is restricted in martensitic transformation.

References

[1] E.O. Fearon, M. Bevis, Acta Metall. 22 (1974), pp. 991-1002.

[2] T.N. Durlu, J. Mater. Sci. 36 (2001), pp. 5665-5671.

[3] M.X. Zhang, P.M. Kelly, Scripta Mater. 47 (2002), pp. 749-755.

[4] S. Morito, X. Huang, T. Furuhara, T. Maki, N. Hansen, Acta Mater. 54 (2006), pp. 5323-5331.

[5] H. Gungunes, E. Yasar , T.N. Durlu, J. Mater. Sci. 42 (2007), pp. 6102-6107.

[6] G. Miyamoto, N. Takayama, T. Furuhara, Scripta Mater. 60 (2009), pp.1113-1116

[7] A. Shibata, T. Furuhara, T. Maki, Acta Mater. 58 (2010), pp. 3477-3492.

[8] X. Chen, J. Gui, R. Wang, J. Wang, J. Liu, F. Chen, D. Wang, Micron 3 (2000), pp. 17-25.

[9] G. Kurdjumov, G. Sachs, Z. Phys, 64 (1930), pp. 325-343.

[10] A.B. Greninger, A.R. Troiano, Trans. ASM 140 (1940), pp. 307-336.

[11] A.B. Greninger, A.R. Troiano, Trans. AIME 145 (1941), pp. 289-291.

[12] Z. Nishiyama, K. Shimizu, Acta Metall. 9 (1961), pp. 980-981.

[13] T. Maki, Mater. Sci. Forum 56–58 (1990), pp. 157-168.

[14] A. Shibata, S. Morito, T. Furuhara, T. Maki, Scripta Mater. 53 (2005), pp. 597-602.

[15] H. Sato, S. Zaefferer, Acta Mater. 57 (2009), pp. 1931–1937.

Chapter 5. Variant selection of martensite transformed from ultrafine-grained (UFG) austenite fabricated by accumulative roll bonding (ARB) process and subsequent annealing

5.1. Introduction

Based on the recent development of severe plastic deformation process [1-5], bulky ultrafine-grained materials having mean grain sizes smaller than 1 μm can be obtained. As has been already described in chapters 3 and 4, ultrafine-grained structure of austenite greatly affects the characteristics of martensite, such as martensite starting (M_s) temperature (chapter 3) and orientation relationship with respect to austenite (chapter 4).

For martensitic transformation in steels, martensite usually satisfies Kurdjumov-Sachs (K-S) orientation relationship with respect to austenite ($\{111\}_A$ // $\{011\}_M$, $<101>_A$ // $<111>_M$, where subscripts of A and M represent austenite and martensite, respectively [6]. When the K-S relationship is maintained, 24 equivalent crystallographic variants of martensite can form from a single crystal (or single grain) of austenite. **Table 5.1** summarizes the orientation relationships between the 24 crystallographic variants (V_1–V_{24}) of martensite and austenite under the K-S orientation relationship. When plastic deformation is applied to austenite before martensitic transformation, the 24 variants of martensite do not form equally but some specific variants are preferentially formed, resulting in the formation of transformation texture. This is so-called variant selection. In this chapter, effect of austenite structure, especially grain size and grain shape, on the variant selection rules of martensitic transformation in the ultrafine-grained Fe-Ni-C alloy fabricated by accumulative roll bonding (ARB) is studied.

Table 5.1. The 24 crystallographic variants of martensite for the K-S orientation relationship.

Variant	Plane parallel	Direction parallel
V_1	$(111)_A // (011)_M$	$[\bar{1}01]_A // [\bar{1}\bar{1}1]_M$
V_2		$[\bar{1}01]_A // [\bar{1}1\bar{1}]_M$
V_3		$[01\bar{1}]_A // [\bar{1}\bar{1}1]_M$
V_4		$[01\bar{1}]_A // [\bar{1}1\bar{1}]_M$
V_5		$[1\bar{1}0]_A // [\bar{1}\bar{1}1]_M$
V_6		$[1\bar{1}0]_A // [\bar{1}1\bar{1}]_M$
V_7	$(\bar{1}11)_A // (011)_M$	$[0\bar{1}1]_A // [\bar{1}\bar{1}1]_M$
V_8		$[0\bar{1}1]_A // [\bar{1}1\bar{1}]_M$
V_9		$[\bar{1}0\bar{1}]_A // [\bar{1}\bar{1}1]_M$
V_{10}		$[\bar{1}0\bar{1}]_A // [\bar{1}1\bar{1}]_M$
V_{11}		$[110]_A // [\bar{1}\bar{1}1]_M$
V_{12}		$[110]_A // [\bar{1}1\bar{1}]_M$
V_{13}	$(1\bar{1}1)_A // (011)_M$	$[10\bar{1}]_A // [\bar{1}\bar{1}1]_M$
V_{14}		$[10\bar{1}]_A // [\bar{1}1\bar{1}]_M$
V_{15}		$[\bar{1}\bar{1}0]_A // [\bar{1}\bar{1}1]_M$
V_{16}		$[\bar{1}\bar{1}0]_A // [\bar{1}1\bar{1}]_M$
V_{17}		$[011]_A // [\bar{1}\bar{1}1]_M$
V_{18}		$[011]_A // [\bar{1}1\bar{1}]_M$
V_{19}	$(11\bar{1})_A // (011)_M$	$[\bar{1}10]_A // [\bar{1}\bar{1}1]_M$
V_{20}		$[\bar{1}10]_A // [\bar{1}1\bar{1}]_M$
V_{21}		$[0\bar{1}\bar{1}]_A // [\bar{1}\bar{1}1]_M$
V_{22}		$[0\bar{1}\bar{1}]_A // [\bar{1}1\bar{1}]_M$
V_{23}		$[101]_A // [\bar{1}\bar{1}1]_M$
V_{24}		$[101]_A // [\bar{1}1\bar{1}]_M$

5.2. Experimental procedure

An Fe-24Ni-0.3C (wt.%) alloy, of which chemical composition was shown in Table 1.2 (chapter 1), was used in the present study. A cast ingot of the alloy was hot-rolled and then cold-rolled to make sheets with thickness of 1 mm. The sheets were austenitized at 1173 K for 3.6 ks to obtain a fully recrystallized and coarse-grained

austenite with a mean grain size of 35 μm. The austenitized sheets were used as the starting material. To fabricate ultrafine-grained austenite structures, the starting material was subjected to the ARB process. The details of the ARB process has been described in chapters 1 and 2. The ARB was repeated up to 6-cycle by pre-heating at 873 K for 0.6 ks, so that the total equivalent strain accumulated was 4.8. The 6-cycle ARB processed specimens were annealed at 773 K or 873 K for 1.8 ks to obtain recovered or recrystallized austenite structures with various grain sizes.

The sheets subjected to the above mentioned treatments were cooled down to 77 K (in liq. N_2) to obtain thermally-induced martensite. The microstructure and texture of the specimens were characterized by electron backscatter diffraction (EBSD) in a scanning electron microscope (SEM) equipped with a field-emission electron gun (Philips XL30S-FEG) operated at 15 kV. For the EBSD observation, the sections parallel to the transverse direction (TD) of the sheets were polished mechanically and then electrolytically in a 900 mL CH_3COOH + 100 mL $HClO_4$ solution at approximately 284 K with a voltage of 20 V. The obtained EBSD data were analyzed by TSL-OIM Analysis software.

5.3. Results and discussion

5.3.1. Transformation texture and variant selection of martensite from coarse-grained austenite (starting material)

Figure 5.1(a) and (b) show an EBSD orientation map and corresponding $\{100\}_A$ pole figure of the starting material. The colors in the orientation map indicates the crystallographic directions of each point parallel to TD of the sheet (the normal direction of the observed plane), according to the stereographic triangle shown in the

figure. The ideal <100>$_A$ axes of typical texture components in f.c.c crystal, i.e., Brass component ({110} <112>$_A$), Copper component ({112} <111>$_A$), S component ({123} <634>$_A$), and Cube component ({100} <001>$_A$) are also indicated in the {100}$_A$ pole figure as circles, triangles, solid rectangles and open rectangles, respectively. The austenite of the starting material consists of equiaxed grains with a mean grain size of 35 μm, and does not have a particular texture, as shown in Fig. 5.1(a) and (b). An EBSD orientation map and corresponding {100}$_M$ pole figure of martensite in the starting material after thermally-induced martensitic transformation are shown in **Fig. 5.1(c) and (d)**. Because the intensities in the pole figure of Fig. 5.1(d) are very weak (max. value is 1.594), it can be said that transformation texture is not developed during thermal martensitic transformation from the starting material having coarse-grained austenite with random texture.

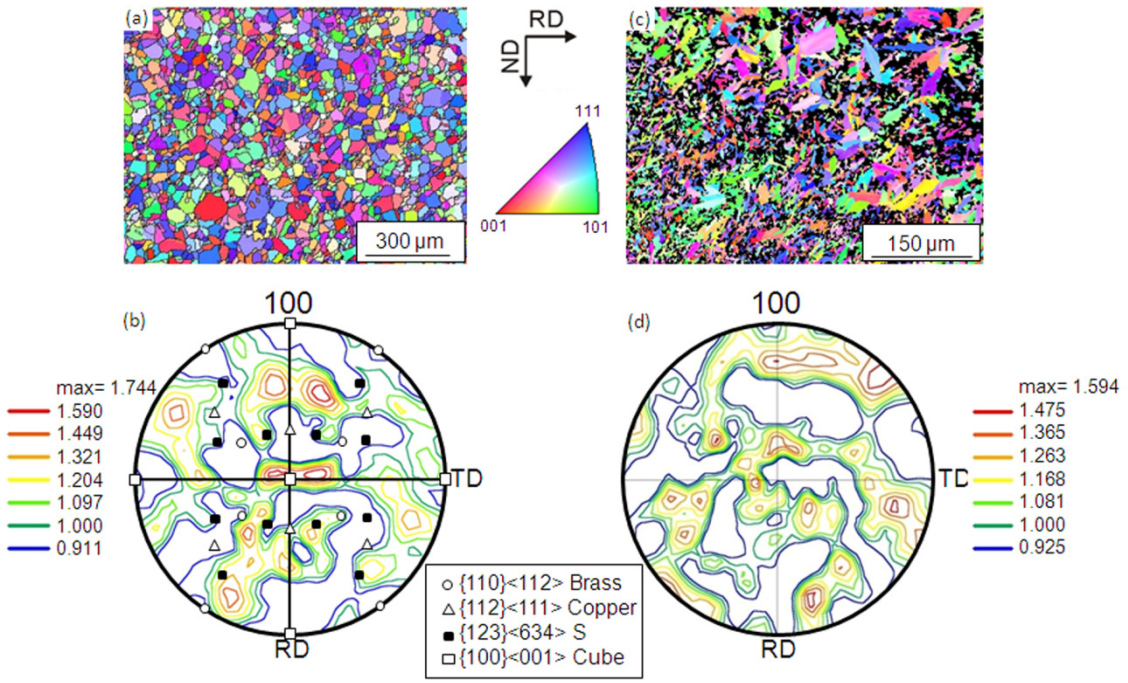

Fig. 5.1. ((a), (b)) EBSD orientation color map and {100} pole figure of austenite before martensitic transformation in the starting material. ((c), (d)) EBSD orientation color map and {100} pole figure of martensite after martensitic transformation in the starting material.

5.3.2. Transformation texture and variant selection of martensite in ARB processed specimen

Figure 5.2(a) and (b) shows an EBSD orientation map and corresponding $\{100\}_A$ pole figure of austenite after 1-cycle ARB process. The colors in the orientation map again indicate the crystallographic directions of each point parallel to TD. The average interval of high angle boundaries along the normal direction (ND) of the sheet is about 18 μm, which agrees well with the size of the initial coarse grains (with initial grain size of 35 μm) after 50% rolling. The $\{100\}_A$ pole figure of Fig. 5.2(b) indicates that the Copper texture is developed by 1-cycle of ARB, i.e., 50% rolling. An EBSD orientation map and corresponding $\{100\}_A$ pole figure of austenite after 6-cycle ARB process are shown in **Fig. 5.2(c) and (d)**. The austenite after 6-cycle ARB process exhibits lamellar structure elongated along the rolling direction (RD) of the sheet. The average interval of high angle boundaries along ND is about 750 nm. This is a typical ultrafine-grained structure fabricated by the ARB process. According to Fig. 5.2(b) and (d), the main texture component of austenite changes from Copper orientation to Brass orientation with increasing the number of ARB cycles.

Figure 5.3 displays EBSD orientation maps and corresponding $\{100\}_M$ pole figures of martensite transformed from the 1-cycle ARB processed specimen having deformed coarse-grained austenite (Fig. 2.2(b)) and the 6-cycle ARB processed specimen having elongated ultrafine-grained austenite (Fig. 2.2(e)). The observed texture of martensite transformed from the 1-cycle ARB processed specimen having deformed coarse-grained austenite (Fig. 5.3(b)) is different from that transformed from the 6-cycle ARB processed specimen having elongated ultrafine-grained austenite (Fig. 5.3(d)). Preferentially formed variants of martensite can be determined by comparing the experimentally measured $\{100\}_M$ pole figure with the stereographic projection on which

$<100>_M$ axes of the ideal 24 variants of martensite are plotted. In order to determine the preferentially formed variants of martensite, the positions of the ideal $<100>_M$ axes for the 24 variants of martensite transformed from the austenite with exact Copper orientation ((112) $[\bar{1}\bar{1}1]_A$) are superimposed on the $\{100\}_M$ pole figure in Fig. 5.3(b). From Fig. 5.3(b), the author can find that the V_2, V_5, V_6, V_{19}, V_{20} and V_{23} are preferentially formed during martensitic transformation from the 1-cycle ARB processed specimen having deformed coarse-grained austenite. These variants are indicated in red circles in Fig. 5.3(b). The positions of the ideal $<100>_M$ axes for the 24 variants of martensite transformed from the austenite with exact Brass orientation ((011) $[2\bar{1}1]_A$) are also plotted in Fig. 5.3(d). It reveals that the V_6, V_{16}, V_{19}, V_{21}, V_{22} and V_{24} are preferentially formed during martensitic transformation from the 6-cycle ARB processed specimen having elongated ultrafine-grained austenite.

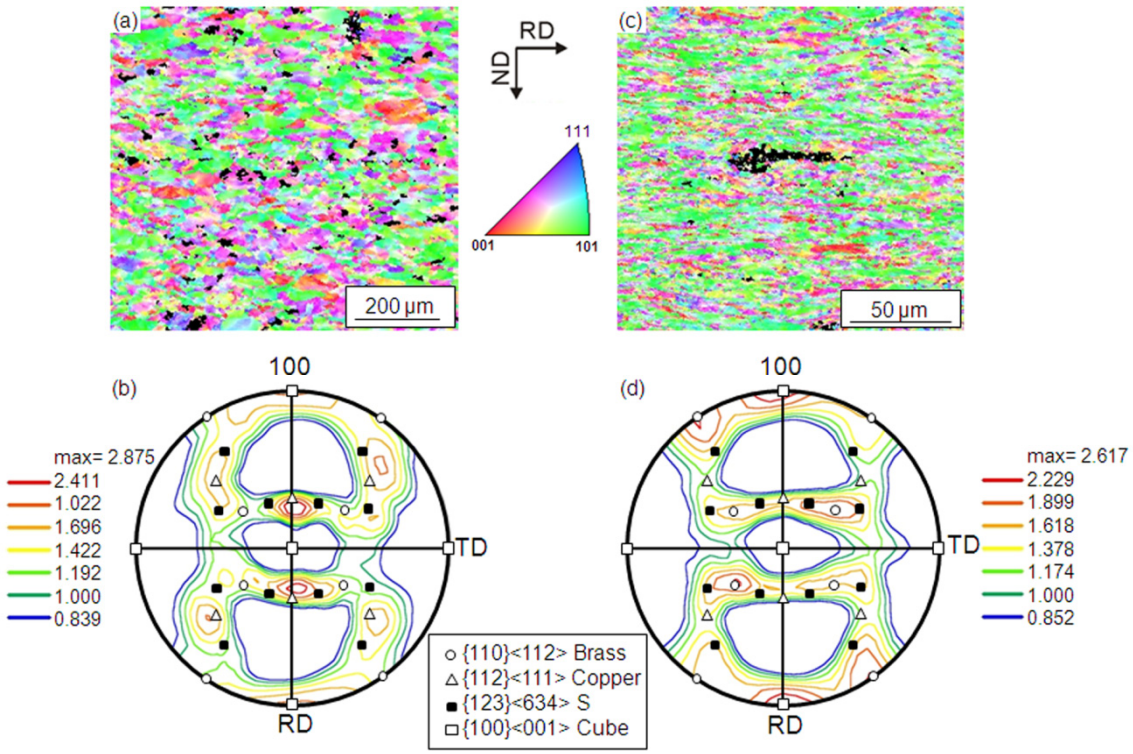

Fig. 5.2. EBSD orientation color maps and $\{100\}_A$ pole figures of austenite after 1-cycle ARB process ((a), (b)) and after 6-cycle ARB process ((c), (d)).

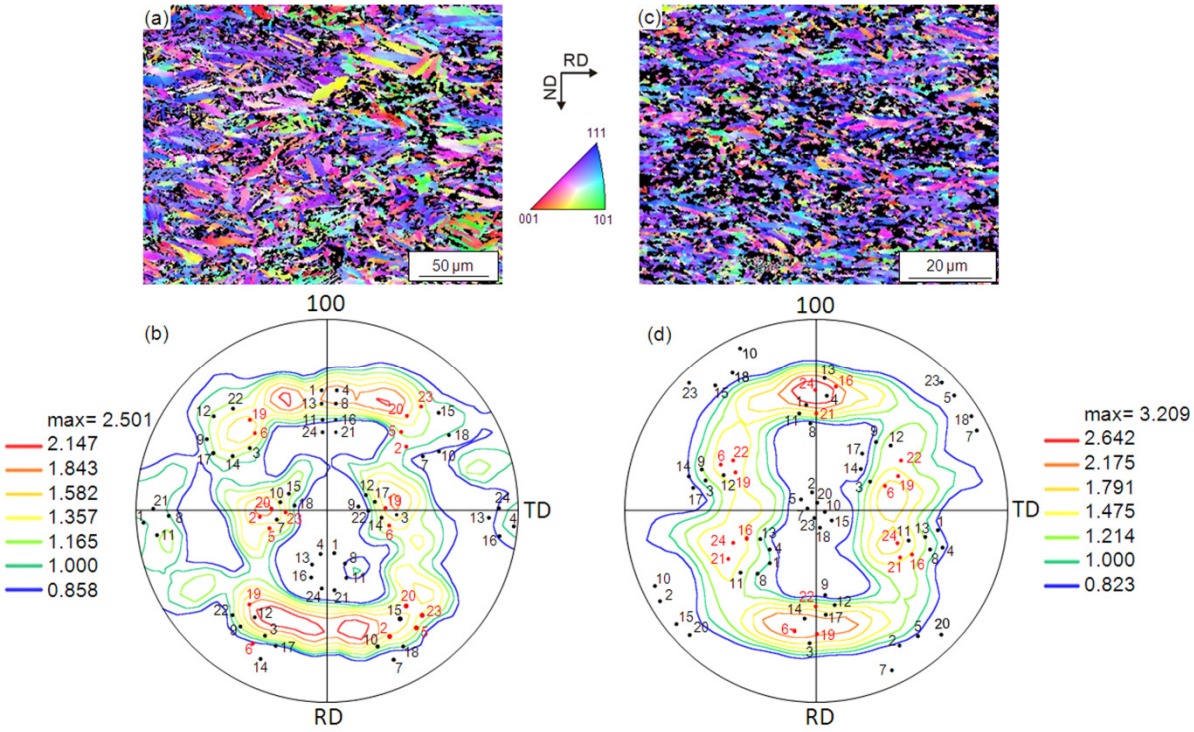

Fig. 5.3. EBSD orientation color maps and $\{100\}_M$ pole figures of martensite transformed from the 1-cycle ARB processed specimen having deformed coarse-grained austenite ((a), (b)), and the 6-cycle ARB processed specimen having elongated ultrafine-grained austenite ((c), (d)). The positions of the ideal $<100>_M$ axes for the 24 variants of martensite transformed from the austenite with exact Copper orientation ((112) $[\bar{1}\bar{1}1]_A$) and from the austenite with exact Brass orientation ((011) $[2\bar{1}1]_A$) are shown by the numbers in $\{100\}_M$ pole figure of (b) and (d), respectively. The preferential variants are indicated by red color.

Kundu [7] demonstrated that variant selection in thermally-induced martensitic transformation from cold-rolled austenite can be predicted from interaction energy between residual stress in the cold-rolled austenite and shape deformation accompanying martensitic transformation. Based on his model, the author discusses the variant selection of martensite transformed from the 1-cycle ARB processed specimen having deformed coarse-grained austenite (Fig. 5.3(b)) and the 6-cycle ARB processed specimen having elongated ultrafine-grained austenite (Fig. 5.3(d)). The interaction energy is given by the equation shown below [8]:

$$U = \sigma_N \delta + \tau s \qquad (5.1)$$

where σ_N is the residual stress component normal to the habit plane, τ is the residual shear stress resolved on the habit plane in the direction of shear, and δ and s are the dilatational and shear strains associated with the shape deformation in martensitic transformation. Because large positive value of the interaction energy means to facilitate the martensitic transformation, it is possible to say that the variants of martensite having large positive value of the interaction energy (U) are preferentially formed. The habit plane orientation, shear direction, δ and s can be obtained from the phenomenological theory of martensite crystallography (PTMC) [9-12]. The calculated habit plane orientation and shear direction of martensite (V_1 in Table 5.1) are $(0.164, 0.753, 0.636)_A$ and $[-0.189, 0.657, -0.730]_A$, respectively, while δ and s are 0.005 and 0.203, respectively. For the PTMC calculation, the lattice parameters of 0.3590 nm (austenite) and 0.2854 nm (martensite) in Fe-33Ni were used [13]. In addition, $(101)[\bar{1}01]_A$ twinning deformation was used as a lattice invariant shear. Wang et al. [14] measured the residual stress tensors for each major texture component of a 50% cold-rolled austenite by neutron diffraction. In the present research, their residual stress tensors measured for Copper and Brass textures (**Table 5.2**) for calculating the interaction energy for each martensite variant is used.

The calculated values of the interaction energy for the 24 variants of martensite transformed from the 1-cycle ARB processed specimen having Copper texture $((112)[\bar{1}\bar{1}1]_A)$ are shown in **Fig. 5.4(a)**. The preferentially formed variants of martensite (indicated by red color) have large positive interaction energy, suggesting that the variant selection in martensitic transformation from the 1-cycle ARB processed specimen having deformed coarse-grained austenite can be well explained by the

interaction energy between the residual stress in the rolled austenite and shape deformation accompanying martensitic transformation.

Figure 5.4(b) shows the interaction energy values for the 24 variants of martensite transformed from the 6-cycle ARB processed specimen having elongated ultrafine-grained austenite with Brass texture ((011) $[2\bar{1}1]_A$). In contrast to Fig. 5.4(a), the preferentially formed variants of martensite transformed from the 6-cycle ARB processed specimen (indicated by red color) have negative interaction energy. Accordingly, the variant selection in martensitic transformation from the ultrafine-grained austenite fabricated by the 6-cycle ARB process is not based on the interaction energy between the residual stress in the ARB processed austenite and shape deformation.

Table 5.2. Residual stress tensors for Brass and Copper textures in cold-rolled austenite measured by Wang et al. [14].

Texture components	σ_{11} / MPa	σ_{22} / MPa	σ_{33} / MPa	σ_{23} / MPa	σ_{13} / MPa	σ_{12} / MPa
Brass {110}<112>	−292	37	73	0	0	±13
Copper {112}<111>	−188	−83	−108	0	±41	0

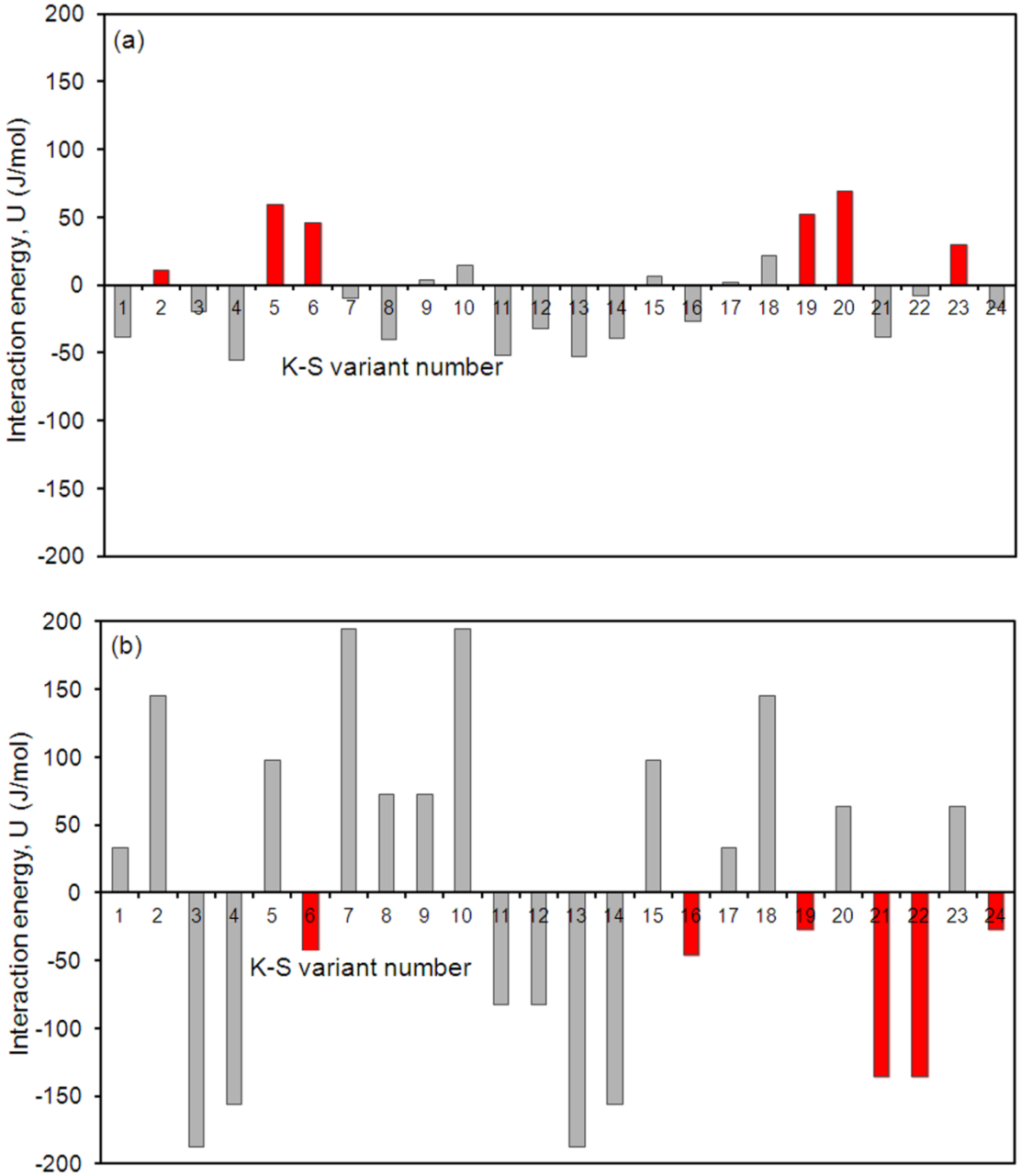

Fig. 5.4. The interaction energy values calculated for the 24 variants of martensite transformed from (a) 1-cycle ARB processed austenite having Copper texture ((112) $[\bar{1}\bar{1}1]_A$), and (b) 6-cycle ARB processed austenite having Brass texture ((011) $[\bar{1}12]_A$). The preferentially formed variants are indicated by red color in (a) and (b).

Since martensite plate cannot grow across high angle boundaries of austenite, it seems that the lamellar shape (elongated along RD) of the ultrafine-grained austenite (Fig. 5.2(c)) affects the variant selection of martensite transformed from the 6-cycle ARB processed specimen. On this basis, habit plane orientations for the 24 variants of

martensite are plotted on the pole figure of which coordinate system corresponds to Brass orientation (RD // $[2\bar{1}1]_A$, ND // $[011]_A$), as shown in **Fig. 5.5**. The pole figure reveals that the normal directions of habit planes for the preferentially formed variants of martensite transformed from the 6-cycle ARB processed specimen (represented by red color) are nearly close to ND (V_6, V_{16}) or TD (V_{19}, V_{21}, V_{22}, V_{24}). The martensite plates of which normal directions of habit planes are close to ND or TD can grow along the elongated direction of the ultrafine-grained austenite in the 6-cycle ARB processed specimen. Therefore, it can be concluded that, in the case of the 6-cycle ARB processed specimen having elongated ultrafine-grained austenite, grain shape of austenite dominantly affects the variant selection of martensitic transformation.

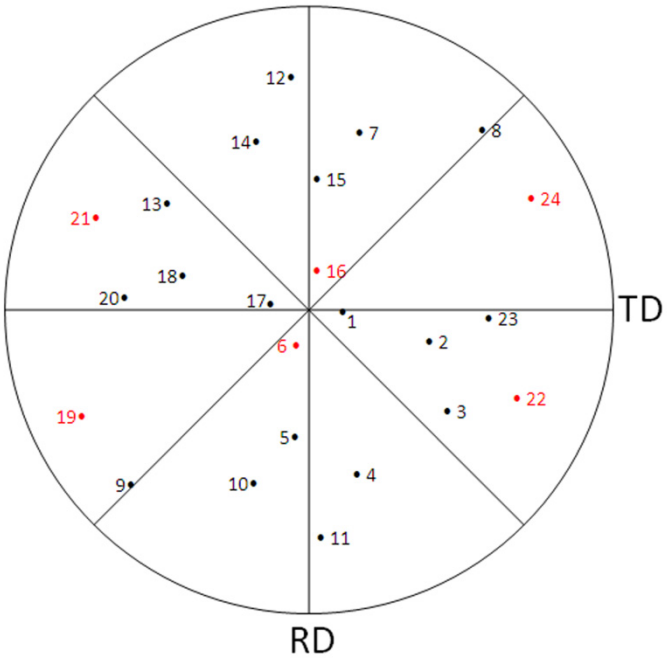

Fig. 5.5. A pole figure showing the habit plane orientation for the 24 variants of martensite. The preferentially formed variants of martensite transformed from the 6-cycle ARB processed specimen having elongated ultrafine-grained austenite are indicated by red color. The coordinate system of the pole figure corresponds to the Brass texture (RD = $[2\bar{1}1]_A$, ND = $[011]_A$), which was found in the 6-cycle ARB processed austenite. The numbers indicate the positions of the habit plane orientation for the 24 variants of martensite transformed from the austenite with exact Brass orientation ((011) $[2\bar{1}1]_A$).

5.3.3. Transformation texture and variant selection of martensite in ARB processed and subsequently annealed specimen

Figure 5.6(a) and (b) shows an EBSD orientation map and corresponding $\{100\}_A$ pole figure of the 6-cycle ARB processed specimen after annealing at 773 K for 1.8 ks. The 6-cycle ARB processed specimen still consists of elongated ultrafine-grained austenite after annealing at 773 K. In addition, Brass texture is kept after annealing at 773 K. This is because annealing at 773 K causes no recrystallization but only recovery, as explained in chapter 2. In contrast, recrystallization occurs by annealing at 873 K for 1.8 ks, resulting in the development of Cube texture as shown in **Fig. 5.6(c) and (d)**.

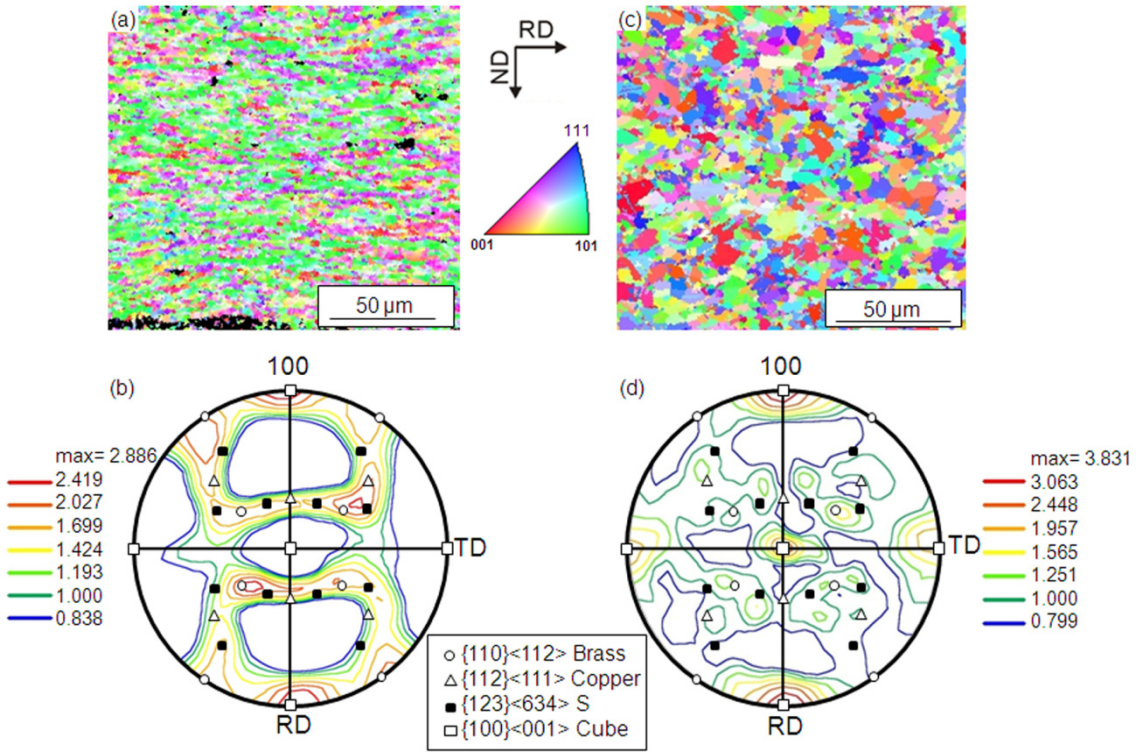

Fig. 5.6. EBSD orientation color maps and $\{100\}_A$ pole figures of austenite in ((a), (b)) the specimen 6-cycle ARB processed and then annealed at 773 K for 1.8 ks, and ((c), (d)) the specimen 6-cycle ARB processed and then annealed at 873 K for 1.8 ks.

Figure 5.7 (a) and (b) displays the EBSD orientation map and corresponding $\{100\}_M$ pole figure of martensite transformed from the austenite 6-cycle ARB processed and then annealed at 773 K for 1.8 ks having elongated ultrafine-grains. The positions of the ideal $<100>_M$ axes for the 24 variants of martensite transformed from the austenite with exact Brass orientation ((011) $[2\bar{1}1]_A$) are plotted in Fig. 5.7(b). The preferentially formed variants of martensite transformed from the 6-cycle ARB processed specimen after annealing at 773 K are V_6, V_{16}, V_{19}, V_{21}, V_{22} and V_{24}, which are completely the same as those transformed from the 6-cycle ARB processed specimen (Fig. 5.3(d)). This fact supports the previous conclusion that the variant selection rule is determined by austenite grain shape, and not by interaction energy between the residual stress of austenite and shape deformation, when the austenite has elongated ultrafine-grained structures, because the residual stress of austenite, which is inherited during the 6-cycle ARB process, is released to some extent by annealing at 773 K.

Figure 5.7 (c) and (d) show an EBSD orientation map and corresponding $\{100\}_M$ pole figure of martensite transformed from the austenite 6-cycle ARB processed and then annealed at 873 K for 1.8 ks having equiaxed (recrystallized) fine-grains. Although the austenite 6-cycle ARB processed and then annealed at 873 K for 1.8 ks has the strong cube texture (Fig. 5.6(c)), the intensities of martensite in the pole figure of Fig. 5.7(d) are very weak. This indicates that there is no variant selection of martensite transformed from the austenite having fully recrystallized and eqiaxed grains even when austenite grain size is very fine.

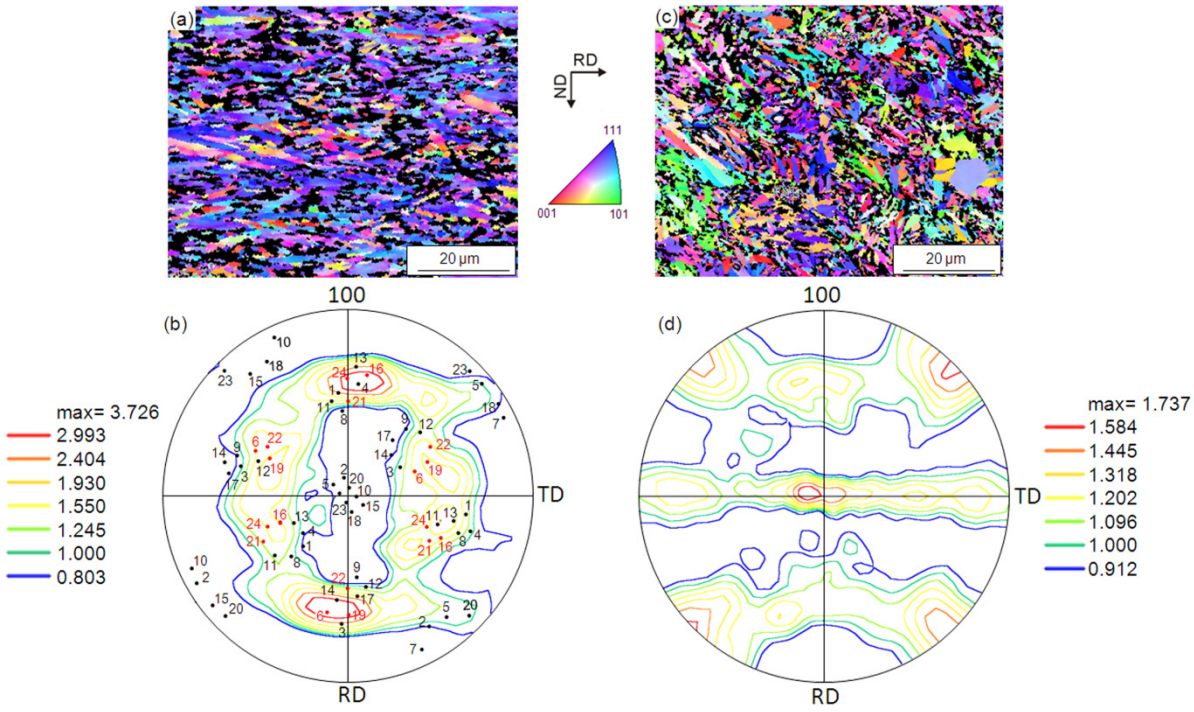

Fig. 5.7. EBSD orientation color maps and $\{100\}_M$ pole figures of martensite transformed from ((a), (b)) the specimen 6-cycle ARB processed and then annealed at 773 K for 1.8 ks, and ((c), (d)) the specimen 6-cycle ARB processed and then annealed at 873 K for 1.8 ks. The positions of the ideal $<100>_M$ axes for the 24 variants of martensite transformed from the austenite with exact Brass orientation ((011) $[2\bar{1}1]_A$) are shown in by the numbers (b). The preferential variants are indicated by red color.

5.4. Conclusion

In this chapter, variant selection of martensite transformed from the ARB processed specimens having different structures, i.e., coarse-grained austenite (the starting material and 1-cycle ARB processed specimen), elongated ultrafine-grained austenite (the 6-cycle ARB processed specimen) and equiaxed fine-grained austenite (the specimen 6-cycle ARB processed and annealed at 873 K for 1.8 ks), was studied in the Fe-24Ni-0.3C alloy. The conclusions are summarized as follows:

(i) The austenite ARB processed by 1-cycle (50% rolled) had Copper texture, while the ultrafine and elongated austenite fabricated by the 6-cycle ARB process showed

Brass texture. Transformation texture of martensite changed with the change of austenite texture, controlled by different variant selection rules.

(ii) The variant selection in martensitic transformation from the 1-cycle ARB processed specimen having deformed coarse-grained austenite can be well explained by the interaction energy between residual stress in the rolled austenite and shape deformation accompanying martensitic transformation. On the other hand, in the case of the 6-cycle ARB processed specimen having elongated ultrafine-grained austenite, the elongated grain shape played an important role for the variant selection of martensite, i.e., the martensite plates which can grow along the elongated direction of the ultrafine-grained austenite were preferentially formed.

(iii) Annealing treatment of the 6-cycle ARB processed specimen at 773 K for 1.8 ks induced no recrystallization but only recovery of austenite, resulting in the same transformation texture and variant selection rule with those in the 6-cycle ARB processed specimen. In contrast, annealing treatment of the 6-cycle ARB processed austenite at 873 K for 1.8 ks suppressed the variant selection by changing the austenite structure from elongated ultrafine-grains to fully-recrystallized and equiaxed fine-grains.

References

[1] R.Z. Valiev, N.A. Krasilnikov, N.K. Tsenev, Mater. Sci. and Eng. A 137 (1991), pp. 35-40.

[2] Z. Horita, D.J. Smith, M. Furukawa, M. Nemoto, R.Z. Valiev, T.G. Langdon, J. Mater. Res. 11 (1996), pp. 1880-1890.

[3] Y. Saito, N. Tsuji, H. Utsunomiya, T. Sakai, Acta Mater. 47 (1999), pp. 579-583.

[4] R.Z. Valiev, M.J. Zehetbauer, Y. Estrin, H.W. Höppel, Y. Ivanisenko, H. Hahn, G. Wilde, H.J. Roven, X. Sauvage, T.G. Langdon, Adv. Eng. Mater. 9 (2007), pp. 527-533.

[5] N. Tsuji, J. of Nanosci. and Nanotech. 7 (2007), pp. 3765-3770.

[6] G. Kurdjumov, G. Sachs, Z. Phys, 64 (1930), pp. 325-343.

[7] S. Kundu, Mater. Sci. and Eng. A 516 (2009), pp. 290-296.

[8] J.R. Patel, M. Cohen, Acta Metall. 1 (1953), pp. 531–538.

[9] M.S. Wechsler, D.S. Lieberman, T.A. Reed, Trans. AIME 197 (1953), pp. 1503–1515.

[10] J.S. Bowles, J. K. Mackenzie, Acta Metall. 2 (1954), pp. 129–137.

[11] J.K. Mackenzie, J.S. Bowles, Acta Metall. 2 (1954), pp. 138–147.

[12] M.S. Wechsler, Acta Metall. 7 (1959), pp. 793–802.

[13] A. Shibata, S. Morito, T. Furuhara, T. Maki, Scripta Mater. 53 (2005), pp. 597-601.

[14] Y.D. Wang, R. Lin Peng, X.L. Wang, R.L. McGreevy, Acta Mater. 50 (2002), pp. 1717-1734.

Chapter 6. Summary and conclusions

As mentioned in the previous chapters, ultrafine-grained (UFG) or nano-structured materials fabricated by severe plastic deformation (SPD) process can exhibit superior and peculiar mechanical properties. Besides the SPD process, another possible way to achieve finer microstructure and good mechanical properties is using phase transformation, especially martensitic transformation in steels. On this basis, the combination of UFG structure and martensitic transformation is desired. In this thesis, characteristics of martensitic transformation from UFG austenite have been clarified. The sheets of a Fe-24wt.%Ni-0.3wt.%C alloy with mean grain size of 35 μm were provided to accumulative roll bonding (ARB) process (with pre-heating at 873 K for 0.6 ks) up to 6 cycles and then subsequently annealed at 773, 823 and 873 K for 1.8 ks to obtain UFG austenite with partly recrystallized or fully recrystallized microstructures. The results achieved in this doctoral thesis can be summarized as follows.

In **chapter 1**, the feasibility and the purpose of this study was indicated, in specific, background of the UFG materials and the previous studies concerning martensitic transformation were elucidated.

In **chapter 2**, characteristics of the UFG austenite processed by the ARB process, i.e., microstructure, texture and mechanical properties, were studied. In addition, the effect of annealing treatment on characteristics of the UFG austenite was investigated. The results indicated that after 6-cycle ARB process, UFG austenite having lamellar grains elongated along the rolling direction (RD) with mean grain thickness of 300 nm was obtained. Annealing treatment at 773-873 K for 1.8 ks of the 6-cycle ARB processed austenite resulted in formation of an austenite having different structures, i.e., partly recrystallized structure and fully recrystallized structure.

Evaluation of texture components in the ARB processed austenite showed that after 1-cycle ARB process, Copper orientation ({112}<111>) was the main texture component. After 2-cycle ARB process, Copper component was weakened and a texture consisting of strong S component ({123}<634>) and weak Brass component ({110}<112>) developed. Increasing ARB cycle up to 6 cycles resulted in the development of strong Brass texture ({110}<112>). By annealing at 773 K for 1.8 ks, texture did not change. However, increase of annealing temperature to 823 ~ 873 K weakened the Brass component but strengthened the Cube component ({100}<001>) considerably.

In the stress-strain curves of the ARB processed austenite, yielding behavior with Lüders band deformation appeared. The Lüders band propagation corresponded to deformation-induced martensitic transformation. The proof strength and tensile strength of austenite increased significantly only after 1-cycle ARB process. With increasing the number of ARB cycles, proof strength increased gradually while tensile strength did not change. The tensile strength of the ARB processed specimens depended on the volume fraction of deformation-induced martensite transformation. The uniform elongation drastically decreased after 1-cycle ARB process, but the ARB processed austenite in the present alloy maintained significantly large tensile elongation compared with other materials ARB processed. Annealing treatment at 773-873 K for 1.8 ks of the 6-cycle ARB processed austenite resulted in significant decrease in proof strength and tensile strength, while uniform elongation did not change.

In **chapter 3**, characteristics of martensite, i.e., microstructure and martensite transformation starting temperature (M_s), transformed from UFG austenite fabricated by ARB process and subsequent annealing were studied in details. The results indicated

that the morphologies of martensite transformed from the coarse-grained austenite and UFG austenite were both lenticular types. However, some martensite plates transformed from the UFG austenite contained low angle boundaries exhibited broken and fragmented shape. The size of the martensite plates decreased with decrease in austenite grain size. However, the ratio of the austenite grain size to the martensite plate size decreased when the austenite grain size was smaller than 2~3 μm. Moreover, the presence of low angle boundaries inside the martensite plates transformed from ARB processed austenite indicated that the low angle boundaries in austenite were not effective for grain refinement by martensite transformation.

Evaluation of the M_s for the ARB processed specimens indicated that it did not change so much, even though the austenite grain size (high angle boundaries) decreased greatly from 35 μm to 750 nm by the 6-cycle ARB process. In contrast, annealing treatment of the 6-cycle ARB processed specimen decreased the M_s significantly. The change in M_s with ARB process and subsequent annealing treatment was consistent with the change in the dislocation density. On the basis of the experimental results, it was concluded that the low angle boundaries or dislocations can act as nucleation sites for martensitic transformation, while high angle boundaries suppress martensitic transformation.

In **chapter 4**, orientation relationship of martensite with respect to the coarse-grained austenite (the starting material), elongated UFG austenite (the 6-cycle ARB processed specimen) and fully-recrystallized fine-grained austenite (the specimen 6-cycle ARB processed and then annealed at 873 K for 1.8 ks) was studied. The orientation relationship of martensite transformed from the coarse-grained austenite was the Greninger-Troiano (G-T) relationship ($\{111\}_A$ 1° from $\{011\}_M$, $<\bar{1}\bar{1}2>_A$ 2.5° from $<0\bar{1}1>_M$, where subscripts of A and M represent austenite and martensite, respectively)

at the middle part of martensite plate, but it shifted to the Kurdjumov-Sachs (K-S) relationship ($\{111\}_A$ // $\{011\}_M$, $<\bar{1}01>_A$ // $<\bar{1}\bar{1}1>_M$) as approaching the interphase boundary. In contrast, the whole area of the martensite plates transformed from the fully recrystallized fine-grained austenite satisfied the G-T relationship. This could be attributed to the smaller size of martensite plate transformed from the fine-grained austenite.

Orientation relationship of martensite transformed from the UFG austenite was the G-T relationship, but the observed orientation relationships were significantly scattered between different martensite plates. This was attributed to the existence of high density of dislocations or low angle boundaries inside the austenite grains resulted in the large scatter of the observed orientation relationships.

In **chapter 5**, variant selection of martensite transformed from the ARB processed specimens having different structures, i.e., coarse-grained austenite, elongated UFG austenite and equiaxed fine-grained austenite, was studied. The austenite ARB processed by 1-cycle (50% rolled) had Copper texture ({112}<111>), while the ultrafine and elongated austenite fabricated by the 6-cycle ARB process showed Brass texture ({110}<112>). Transformation texture of martensite changed with the change of austenite texture, controlled by different variant selection rules.

The variant selection in martensitic transformation from the 1-cycle ARB processed specimen having the deformed coarse-grained austenite can be well explained by the interaction energy between residual stress in the rolled austenite and shape deformation accompanying martensitic transformation. On the other hand, in the case of the 6-cycle ARB processed specimen having elongated UFG austenite, the elongated grain shape played an important role for the variant selection of martensite, i.e., the martensite

plates which could grow along the elongated direction of the UFG austenite were preferentially formed.

Annealing treatment of the 6-cycle ARB processed specimen at 773 K for 1.8 ks induced no recrystallization but only recovery of austenite, resulting in the same transformation texture and variant selection rule as those in the 6-cycle ARB processed specimen. In contrast, annealing treatment of the 6-cycle ARB processed austenite at 873 K for 1.8 ks suppressed the variant selection by changing the austenite structure from elongated ultrafine-grains to fully-recrystallized and equiaxed fine-grains.

Acknowledgements

I am indebted to many people for completing this dissertation. Especially I would like to give great appreciation to my principle advisor, **Professor Nobuhiro Tsuji** of Kyoto University for his excellent scientific guidance, inspiration, and trust. Without his endless support, it is impossible for me to finish my Ph.D. study and this dissertation. Also, I would like to thank deeply from my co-advisor, **Dr. Akinobu Shibata** of Kyoto University, for his warm encouragements, helpful discussions, great advices and proper suggestions. Indeed, they provided for me the best academic environments, supervised my dissertation, and taught me the qualified research method. I also want to express my sincerest appreciation to my thesis committee members, **Professor Yasuharu Shirai** and **Professor Haruyuki Inui** for accepting to evaluate my thesis and their excellent advises. In addition, I am thankful for the help and support provided by all of my laboratory members.

I also would like to express sincere thanks from the Ministry of Science, Research and Technology (MSRT) of Iran for supporting me to do PhD in Japan. The support is gratefully appreciated.

List of publications

a) International Journal papers

1. **H. R. Jafarian**, E. Borhani, A. Shibata, D. Terada, N. Tsuji, "Martensite/austenite interfaces in ultrafine grained Fe–Ni–C alloy", Journal of Materials Science Vol. 46 (2011), pp. 4216-4220.

2. **H. R. Jafarian**, E. Borhani, A. Shibata, D. Terada, N. Tsuji, "Martensitic transformation from ultrafine-grained austenite fabricated by ARB in Fe-24Ni-0.3C", Materials Science Forum Vols. 667-669 (2011), pp 361-366.

3. A. Shibata, **H. R. Jafarian**, D. Terada, N. Tsuji, " Crystallographic Features of Martensite Transformed from Ultrafine Grained Austenite Fabricated by Severe Plastic Deformation", Materials Science Forum, Accepted.

4. A. Shibata, **H. R. Jafarian**, N. Tsuji, "Microstructure and crystallographic features of martensite transformed from ultrafine-grained austenite in Fe-24Ni-0.3C alloy ", Materials Transactions, Accepted.

5. **H. R. Jafarian**, E. Borhani, A. Shibata, N. Tsuji, "Variant selection of martensite transformation from ultrafine-grained austenite in Fe-Ni-C alloy ", Journal of Alloys and Compounds, Submitted.

b) Presentation in Japanese meeting

1. **H. R. Jafarian**, E. Borhani, D. Terada, Y. Miyajima and N. Tsuji, ″Martensitic transformation from ARB processed and annealed metastable austenite″, Proceeding of meeting of the Japan Institute of Metals, 2009 autumn, Kyoto University, p. 526.

2. **H. R. Jafarian**, E. Borhani, A. Shibata, D. Terada, and N. Tsuji, ″Transformation texture in ultrafine grained metastable austenitic steel″, Proceeding of meeting of the Japan Institute of Metals, 2010 autumn, Hokkaido